In presenting the dissertation as a partial fulfillment of the requirements for an advanced degree from the Georgia Institute of Technology, I agree that the Library of the Institute shall make it available for inspection and circulation in accordance with its regulations governing materials of this type. I agree that permission to copy from, or to publish from, this dissertation may be granted by the professor under whose direction it was written, or, in his absence, by the Dean of the Graduate Division when such copying or publication is solely for scholarly purposes and does not involve potential financial gain. It is understood that any copying from, or publication of, this dissertation which involves potential financial gain will not be allowed without written permission.

_____

_____

7/25/68

LOW REYNOLDS NUMBER FLOW PERPENDICULAR TO A CIRCULAR CYLINDER WITH SURFACE MASS TRANSFER

A THESIS

Presented to

The Faculty of the Graduate Division

by

Han-Chuan Wu

In Partial Fulfillment

of the Requirements for the Degree

Doctor of Philosophy

in the School of Chemical Engineering

Georgia Institute of Technology

December, 1971

LOW REYNOLDS NUMBER FLOW PERPENDICULAR TO A CIRCULAR CYLINDER

WITH SURFACE MASS TRANSFER

Approved:

Chairman

Date approved by Chairman: 1/18/72

ACKNOWLEDGMENTS

The author wishes to express his sincere appreciation to his thesis advisor, Dr. Henderson C. Ward, for suggesting this problem and for his encouragement and guidance throughout the progress of this study. He is also indebted to Dr. Charles W. Gorton and Dr. Jude T. Sommerfeld, who served as members of the thesis committee, for their many helpful suggestions and careful review of the entire thesis.

Acknowledgment is also due to the Georgia Institute of Technology Rich Electronic Computer Center for the use of its computers. Thanks are also given to Dr. Homer V. Grubb for providing the author a graduate teaching assistantship.

TABLE OF CONTENTS

LIST OF TABLES

LIST OF ILLUSTRATIONS

NOMENCLATURE

In this tabulation, the principal symbols are shown. Symbols which have only a temporary significance are defined in the text and are not listed here.

Roman Letter	Definition
a	radius of circular cylinder
A	component A of binary solution
B	component B of binary solution
C	dimensionless mass concentration of component A
C_D	total drag coefficient
C_{DF}	friction drag coefficient
C_{DP}	pressure drag coefficient
$C_{D(\infty)}$	total drag coefficient extrapolated to infinite boundary position
C_P	pressure coefficient
D	diameter
$\mathscr{D}$	diffusivity of binary solution
f	function of a variable
G	radial suction mass flux in gallons/day/ft^2
I	positive integer in angular direction
J	positive integer in radial direction
$k_{x,loc}$	local mass-transfer coefficient
L1,L3,L4	coefficients for numerical analysis in diffusion equation

Roman Letter	Definition
M	number of grid spacings in angular direction
N	number of grid spacings in radial direction
n_{AO}	radial mass flux of component A at the surface
n_{BO}	radial mass flux of component B at the surface
Nu_{loc}	local Nusselt number, $\frac{2ak_{x,loc}}{C\mathcal{D}}$
$Nu_{overall}$	overall Nusselt number
p	dimensional pressure
P	dimensionless pressure with respect to ρU_∞^2
P_0	dimensionless pressure at front stagnation point
P_∞	dimensionless pressure in uniform stream
Pe	Peclet number, $\frac{2aU_\infty}{\mathcal{D}}$
r	radial distance in cylindrical coordinates, dimensional or dimensionless
r_∞	outer boundary position
Δr	mesh size in radial direction
R	Reynolds number, $\frac{2aU_\infty\rho}{\mu}$
Sch	Schmidt number, $\frac{\nu}{\mathcal{D}}$
U_∞	uniform stream velocity
v_0	dimensional radial velocity at the surface
v_r	dimensional radial velocity
v_θ	dimensional angular velocity
V_0	dimensionless radial velocity at the surface
V_x	dimensionless angular velocity
V_z	dimensionless radial velocity

Roman Letter	Definition
w_A	mass fraction of component A
x	angle in cylindrical coordinates, same as θ
Δx	mesh size in angular direction
z	axial distance normal to flow direction or radial distance from the cylinder wall
Δz	mesh size in radial direction

Greek Letter	Definition
α	relaxation factor in stream function equation
β	relaxation factor in vorticity equation
γ	Euler's constant, 0.57721
Γ	concentration polarization
ρ	mass density of binary solution
ρ_A	mass concentration of component A
μ	viscosity
ν	kinematic viscosity
θ	angle in cylindrical coordinates
∇^2	Laplacian operator
ψ	the stream function
ζ	vorticity
π	3.14159

Subscript	Definition
0	refers to quantity evaluated at the surface of the cylinder
∞	refers to quantity in the uniform stream
I	positive integer denotes a grid point whose angular coordinate is $x = I\Delta x$

Subscript	Definition
J	positive integer denotes a grid point whose radial coordinate is $z = J\Delta z$

SUMMARY

A study of low Reynolds number flow perpendicular to a circular cylinder with constant radial suction mass flux at the surface was carried out by a numerical method. The system considered was a binary solution of A and B flowing perpendicular to the cylinder with one component, say B, being removed at the surface. The investigation was limited to high Schmidt numbers and Reynolds numbers from 0.5 to 10. The Schmidt number used in this study was 560 and corresponds to that of a dilute salt-water solution, which is the fluid of interest in desalination by reverse osmosis. The total density, viscosity, and diffusivity of the binary solution were assumed to be constant throughout the entire flow field.

The purpose of this study was to determine the concentration buildup along the cylindrical surface, the local and overall mass-transfer coefficients at the wall, and the effects of constant radial suction mass flux on the flow pattern, drag coefficient, and the surface pressure distribution.

This study required the solution of the Navier-Stokes equation, the equation of continuity, and the diffusion equation, subject to specified boundary conditions. This system of equations is non-linear, and no analytical solution could be obtained. Therefore, the solution was obtained by numerical means. The whole flow field was covered by a rectangular grid with a constant step size in the angular direction and with a small step size close to and a larger step size far away from the cylinder

in the radial direction. The variable values were then considered as point functions at these grid points. The equation of motion was reduced to a single partial differential equation by introducing the stream function and eliminating the terms containing the pressure components. The resulting fourth-order partial differential equation in the stream function was split into two second-order partial differential equations, which were then approximated by finite difference equations which related the values of neighboring points in the flow field. Since both second-order partial differential equations were of elliptic form, a successive over-relaxation technique was used. Relaxation factors, which were found by trial and error, were introduced in order to achieve faster rates of convergence for the solutions of the stream function and vorticity. Further flow characteristics were then calculated from the known values of the stream function and vorticity. The flow patterns around the cylinder were obtained with the aid of a contouring program.

Without radial suction flux at the wall, the flow patterns are almost symmetrical fore and aft at a Reynolds number of 1. As the Reynolds number is increased, asymmetry becomes more pronounced. At Reynolds numbers of 7 and 10, the flow patterns show flow separation and the appearance of a pair of standing eddies behind the cylinder. However, with radial suction flux, the flow patterns show better fore-and-aft symmetry near the cylinder body. The constant streamlines have moved closer to the cylinder and their locations are dependent on the magnitude of the radial suction flux. Thus, when there is a radial suction flux at the wall, flow separation will be eliminated or delayed, depending on the magnitude of the radial suction flux and the Reynolds number.

The drag coefficient increases as the radial suction flux is increased. However, the friction drag coefficient increases more rapidly than does the pressure drag coefficient. This result correlates with the fact that the surface vorticity increases significantly with increasing radial suction flux, but the surface pressure distribution is relatively insensitive to this process.

The Crank-Nicholson implicit finite difference technique was used to approximate the convective diffusion equation. The derivative in the angular direction was approximated by the Crank-Nicholson half-way point method. The derivative in the radial direction was given by the average values over two succeeding angular increments. The concentration profiles were then calculated down the stream. At each angular increment, there resulted N-1 simultaneous equations in N-1 unknowns for which the matrix of coefficients was tridiagonal in form. The method of Thomas was used in solving these simultaneous equations.

The maximum local Nusselt number occurs at the front stagnation point. The local Nusselt number decreases with increasing distance from the front stagnation point and would continue to decrease if there were no flow separation. The contribution of the rear region to the overall mass transfer is very small. The overall mass-transfer coefficient can be approximated by the relation

$$Nu_{overall}/Sch^{1/3} = b + 0.75\ R^{1/2}$$

where b depends on the magnitude of the radial suction flux.

The results of the present analysis without radial suction flux at the wall agree very well with those of other numerical studies and experimental investigations.

CHAPTER I

INTRODUCTION

For more than a century, incompressible flow past a circular cylinder submerged in a viscous fluid has attracted considerable attention. However, no investigation to date has been done at low Reynolds numbers to include the case of constant radial suction mass flux at the cylinder wall. Since this problem is of practical interest in desalination operations by reverse osmosis, it was decided to study low Reynolds number flow perpendicular to a circular cylinder with constant radial suction mass flux at the surface.

Previous Work and Results

The study of the flow past a circular cylinder at low Reynolds numbers requires the solution of the Navier-Stokes equation and the equation of continuity, subject to specified boundary conditions. The complete Navier-Stokes equation is so complicated that no analytical solution has been obtained. As early as 1851, Stokes (1) argued that the inertia forces, exhibited by the convective terms, were small in comparison with the viscous forces. He thus neglected the inertia terms, thereby obtaining Stokes' approximation for the Navier-Stokes equation. Stokes' approximation has been successfully used in the study of the flow characteristics in the neighborhood of a sphere. However, when applied to the case of a cylinder, the solution of Stokes' approximation can not be resolved,

because there exists no solution that satisfies both surface and infinite boundary conditions. This situation is known as Stokes' paradox.

Stokes' paradox was shown by Oseen (2) to arise from the singular nature of flow at low Reynolds numbers. He argued that the ratio of inertia forces to viscous forces became arbitrarily large at sufficiently great distances from the surface, regardless of how small the Reynolds number might be. Rather than neglect the inertia terms altogether, Oseen approximated them by their linearized forms valid far from the cylinder, where the difficulty arose. Thus Oseen's equation provides a uniformly valid first approximation.

Later, Lamb (3) gave the solution of Oseen's equation. For low Reynolds number flow perpendicular to a submerged cylinder, Lamb's result for the drag coefficient is

$$C_D = \frac{8\pi}{R}\left(\frac{1}{2} - \gamma - \ln\left(\frac{R}{8}\right)\right)^{-1} \qquad (1\text{-}1)$$

where γ is Euler's constant 0.57721.

Tomotika and Aoi (4) studied in detail the flow patterns around a circular cylinder. An analytical solution of Oseen's equation for arbitrary Reynolds numbers was obtained. They concluded the surprising result that a pair of standing eddies were formed behind the cylinder, even when the Reynolds number was as small as 0.05. This is contrary to experimental observations (5). Yamada (6) treated the same problem by the same equation but in a somewhat different way, with the view of determining the Reynolds number at which standing eddies make their appearance. He

concluded that Oseen's equation is valid only at very low Reynolds numbers. Therefore Tomotika and Aoi's results are doubtful.

A perturbation technique has also been used to obtain the asymptotic solution, with Reynolds number as a perturbation parameter. The straightforward perturbation solution is not uniformly valid throughout the whole flow field. Kaplun (7) and Prounman and Pearson (8) independently studied the higher approximations to the flow past a circular cylinder at low Reynolds number by the method of matched asymptotic expansions. Stokes' and Oseen's approximations were used in the region close to and far from the cylinder, respectively. However, the fact that the two expansions are both derived from the same exact solution leads to a matched procedure which yields further boundary conditions for each expansion. Thus it was possible to determine alternately successive terms in each expansion. Kaplun determined the drag coefficient as

$$C_D = \frac{8\pi}{R}\left(\Delta_1(R) - 0.87\ \Delta_1^3(R)\right) \qquad (1\text{-}2)$$

where $\Delta_1(R) = \left(\ln \frac{8}{R} - \gamma + \frac{1}{2}\right)^{-1}$

These results are valid only at very low Reynolds numbers ($R < 2$).

At higher Reynolds numbers ($R > 2$), almost every study has been done by experimentation or numerical analysis. Taneda (5) and Tritton (9) have carried out some valuable experiments, whose results have been used for comparison with numerical studies.

The numerical study of the Navier-Stokes equation for viscous flow past a circular cylinder is very tedious and time-consuming when done

without machine aid. Therefore, not much had been done until recently when high speed electronic computers became available. The first attempt to study this problem numerically was reported by Thom (10,11) at Reynolds numbers of 10 and 20. The fourth-order differential equation in the stream function was split into two second-order differential equations, which were then approximated by finite difference equations which related the values of neighboring points on a flow grid. Since both equations were elliptic partial differential equations, an iteration technique was used to obtain solution in the form of the stream function and vorticity. Kawaguti (12) used the same technique and studied the same problem at a Reynolds number of 40. These calculations were performed by desk calculator and were very time-consuming, even with fairly large mesh size. For example, Kawaguti's study on this subject took about a year and a half with twenty working hours every week.

Allen and Southwell's numerical study (13) by a relaxation method on this problem is not in accord with previous investigations. As criticized by Kawaguti (14), their results showing the Reynolds number dependency on the length of standing eddies behind a circular cylinder were inconsistent with experimental and numerical results.

Dennis and Shimshoni (15) reduced the equations of motion to a series of ordinary differential equations and solved these equations by a numerical method over the Reynolds number range of 0.01 to 10^5. Their results have been questioned by Underwood (16), who used a semi-analytic method of series truncation developed by Van Dyke (17). Underwood also reduced the governing partial differential equations to a system of ordinary differential equations which were then integrated numerically. A

fifth-truncation solution was shown to be accurate. His results for Reynolds numbers from 0.1 to 10 gave good agreement with other numerical studies.

Several unsteady state approaches of incompressible viscous flow past a circular cylinder were also investigated to determine the existence of steady state solutions at higher Reynolds numbers. Payne (18) obtained the numerical results at Reynolds numbers of 40 and 100 but did not extend his calculations far enough to reach steady state. Further, because his mesh size and time interval were large, solution errors were not minimized. Later, Kawaguti and Jain (19) employed a finite difference expression in explicit form to calculate the stream function and vorticity at a later time, but they did not check their solution accuracy by varying the mesh size and time interval.

Finally Son and Hanratty (20) employed the implicit-alternating direction technique, developed by Peaceman and Rachford (21), to obtain some insight into the nature of the steady flow field at infinite Reynolds number. Their results indicate that steady state features can be expected for Reynolds number up to 200. However Son and Hanratty did not obtain a complete solution at a Reynolds number of 500, because of the excess computation time required.

For the numerical study of viscous flow past a circular cylinder in an infinite fluid, the computational field was restricted within an outer circular boundary. The outer boundary must be at a relatively large radial distance for low Reynolds numbers study. Extrapolation to an infinite boundary is required in order to obtain an accurate result. The extrapolation procedure used by Keller and Takami (22) to obtain results

applicable to a cylinder in a fluid of infinite extent was considered inadequate by Hamielec and Raal (23), who developed an extrapolation technique to obtain an asymptotic solution. Hamielec and Raal's extensive numerical calculations showed that smaller step sizes were required for higher Reynolds number calculations.

An understanding of the hydrodynamic behavior was essential to the study of the convective diffusion problem. In all previous studies mentioned, drag coefficients, pressure distributions, and flow patterns were the quantities investigated. Very few studies on mass transfer in this system have been done. Lohrisch (24) observed the absorption of water vapor on caustic cylinders and ammonia on cylinders wetted with phosphoric acid. Linton and Sherwood (25) measured the rate of solution of cast cylinders of organic acids in a stream of water. Dobry and Finn (26) studied experimentally the mass transfer to a cylinder at low Reynolds numbers by using a diffusion-limited electrode reaction occurring at the surface of the cylinder. Their results gave good agreement with heat-transfer data obtained by Davis (27) at Prandtl numbers from 860 to 1240. Friedlander (28) applied the boundary-layer concept and obtained a theoretical solution for mass transfer to cylinders at low Reynolds numbers. His results were not reliable because he used the incorrect velocity profile of Tomotika and Aoi.

By using the von Mises transformation, Lighthill (29) reduced the diffusion equation to the heat conduction equation, which was then integrated analytically. Thus, a concentration distribution near the surface was obtained for the case of constant surface concentration. As pointed

out by Sih and Newman (30) and Newman (31), the diffusion-layer solution is in error at the rear of the cylinder because the diffusion layer becomes too thick for the theory to apply.

Based on the idea that mass transfer from interfaces are influenced by the fluid-dynamic condition, an expression relating mass transfer to hydrodynamic conditions over the entire surface of the cylinder was developed by Grafton (32). At the front stagnation point, the mass-transfer coefficient was expressed as

$$Nu_{loc} = 1.51\ Sch^{1/3}\ R^{1/2} \qquad (1\text{-}3)$$

While not much has been done on mass transfer to a circular cylinder at low Reynolds numbers, many corresponding heat transfer problems have been treated. It is well known that the diffusion of heat and the diffusion of mass are analogous under certain conditions. For example, for heat transfer the Nusselt number is a function of the Prandtl and Reynolds numbers, while for mass transfer at low mass-transfer rates it is the same function of the Schmidt and Reynolds numbers. Thus mass transfer results at low mass-transfer rates may be predicted from heat-transfer data by simply replacing the Prandtl number with the Schmidt number.

McAdams (33) has reviewed most of the literature on heat transfer to cylinders. Piret, James, and Stacy (34) studied heat transmission from fine wires to water. Eckert and Soehngen (35) measured the heat-transfer coefficients around circular cylinders at Reynolds numbers from 20 to 500. Soehngen (36) extended the range of data into the regime of Reynolds numbers lower than 0.1. Cole and Roshko (37) and Ellingworth (38) also

studied the heat transfer from a circular cylinder at low Reynolds numbers. By using more accurate velocity profiles, Wood (39) and Hieber and Gebhart (40) studied the same problem and obtained a solution containing higher order approximations.

Scope and Purpose of the Study

In this study, a binary solution flowing perpendicular to a circular cylinder at a Schmidt number of 560 and Reynolds numbers from 0.5 to 10 was considered. The Schmidt number of 560 is that of a dilute salt-water solution at 25°C. The circular cylinder was assumed to be made of a semipermeable membrane which permitted the passage of one component uniformly. The total density, viscosity, and diffusivity of the binary solution were assumed to be constant throughout the whole flow field.

The purpose of this analysis was to determine the concentration buildup along the cylindrical surface, the local and overall mass-transfer coefficients at the cylinder wall, and the effects of constant radial suction mass flux on the flow pattern, drag coefficient, and the surface pressure distribution. The results of this analysis can be applied to the design and operation of hollow-fiber reverse osmosis desalination units.

CHAPTER II

MATHEMATICAL DESCRIPTION OF THE PROBLEM

Statement of the Problem

The system considered consists of a binary solution of A and B flowing perpendicular to a circular cylinder with one component, say B, being removed at the surface. This investigation is limited to high Schmidt numbers and low Reynolds numbers. The surface mass flux, n_{BO}, is assumed to be uniform and the physical properties of the binary solution are assumed to be constant. The following assumptions are also made in this study:

(1) The flow is steady, isothermal, and two-dimensional with uniform stream velocity U_∞.

(2) The fluid is Newtonian and of constant viscosity μ.

(3) The mass density ρ and the diffusivity $\mathcal{D}$ of the solution are constant.

(4) There is no wall slip.

(5) There are no external forces acting on the system.

(6) Angular symmetry is present.

It was desired to determine the concentration buildup along the cylindrical surface, and the local and overall mass-transfer coefficients at the cylinder wall. In addition, the effects of constant radial suction mass flux on various flow characteristics were studied.

The difficulties encountered in the mathematical solution of this system were: 1) no accurate description of the flow field was available, and 2) the hydrodynamic boundary layer was too thick for boundary-layer theory to apply. The governing equations which describe the physical problem can be found in references (41, 42).

Fluid Flow Equations and Boundary Conditions

The system studied here is represented in the cylindrical coordinate system, with the angle θ measured from the upstream axis and the distance z measured along the cylinder axis. The flow diagram is shown in Figure 1.

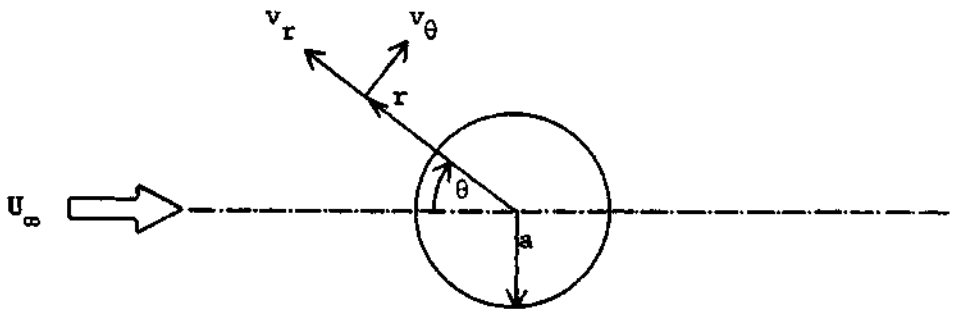

Figure 1. Cylindrical Coordinate System

The term "a" is the radius of the cylinder, and v_r and v_θ are the velocity components in the r- and θ-directions, respectively. Under the assumption of two-dimensional flow, there will be no flow in the z-direction and the velocity component in the z-direction, v_z, and all derivatives with respect to z are zero. Therefore, the governing differential equations of the system can be written as

Equation of Continuity

$$\frac{\partial v_r}{\partial r} + \frac{v_r}{r} + \frac{1}{r}\frac{\partial v_\theta}{\partial \theta} = 0 \tag{2-1}$$

Equation of Motion in r-Direction

$$\rho\left(v_r \frac{\partial v_r}{\partial r} + \frac{v_\theta}{r}\frac{\partial v_r}{\partial \theta} - \frac{v_\theta^2}{r}\right) = -\frac{\partial p}{\partial r} \tag{2-2}$$

$$+ \mu\left(\frac{\partial^2 v_r}{\partial r^2} + \frac{1}{r}\frac{\partial v_r}{\partial r} - \frac{v_r}{r^2} + \frac{1}{r^2}\frac{\partial^2 v_r}{\partial \theta^2} - \frac{2}{r^2}\frac{\partial v_\theta}{\partial \theta}\right)$$

Equation of Motion in θ-Direction

$$\rho\left(v_r \frac{\partial v_\theta}{\partial r} + \frac{v_\theta}{r}\frac{\partial v_\theta}{\partial \theta} + \frac{v_r v_\theta}{r}\right) = -\frac{1}{r}\frac{\partial p}{\partial \theta} \tag{2-3}$$

$$+ \mu\left(\frac{\partial^2 v_\theta}{\partial r^2} + \frac{1}{r}\frac{\partial v_\theta}{\partial r} - \frac{v_\theta}{r^2} + \frac{1}{r^2}\frac{\partial^2 v_\theta}{\partial \theta^2} + \frac{2}{r^2}\frac{\partial v_r}{\partial \theta}\right)$$

Boundary Conditions

$$\text{at } r = a, \quad v_r(r,\theta) = v_0$$

$$\text{and} \quad v_\theta(r,\theta) = 0 \tag{2-4}$$

$$\text{at } r = \infty, \quad v_r(r,\theta) = -U_\infty \cos\theta$$

$$\text{and} \quad v_\theta(r,\theta) = U_\infty \sin\theta$$

where v_0 is the uniform radial suction velocity at the surface.

Dimensionless Forms of Flow Equations and Boundary Conditions

The flow equations and boundary conditions can be made dimensionless by defining suitable dimensionless variables. For the problem of interest, the uniform stream conditions were used as reference quantities and the radius of the cylinder was used as a characteristic length. The dimensionless variables are defined by

$$V_r = v_r/U_\infty \qquad V_\theta = v_\theta/U_\infty \qquad V_0 = v_0/U_\infty \tag{2-5}$$

$$P = p/\rho U_\infty^2 \qquad R = 2aU_\infty\rho/\mu$$

where R is the Reynolds number.

By introducing the above dimensionless variables into the governing Equations (2-1) through (2-4), the dimensionless forms of the equations of continuity and motion together with the boundary conditions take the following form:

Equation of Continuity

$$\frac{\partial V_r}{\partial r} + \frac{V_r}{r} + \frac{1}{r}\frac{\partial V_\theta}{\partial \theta} = 0 \tag{2-6}$$

Equation of Motion in r-Direction

$$V_r \frac{\partial V_r}{\partial r} + \frac{V_\theta}{r}\frac{\partial V_r}{\partial \theta} - \frac{V_\theta^2}{r} = -\frac{\partial P}{\partial r} \tag{2-7}$$

$$+ \frac{2}{R}\left(\frac{\partial^2 V_r}{\partial r^2} + \frac{1}{r}\frac{\partial V_r}{\partial r} - \frac{V_r}{r^2} + \frac{1}{r^2}\frac{\partial^2 V_r}{\partial \theta^2} - \frac{2}{r^2}\frac{\partial V_\theta}{\partial \theta}\right)$$

Equation of Motion in θ-Direction

$$V_r \frac{\partial V_\theta}{\partial r} + \frac{V_\theta}{r} \frac{\partial V_\theta}{\partial \theta} + \frac{V_r V_\theta}{r} = - \frac{1}{r} \frac{\partial P}{\partial \theta} \tag{2-8}$$

$$+ \frac{2}{R}\left(\frac{\partial^2 V_\theta}{\partial r^2} + \frac{1}{r} \frac{\partial V_\theta}{\partial r} - \frac{V_\theta}{r^2} + \frac{1}{r^2} \frac{\partial^2 V_\theta}{\partial \theta^2} + \frac{2}{r^2} \frac{\partial V_r}{\partial \theta} \right)$$

Boundary Conditions

$$\text{at } r = 1, \; V_r(r,\theta) = V_0 \tag{2-9}$$

$$\text{and} \quad V_\theta(r,\theta) = 0$$

$$\text{at } r = \infty, \; V_r(r,\theta) = - \cos\theta$$

$$\text{and} \quad V_\theta(r,\theta) = \sin\theta$$

Note that, in the dimensionless equations, r is the radial distance divided by the radius a.

Diffusion Equation and Boundary Conditions

The equation of continuity of component A can be written as

$$v_r \frac{\partial \rho_A}{\partial r} + \frac{v_\theta}{r} \frac{\partial \rho_A}{\partial \theta} = \mathcal{D}\left(\frac{\partial^2 \rho_A}{\partial r^2} + \frac{1}{r} \frac{\partial \rho_A}{\partial r} + \frac{1}{r^2} \frac{\partial^2 \rho_A}{\partial \theta^2} \right) \tag{2-10}$$

with the boundary conditions

$$\text{at } r = \infty, \; \rho_A(r,\theta) = \rho_{A\infty} \tag{2-11}$$

$$\text{at } \theta = 0, \; \partial \rho_A / \partial \theta = 0$$

in which ρ_A is the mass concentration of component A. The subscript ∞ indicates the quantity in the uniform stream.

Fick's first law of diffusion can be written in terms of the mass flux at the surface of the cylinder as

$$n_{AO} = w_{AO}\left(n_{AO} + n_{BO}\right) - \rho\mathcal{D}\left(\frac{\partial w_A}{\partial r}\right)_{r=a} \tag{2-12}$$

in which the subscript O indicates values evaluated at the surface of the cylinder.

Since component A is completely rejected at the surface of the cylinder, n_{AO} must be zero. Substitution of $n_{BO} = \rho v_0$ and $w_A = \rho_A/\rho$ into Equation (2-12) gives the third boundary condition for the diffusion equation

$$\frac{1}{\rho_A}\left(\frac{\partial \rho_A}{\partial r}\right)_{r=a} = \frac{v_0}{\mathcal{D}} \tag{2-13}$$

Dimensionless Forms of Diffusion Equation and Boundary Conditions

Equations (2-10), (2-11), and (2-13) can be made dimensionless by defining the following dimensionless mass concentration

$$C = \rho_A/\rho_{A\infty}$$

Therefore the governing diffusion equation together with its boundary conditions becomes

$$V_r\frac{\partial C}{\partial r} + \frac{V_\theta}{r}\frac{\partial C}{\partial \theta} = \frac{2}{Pe}\left(\frac{\partial^2 C}{\partial r^2} + \frac{1}{r}\frac{\partial C}{\partial r} + \frac{1}{r^2}\frac{\partial^2 C}{\partial \theta^2}\right) \tag{2-14}$$

$$\text{at } r = \infty,\ C(r,\theta) = 1.0 \qquad (2\text{-}15)$$

$$\text{at } \theta = 0,\ \partial C/\partial\theta = 0.0$$

$$\text{at } r = 1,\ \frac{1}{C}\frac{\partial C}{\partial r} = \frac{aV_0}{\mathcal{D}}$$

where Pe is the Peclet number defined as

$$Pe = 2aU_\infty/\mathcal{D}$$

The resulting diffusion Equation (2-14) can be further simplified by performing a qualitative "order of magnitude" analysis. This method was originally devised by Prandtl (42) to show that the Navier-Stokes equation could be simplified to yield approximate solutions for many fluid flow problems.

Assuming that diffusion in the angular direction can be neglected at high Schmidt numbers, the governing diffusion equation is given by the parabolic differential equation

$$V_r\frac{\partial C}{\partial r} + \frac{V_\theta}{r}\frac{\partial C}{\partial\theta} = \frac{2}{Pe}\left(\frac{\partial^2 C}{\partial r^2} + \frac{1}{r}\frac{\partial C}{\partial r}\right) \qquad (2\text{-}16)$$

A similar approximation was employed by Levich (43) for convective diffusion to a sphere.

The resulting equations of continuity, motion, and diffusion together with the boundary conditions in dimensionless form, Equations (2-6), (2-7), (2-8), (2-9), (2-15), and (2-16), constitute the mathematical description of the physical problem of this study. These equations were solved numerically as described in the next chapter.

CHAPTER III

TECHNIQUE FOR NUMERICAL SOLUTION

Many differential equations describing a physical problem are so complicated that their analytical solutions can not be found. Numerical techniques are often used to overcome this difficulty. The finite difference approximation method has become a very powerful tool for solving many fluid flow problems, especially with the aid of modern high speed computers. As its name implies, the finite difference approximation method is an approximate technique. However, by using smaller step sizes (at the expense of computation time), the errors involved in solving the complete equations can be minimized.

In order to obtain the numerical solution, the differential equation has to be converted into some special form suitable for numerical operations. The system of interest is divided into finite grid points. The values of a variable are then considered as point functions on these grid points. The derivatives and variables appearing in the differential equation must first be replaced by some approximate finite difference form, with the result that the differential equation is replaced by a finite difference equation. The resulting finite difference equation can then be solved by algebraic and arithmetic procedures.

System of Grid Points

Let the flow field be covered by the cylindrical grid system shown

in Figure 2, where $\Delta\theta$ and Δr are angular and radial increments, respectively. For computational efficiency the radial coordinate will be replaced by

$$r = e^z$$

with a constant step size in z. For convenience θ will be replaced by x. The flow field can then be represented by the rectangular grid system shown in Figure 3, with constant step sizes of Δz and Δx in the z- and x-directions, respectively. I and J are positive integers denoting the location of a grid point. Thus a grid point represented by (I,J) has the space coordinates $x = I\Delta x$ and $z = J\Delta z$.

Approximations of Derivatives by Finite Differences

Depending on the accuracy desired, derivatives may be approximated by several different finite difference forms. The basic principle in establishing a finite difference approximation to the derivative of a dependent variable at a point is the application of a Taylor's series expansion to the value of that variable in the vicinity of that point. Referring to Figure 3, the value of a variable at a grid point (I,J) can be expressed as

$$f_{I,J} = f(I\Delta x, J\Delta z) \tag{3-1}$$

Using Taylor's series expansion and assuming that sufficient numbers of derivatives exist, the values of a variable at two points (x,z) and $(x+\Delta x, z+\Delta z)$ may be related by

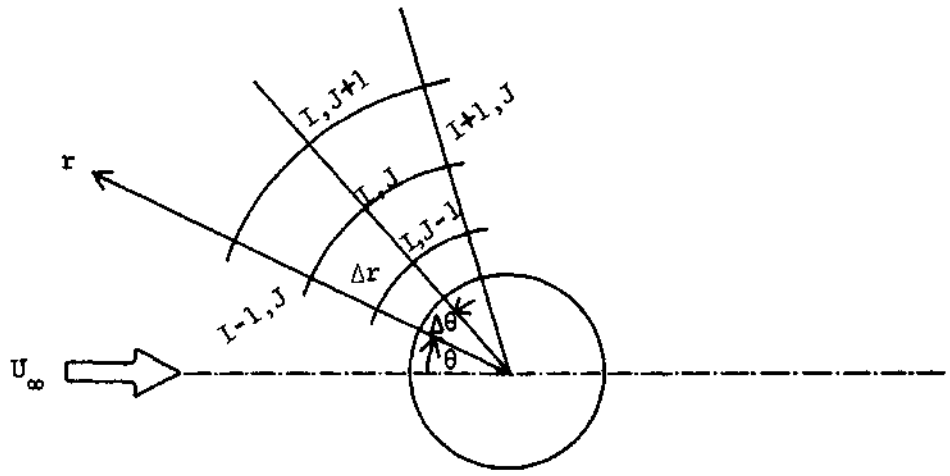

Figure 2. Cylindrical Grid System

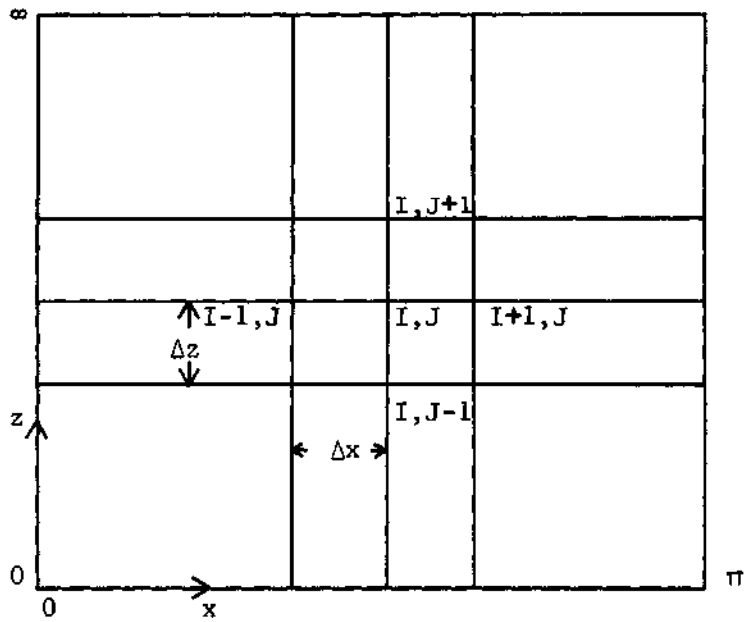

Figure 3. Rectangular Grid System

$$f(x + \Delta x,\ z + \Delta z) = f(x,z) + \left(\Delta x \frac{\partial}{\partial x} + \Delta z \frac{\partial}{\partial z}\right) f(x,z) \qquad (3\text{-}2)$$

$$+ \frac{1}{2!}\left(\Delta x \frac{\partial}{\partial x} + \Delta z \frac{\partial}{\partial z}\right)^2 f(x,z) + \ldots$$

$$+ \frac{1}{(n-1)!}\left(\Delta x \frac{\partial}{\partial x} + \Delta z \frac{\partial}{\partial z}\right)^{n-1} f(x,z) + R_n$$

where the remainder term is given by

$$R_n = \frac{1}{n!}\left(\Delta x \frac{\partial}{\partial x} + \Delta z \frac{\partial}{\partial z}\right)^n f(x + \xi\Delta x,\ z + \xi\Delta z) \qquad (3\text{-}3)$$

with $0 < \xi < 1$.

That is

$$R_n = 0((|\Delta x| + |\Delta z|)^n) \qquad (3\text{-}4)$$

Equation (3-4) means there exists a positive constant M such that $|R_n| \leq M(|\Delta x| + |\Delta z|)^n$ as both Δx and Δz tend to zero.

Based on Taylor's series expansion and the convention of Equation (3-1), expansions for $f_{I+1,J}$ and $f_{I-1,J}$ about its value at the central point result in

$$f_{I+1,J} = f_{I,J} + \Delta x \frac{\partial f}{\partial x} + \frac{\Delta x^2}{2!}\frac{\partial^2 f}{\partial x^2} + \frac{\Delta x^3}{3!}\frac{\partial^3 f}{\partial x^3} + \frac{\Delta x^4}{4!}\frac{\partial^4 f}{\partial x^4} + \ldots \qquad (3\text{-}5)$$

$$f_{I-1,J} = f_{I,J} - \Delta x \frac{\partial f}{\partial x} + \frac{\Delta x^2}{2!}\frac{\partial^2 f}{\partial x^2} - \frac{\Delta x^3}{3!}\frac{\partial^3 f}{\partial x^3} + \frac{\Delta x^4}{4!}\frac{\partial^4 f}{\partial x^4} + \ldots \qquad (3\text{-}6)$$

where all derivatives are evaluated at the point (I,J). As long as Δx is

sufficiently small, terms of the order of Δx^2 and higher may be neglected. Then from Equation (3-5), a first approximation to $\partial f/\partial x$ is

$$\frac{\partial f}{\partial x} = \frac{f_{I+1,J} - f_{I,J}}{\Delta x} + 0(\Delta x) \tag{3-7}$$

and from Equation (3-6), another expression is obtained

$$\frac{\partial f}{\partial x} = \frac{f_{I,J} - f_{I-1,J}}{\Delta x} + 0(\Delta x) \tag{3-8}$$

If Equation (3-6) is subtracted from Equation (3-5) and terms of the order of Δx^3 and higher are neglected, then

$$\frac{\partial f}{\partial x} = \frac{f_{I+1,J} - f_{I-1,J}}{2\Delta x} + 0(\Delta x^2) \tag{3-9}$$

where $0(\Delta x^n)$ is the truncation error, which is the difference between the derivative and the finite difference approximation used to represent it. When a certain expression has a truncation error of the order of Δx^n, it means the error involved is no greater than some positive constant multiplied by Δx^n. Equations (3-7), (3-8), and (3-9) are called the forward, backward, and central difference approximations, respectively.

Adding Equations (3-5) and (3-6) and neglecting terms of the order of Δx^3 and higher, a first approximation to $\partial^2 f/\partial x^2$, correct to the second order, is

$$\frac{\partial^2 f}{\partial x^2} = \frac{f_{I+1,J} - 2f_{I,J} + f_{I-1,J}}{\Delta x^2} + 0(\Delta x^2) \tag{3-10}$$

There are many ways of approximating the same derivative. The particular choice of method depends on the accuracy desired and determines the computational procedures to be used.

The finite difference approximation having higher than second order truncation errors can be obtained by considering additional points such as (I-2,J) and (I+2,J). Also it is necessary to find an approximation of $\partial f/\partial x$ to be used on or adjacent to the boundary points. Therefore several different expressions of $\partial f/\partial x$ which were used are

$$\frac{\partial f}{\partial x} = \frac{-2f_{I-1,J} - 3f_{I,J} + 6f_{I+1,J} - f_{I+2,J}}{6\Delta x} + O(\Delta x^3) \qquad (3\text{-}11)$$

$$\frac{\partial f}{\partial x} = \frac{f_{I-2,J} - 8f_{I-1,J} + 8f_{I+1,J} - f_{I+2,J}}{12\Delta x} + O(\Delta x^4) \qquad (3\text{-}12)$$

$$\frac{\partial f}{\partial x} = \frac{-11f_{I,J} + 18f_{I+1,J} - 9f_{I+2,J} + 2f_{I+3,J}}{6\Delta x} + O(\Delta x^3) \qquad (3\text{-}13)$$

$$\frac{\partial f}{\partial x} = \frac{-3f_{I,J} + 4f_{I+1,J} - f_{I+2,J}}{2\Delta x} + O(\Delta x^2) \qquad (3\text{-}14)$$

Many more finite difference representations for the derivatives are given by Lapidus (44).

Dimensionless Forms of Equations of Motion in Terms of the Stream Function and Vorticity

Equations (2-6), (2-7), and (2-8) can be combined into a single partial differential equation by introducing a new variable, the stream function. The stream function ψ is defined as

$$V_r = -\frac{1}{r}\frac{\partial \psi}{\partial \theta} \qquad (3\text{-}15)$$

$$V_\theta = \frac{\partial \psi}{\partial r}$$

such that the equation of continuity (2-6) is automatically satisfied. If the equations of motion in the r- and θ-directions are differentiated with respect to θ and r respectively, the two resulting equations can be combined to eliminate the terms containing the pressure components. After doing some mathematical manipulation and using the equation of continuity to simplify the equation, there results the fourth-order differential equation for the stream function

$$\nabla^4 \psi + \frac{R}{2r}\left(\frac{\partial \psi}{\partial \theta}\frac{\partial}{\partial r} - \frac{\partial \psi}{\partial r}\frac{\partial}{\partial \theta}\right)\nabla^2 \psi = 0 \qquad (3\text{-}16)$$

where the Laplacian operator ∇^2 is defined by

$$\nabla^2 = \frac{\partial^2}{\partial r^2} + \frac{1}{r}\frac{\partial}{\partial r} + \frac{1}{r^2}\frac{\partial^2}{\partial \theta^2}$$

A dimensionless vorticity ζ is defined by

$$\zeta = \nabla^2 \psi \qquad (3\text{-}17)$$

which enables Equation (3-16) to be rewritten as

$$\nabla^2 \zeta + \frac{R}{2r}\left(\frac{\partial \psi}{\partial \theta}\frac{\partial}{\partial r} - \frac{\partial \psi}{\partial r}\frac{\partial}{\partial \theta}\right)\zeta = 0 \qquad (3\text{-}18)$$

Since the stream function and vorticity vary most rapidly near the cylinder surface, a smaller step size is required in this region. The

step size used in the radial direction is increased as r increases, according to the relation

$$r = e^{z} \tag{3-19}$$

Thus, far from cylinder surface, a larger step size is used. This device will considerably reduce the computation time.

With the substitutions of Equation (3-19) and $\theta \approx x$ back into the equations of motion, the dimensionless forms of the flow equations may be expressed in terms of the new set of dependent variables ψ, ζ, z, and x as follows:

Stream Function Equation

$$\frac{\partial^2 \zeta}{\partial x^2} + \frac{\partial^2 \zeta}{\partial z^2} + \frac{R}{2}\left(\frac{\partial \psi}{\partial x}\frac{\partial \zeta}{\partial z} - \frac{\partial \psi}{\partial z}\frac{\partial \zeta}{\partial x}\right) = 0 \tag{3-20}$$

Vorticity Equation

$$\frac{\partial^2 \psi}{\partial x^2} + \frac{\partial^2 \psi}{\partial z^2} = e^{2z}\,\zeta \tag{3-21}$$

Velocity Equation

$$V_x = \frac{1}{e^z}\frac{\partial \psi}{\partial z} \tag{3-22}$$

$$V_z = -\frac{1}{e^z}\frac{\partial \psi}{\partial x}$$

Boundary Conditions

$$\text{at } x = 0,\ \psi = 0,\ \zeta = 0 \tag{3-23}$$

$$\text{at } x = \pi,\ \psi = -V_0\pi,\ \zeta = 0$$

$$\text{at } z = 0,\ \psi = -V_0 x,\ \zeta = \frac{\partial^2 \psi}{\partial x^2} + \frac{\partial^2 \psi}{\partial z^2}$$

$$\text{at } z = \infty,\ \psi = e^z \sin x - V_0 x,\ \zeta = 0$$

Dimensionless Governing Diffusion Equation in Terms of New Variables

The diffusion equation together with its boundary conditions can be rewritten as follows:

$$V_z\, e^z \frac{\partial C}{\partial z} + V_x\, e^z \frac{\partial C}{\partial x} = \frac{2}{Pe} \frac{\partial^2 C}{\partial z^2} \tag{3-24}$$

$$\text{at } x = 0,\ \frac{\partial C}{\partial x} = 0 \tag{3-25}$$

$$\text{at } z = \infty,\ C = 1$$

$$\text{at } z = 0,\ \frac{1}{C} \frac{\partial C}{\partial z} = \frac{aV_0}{\mathcal{D}}$$

The last boundary condition can not be applied directly. Assuming a starting concentration at the surface, the concentration at every grid point will be calculated and then used to recalculate a better value of surface concentration according to the satisfaction of the boundary condition.

Outline of Numerical Solution

By using the derivatives given in the previous section, the finite

difference forms of the governing equations are first derived. The procedure of the numerical technique is given in the following section.

Finite Difference Forms of the Stream Function and Vorticity Equations

Using the approximation of derivatives accurate to the second order, the stream function and vorticity equations can be approximated by

$$\psi_{I,J} = \frac{1}{2\left(1 + \frac{\Delta x^2}{\Delta z^2}\right)} \left[\psi_{I+1,J} + \psi_{I-1,J} + \left(\psi_{I,J+1} + \psi_{I,J-1}\right)\frac{\Delta x^2}{\Delta z^2} - \Delta x^2 e^{2z} \zeta_{I,J}\right] \quad (3\text{-}26)$$

and

$$\zeta_{I,J} = \frac{1}{2\left(1 + \frac{\Delta x^2}{\Delta z^2}\right)} \left\{\zeta_{I+1,J} + \zeta_{I-1,J} + \left(\zeta_{I,J+1} + \zeta_{I,J-1}\right)\frac{\Delta x^2}{\Delta z^2} + \frac{R}{8}\frac{\Delta x}{\Delta z}\left[\left(\psi_{I+1,J} - \psi_{I-1,J}\right)\left(\zeta_{I,J+1} - \zeta_{I,J-1}\right) - \left(\psi_{I,J+1} - \psi_{I,J-1}\right)\left(\zeta_{I+1,J} - \zeta_{I-1,J}\right)\right]\right\} \quad (3\text{-}27)$$

or

$$\psi'_{I,J} = \psi_{I,J} + \frac{\alpha}{2\left(1 + \frac{\Delta x^2}{\Delta z^2}\right)} \left[\psi_{I+1,J} + \psi_{I-1,J} + \left(\psi_{I,J+1} + \psi_{I,J-1}\right)\frac{\Delta x^2}{\Delta z^2} - 2\left(1 + \frac{\Delta x^2}{\Delta z^2}\right)\psi_{I,J} - \Delta x^2 e^{2z} \zeta_{I,J}\right] \quad (3\text{-}28)$$

and

$$\zeta'_{I,J} = \zeta_{I,J} + \frac{\beta}{2\left(1 + \frac{\Delta x^2}{\Delta z^2}\right)} \left\{\zeta_{I+1,J} + \zeta_{I-1,J} \right. \tag{3-29}$$

$$+ \left(\zeta_{I,J+1} + \zeta_{I,J-1}\right)\frac{\Delta x^2}{\Delta z^2}$$

$$+ \frac{R}{8}\frac{\Delta x}{\Delta z}\left[\left(\psi_{I+1,J} - \psi_{I-1,J}\right)\left(\zeta_{I,J+1} - \zeta_{I,J-1}\right)\right.$$

$$\left. - \left(\psi_{I,J+1} - \psi_{I,J-1}\right)\left(\zeta_{I+1,J} - \zeta_{I-1,J}\right)\right]$$

$$\left. - 2\left(1 + \frac{\Delta x^2}{\Delta z^2}\right)\zeta_{I,J}\right\}$$

where α and β are called relaxation factors, the values of which are found by trial and error so as to achieve faster convergences for the solutions of the stream function and vorticity. A successive over-relaxation method (44,45) will be used to calculate the values of ψ and ζ. As soon as a new value ($\psi'_{I,J}$, $\zeta'_{I,J}$) is calculated, the old value will be replaced. Therefore the most recent estimates of ψ and ζ are always used in the iteration procedure.

The vorticity distribution on the cylinder surface must be known in order to proceed with the calculation. This can be obtained from the values of ψ near the cylinder surface. If ψ can be expressed as a polynomial function of z, as was done by Jenson (46) in the study of viscous flow round a sphere

$$\psi = a + bz + cz^2 + dz^3 \tag{3-30}$$

and since $V_x = 0$ and $\psi = - V_0 x$ on the cylinder surface, Equation (3-30) reduces to

$$\psi = - V_0 x + cz^2 + dz^3 \tag{3-31}$$

hence

$$\frac{d^2\psi}{dz^2} = 2c + 6z \tag{3-32}$$

Therefore the vorticity distribution on the surface is

$$\zeta_{I,0} = \left(\frac{d^2\psi}{dz^2}\right)_{z=0} \tag{3-33}$$

or

$$\zeta_{I,0} = \frac{8\psi_{I,1} - \psi_{I,2} - 7\psi_{I,0}}{2\Delta z^2} \tag{3-34}$$

Finite Difference Form of Governing Diffusion Equation

The Crank-Nicholson implicit finite difference technique (47) is used to approximate the diffusion equation. The derivative in the angular direction is approximated by the Crank-Nicholson half-way point method. The radial derivatives are given by the average values over two succeeding angular increments. The following finite difference forms are used for the differential terms

$$\frac{\partial C}{\partial x} = \frac{C_{I+1,J} - C_{I,J}}{\Delta x} + 0(\Delta x^2) \tag{3-35}$$

$$\frac{\partial C}{\partial z} = \frac{1}{2}\left(\frac{C_{I+1,J+1} - C_{I+1,J-1}}{2\Delta z} + \frac{C_{I,J+1} - C_{I,J-1}}{2\Delta z}\right) + 0(\Delta z^2)$$

$$\frac{\partial^2 C}{\partial z^2} = \frac{1}{2}\left(\frac{C_{I+1,J+1} - 2C_{I+1,J} + C_{I+1,J-1}}{\Delta z^2} + \frac{C_{I,J+1} - 2C_{I,J} + C_{I,J-1}}{\Delta z^2}\right) + O(\Delta z^2)$$

From Equation (3-24) the following finite difference approximation is obtained

$$(L1 + L3)C_{I+1,J-1} - (2L1 + L4)C_{I+1,J} + (L1 - L3)C_{I+1,J+1} = \qquad (3\text{-}36)$$

$$- (L1 + L3)C_{I,J-1} + (2L1 - L4)C_{I,J} - (L1 - L3)C_{I,J+1}$$

where

$$L1 = 1/(Pe\Delta z^2) \qquad (3\text{-}37)$$

$$L3 = e^z(V_{z_{I+1,J}} + V_{z_{I,J}})/(8\Delta z)$$

$$L4 = e^z(V_{x_{I+1,J}} + V_{x_{I,J}})/(2\Delta x)$$

At the front stagnation line, the following finite difference approximation is used:

$$\left(\frac{1}{\Delta z^2 Pe} + \frac{e^z}{4\Delta z} V_{z_{0,J}}\right)C_{0,J-1} - \frac{2}{\Delta z^2 Pe} C_{0,J} \qquad (3\text{-}38)$$

$$+ \left(\frac{1}{\Delta z^2 Pe} - \frac{e^z}{4\Delta z} V_{z_{0,J}}\right)C_{0,J+1} = 0$$

The concentration profiles will be calculated down the stream. At each angular increment, Equation (3-36) is written once for each point from

J equal to 1 to J equal to N-1. This results in N-1 simultaneous equations with N-1 unknowns for which the matrix of coefficients is tridiagonal in form. The method of Thomas (48) is particularly useful in solving these special simultaneous equations. It holds the advantages over the Gaussian Elimination Method in that it avoids the error growth associated with the back solution of the elimination method and in that it minimizes the storage problem in machine computation. The algorithm of the method of Thomas is given in Appendix A.

The concentration on the cylinder surface, C^*, is guessed first to start the calculation of the concentration profile. A new value of C^* is then calculated from Equation (3-25c). A test is made to see if the difference between the guessed value and the new value is less than 1.0×10^{-6}. If not, the method is repeated using the new value of C^* as the next guess.

Procedure of Numerical Calculations

The sequence of operations which must be performed in order to compute the desired quantity can be summarized by the following steps

(1) The values of ζ are set equal to zero. The initial values of ψ at every interior point are assumed equal to the ideal flow solution given by $\psi = r \sin x$.

(2) Iterative calculation of ψ using Equation (3-28) along with the appropriate boundary conditions is continued until the difference in the values of ψ between successive calculations is less than 1.0×10^{-6}.

(3) The values of ζ on the surface are then calculated from Equation (3-34).

(4) New values of ψ are calculated using Equation (3-28) with its boundary conditions.

(5) Step (3) is repeated.

(6) New values of ζ are calculated using Equation (3-29) with its boundary conditions.

(7) Repeat steps (4) through (6) until changes in the values of ψ and ζ from previous calculations are each less than 1.0×10^{-6}. Note that the most recently calculated values of ψ and ζ are always used in steps (4) and (6).

(8) V_x and V_z are calculated from Equation (3-15) by using a higher order approximation to the derivative.

(9) Drag coefficient and surface pressure distribution are then calculated from the convergent values of the stream function and vorticity.

(10) The concentration distribution and mass-transfer coefficient are obtained using Equation (3-36).

Other Flow Characteristics

Pressure Distribution on the Surface of the Cylinder

The pressure distribution along the cylinder can be obtained from the equations of motion. Since V_θ and $\partial V_r/\partial\theta$ are both equal to zero at the front stagnation line, the equation of motion in the r-direction can be reduced to

$$V_r \frac{\partial V_r}{\partial r} + \frac{\partial P}{\partial r} = \frac{2}{R}\left(\frac{\partial^2 V_r}{\partial r^2} + \frac{1}{r}\frac{\partial V_r}{\partial r} - \frac{V_r}{r^2} + \frac{1}{r^2}\frac{\partial^2 V_r}{\partial \theta^2} - \frac{2}{r^2}\frac{\partial V_\theta}{\partial \theta}\right) \qquad (3\text{-}39)$$

Hence

$$V_r \frac{\partial V_r}{\partial r} + \frac{\partial P}{\partial r} = - \frac{2}{Rr} \left(\frac{\partial \zeta}{\partial \theta}\right)_{\theta=0}$$

Integrating with respect to r

$$P_0 - P_\infty = \frac{1}{2}\left(1 - V_0^2\right) + \frac{2}{R}\int_0^\infty \left(\frac{\partial \zeta}{\partial \theta}\right)_{\theta=0} dz \qquad (3\text{-}40)$$

In Equation (3-40) the quantity P_∞ is the pressure in the plane $\theta = 0$ far from the cylinder, and P_0 is the pressure at the front stagnation point.

On the surface of the cylinder since V_θ and all derivatives with respect to θ are zero, the equation of motion in the θ-direction can be reduced to

$$V_r \frac{\partial V_\theta}{\partial r} + \frac{1}{r}\frac{\partial P}{\partial \theta} = \frac{2}{R}\left(\frac{\partial^2 V_\theta}{\partial r^2} + \frac{1}{r}\frac{\partial V_\theta}{\partial r}\right) \qquad (3\text{-}41)$$

On the surface

$$\left(\frac{\partial V_\theta}{\partial r}\right)_{r=1} = \zeta_{z=0} \qquad (3\text{-}42)$$

hence

$$\left(\frac{\partial P}{\partial \theta}\right)_{z=0} = \frac{2}{R}\left(\frac{\partial \zeta}{\partial z}\right)_{z=0} - V_0\ \zeta_{z=0} \qquad (3\text{-}43)$$

Integrating with respect to θ

$$P - P_0 = \frac{2}{R}\int_0^\theta \left(\frac{\partial \zeta}{\partial z}\right)_{z=0} d\theta - V_0 \int_0^\theta \zeta_{z=0} d\theta \qquad (3\text{-}44)$$

where P is the pressure at any point on the surface. From Equations (3-40) and (3-44) the pressure distribution on the surface of the cylinder is obtained and is given in the form of the pressure coefficient defined as

$$C_P = \frac{P - P_\infty}{\frac{1}{2}\rho U_\infty^2} \tag{3-45}$$

Drag Coefficient

The drag on the cylinder is usually expressed in terms of a dimensionless drag coefficient

$$\text{drag coefficient} = \frac{\text{drag force in the flow direction}}{\text{projected area normal to the direction of flow} \times \text{kinetic energy}}$$

The drag coefficient due to the pressure C_{DP} is given by

$$C_{DP} = 2 \int_0^\pi P \cos\theta \, d\theta \tag{3-46}$$

The frictional drag coefficient C_{DF} is given by

$$C_{DF} = \frac{4}{R} \int_0^\pi \zeta_{z=0} \sin\theta \, d\theta \tag{3-47}$$

Mass-Transfer Coefficient

A local mass-transfer coefficient $k_{x,loc}$ may be defined as

$$k_{x,loc} \frac{C_0 - C_\infty}{C} = - \mathcal{D} \frac{C_\infty}{a} \left(\frac{\partial C}{\partial r}\right)_{r=1} \tag{3-48}$$

The corresponding local Nusselt number for mass transfer is

$$Nu_{loc} = \frac{2ak_{x,loc}}{C\mathcal{D}} = -2\left(\frac{1}{C-1}\frac{\partial C}{\partial r}\right)_{r=1} \qquad (3\text{-}49)$$

and the overall Nusselt number for mass transfer is

$$Nu_{overall} = \int_0^A Nu_{loc}\, dA = -\frac{2}{\pi}\int_0^{\pi}\left(\frac{1}{C-1}\frac{\partial C}{\partial r}\right)_{r=1} d\theta \qquad (3\text{-}50)$$

CHAPTER IV

RESULTS AND DISCUSSION

Introduction

Numerical solutions of the equations describing the mathematical model were obtained with the aid of an Univac-1108 electronic digital computer. The complete computer program for the numerical calculations of this study, together with its subroutines, is given in Appendix B. The program is written in the Fortran V language.

Calculations were made for a Schmidt number of 560 and Reynolds numbers from 0.5 to 10. Although this study could have been extended to higher Reynolds numbers without any modification, the computation time became impractical at higher Reynolds numbers. For example, initial calculations at a Reynolds number of 40 were made to test the computer program, and the computation time was found to be excessive (18 minutes). Since no study was made for Reynolds numbers between 10 and 40, the results for a Reynolds number of 40 are not included.

For each run, the convergent values of the stream function and vorticity were first calculated and these values were then used to compute other flow characteristics. Since both the stream function and vorticity equations were of elliptic form, a successive over-relaxation technique was used. Relaxation factors, which were found by trial and error, were introduced in order to achieve faster rates of convergence. The term "convergence" is used to connote that when the difference in the values

of a physical quantity between two successive calculations is less than the error specified, the quantity has converged.

Various angular and radial step sizes were used to test the convergence of the computations and the accuracy of the solutions. The majority of computations were performed using a 31 by 46 or a 31 by 61 grid with the totals of 1426 and 1891 grid points respectively. The step size used in the radial direction and the number of grid points (and therefore the outer boundary position) varied with the Reynolds number and the radial suction flux. Computation time was found to increase remarkably as the outer boundary was moved away from the cylinder, and this increase was further magnified as the Reynolds number was increased. For a typical run with a 31 by 61 grid at a Reynolds number of 1, the execution time was about 140 seconds. The execution time was nearly doubled for the same run but with a 61 by 61 grid. At higher Reynolds numbers, the execution time was much longer, for the solution converged more slowly.

The results of this study are presented in two sections: zero radial suction mass flux and constant radial suction mass flux. The former is a special case of the latter. The study of zero radial suction mass flux was undertaken to ascertain the reliability and the accuracy of the finite-difference technique and the computer program by comparing the results obtained in the present study with the results of other numerical studies and experimental investigations.

Zero Radial Suction Mass Flux

Drag Coefficient

The drag coefficient has been the most popular quantity investigated

in the study of incompressible flow past a circular cylinder submerged in a viscous fluid. The results of the present study are summarized in Table 1. Also shown in Table 1 are step sizes, outer boundary position, and relaxation factors used.

The effect of step size on the accuracy of the solution for a Reynolds number of 1 was investigated in detail and is shown in Table 1. For Reynolds numbers other than 1, various radial step sizes and a constant angular step size were used. The results indicate an angular step size of 6° and a radial step size (Δz) of 0.1047 were fine enough to obtain an accurate solution.

The drag coefficient at any given Reynolds number was obtained by numerical integration of Equations (3-46) and (3-47), using Simpson's rule. For numerical analysis purpose, the field of computation must be restricted within an outer circular boundary. It was found that the outer boundary for undisturbed flow must be at a relatively large radial distance for low Reynolds numbers. This wall effect was very serious for Reynolds numbers less than 5. In the present study, the drag coefficient at infinite boundary position $C_{D(\infty)}$ was obtained from the intercept of a plot of C_D against the reciprocal of the radial position of the outer boundary r_∞. Figure 4 shows such a plot. A nearly straight line was obtained for each Reynolds number studied. It is seen that the slope of each curve approaches zero as the Reynolds number increases. Hamielec and Raal's extrapolation technique which suggests a plot of C_D against the reciprocal of the square of the outer boundary position was found to be not suitable for extrapolation in this study.

Table 1. Computational Parameters Used and Drag Coefficients Calculated

R	Δx	Δz	r_∞	grid	α	β	C_{DF}	C_{DP}	C_D	$C_{D(\infty)}$
1	6°	0.080	36.60	31 x 46	1.835	1.10	5.919	6.060	11.979	
1	6°	0.095	71.88	31 x 46	1.835	1.20	5.515	5.636	11.151	
1	6°	0.1047	111.32	31 x 46	1.825	0.90	5.373	5.485	10.858	10.34
1	3°	0.1047	111.32	61 x 46	1.90	1.20	5.376	5.487	10.863	
1	6°	0.092	249.64	31 x 61	1.835	0.45	5.224	5.327	10.551	
2	6°	0.080	36.60	31 x 46	1.835	1.10	3.602	3.799	7.401	
2	6°	0.095	71.88	31 x 46	1.835	0.75	3.419	3.598	7.017	6.62
2	6°	0.1047	111.32	31 x 46	1.825	0.45	3.355	3.525	6.880	
4	6°	0.080	36.60	31 x 46	1.835	0.65	2.271	2.539	4.810	
4	6°	0.095	71.88	31 x 46	1.835	0.40	2.183	2.429	4.612	4.41
4	6°	0.1047	111.32	31 x 46	1.825	0.25	2.154	2.392	4.546	
7	6°	0.080	36.60	31 x 46	1.835	0.50	1.592	1.918	3.510	
7	6°	0.095	71.88	31 x 46	1.835	0.25	1.541	1.846	3.387	3.28
7	6°	0.1047	111.32	31 x 46	1.825	0.165	1.526	1.822	3.348	
10	6°	0.080	36.60	31 x 46	1.835	0.35	1.275	1.636	2.911	
10	6°	0.095	71.88	31 x 46	1.835	0.19	1.239	1.579	2.818	2.73
10	6°	0.1047	111.32	31 x 46	1.825	0.125	1.229	1.560	2.789	

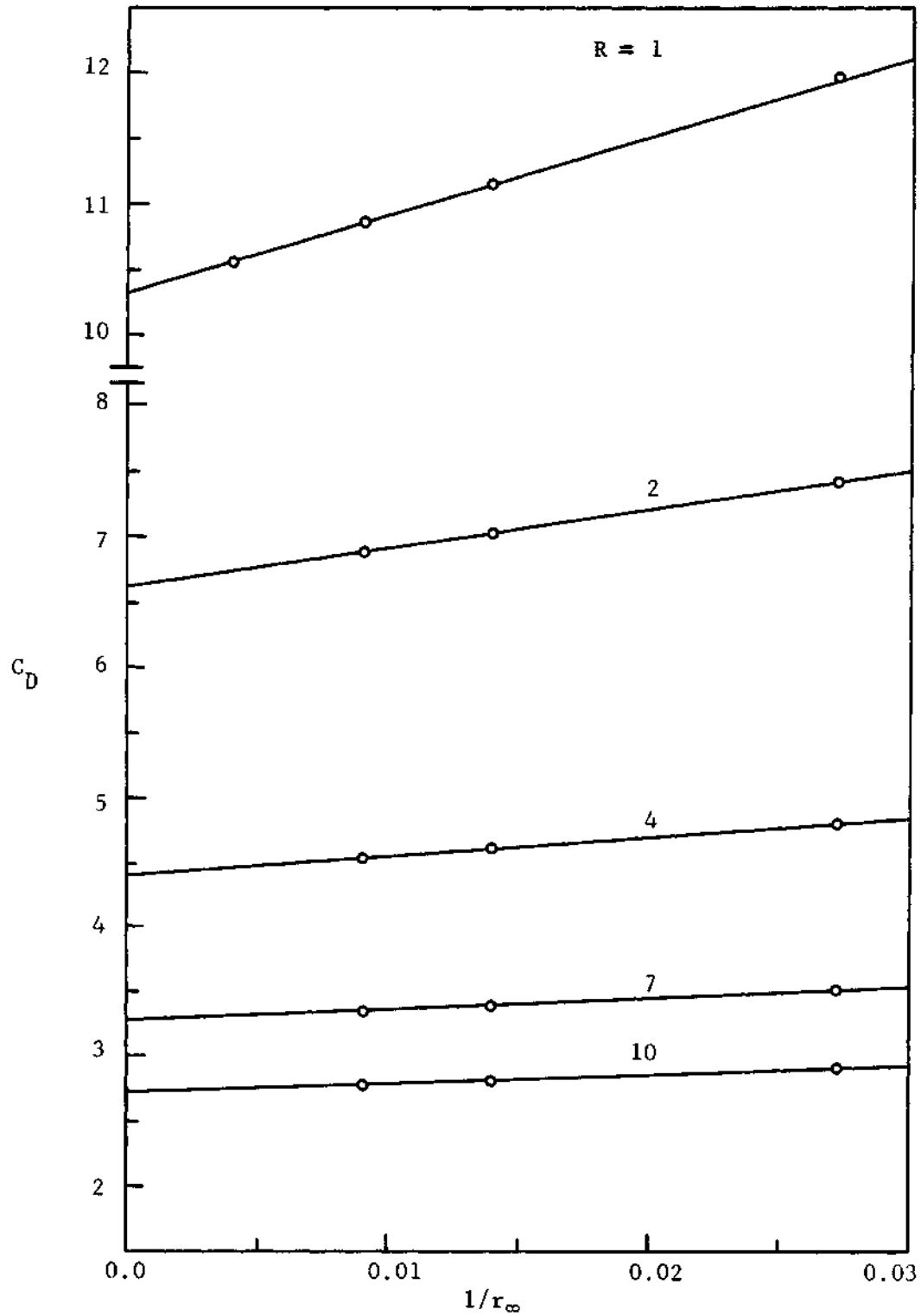

Figure 4. Variation of Drag Coefficient with the Position of Infinite Boundary

Drag coefficients at infinite boundary position $C_{D(\infty)}$ are plotted against Reynolds numbers in Figure 5 and compared with numerical solutions by Keller and Takami, Hamielec and Raal, and Underwood, and also with experimental data by Tritton. The agreement for the Reynolds numbers reported is very good. The larger values of $C_{D(\infty)}$ observed in the experiments by Tritton and the larger values calculated by Underwood are interpreted as due to wall effect. Hamielec and Raal's results showed slight differences from the present study. The differences mainly came from the calculation of C_{DP}, which required double integration of Equation (3-46) by Simpson's rule. The results of the present study and those of other numerical studies are also tabulated in Table 2 for the various Reynolds numbers reported.

Table 2. Drag Coefficients Calculated by Various Workers

R	$C_{D(\infty)}$			
	Underwood	Hamielec & Raal	Keller & Takami	Present Study
0.4	20.11			
1.0		10.97		10.34
1.6	8.67			
2.0		6.83	6.64	6.62
4.0		4.52	4.43	4.41
6.4	3.97			
7.0				3.28
10.0	2.88	2.75	2.74	2.73

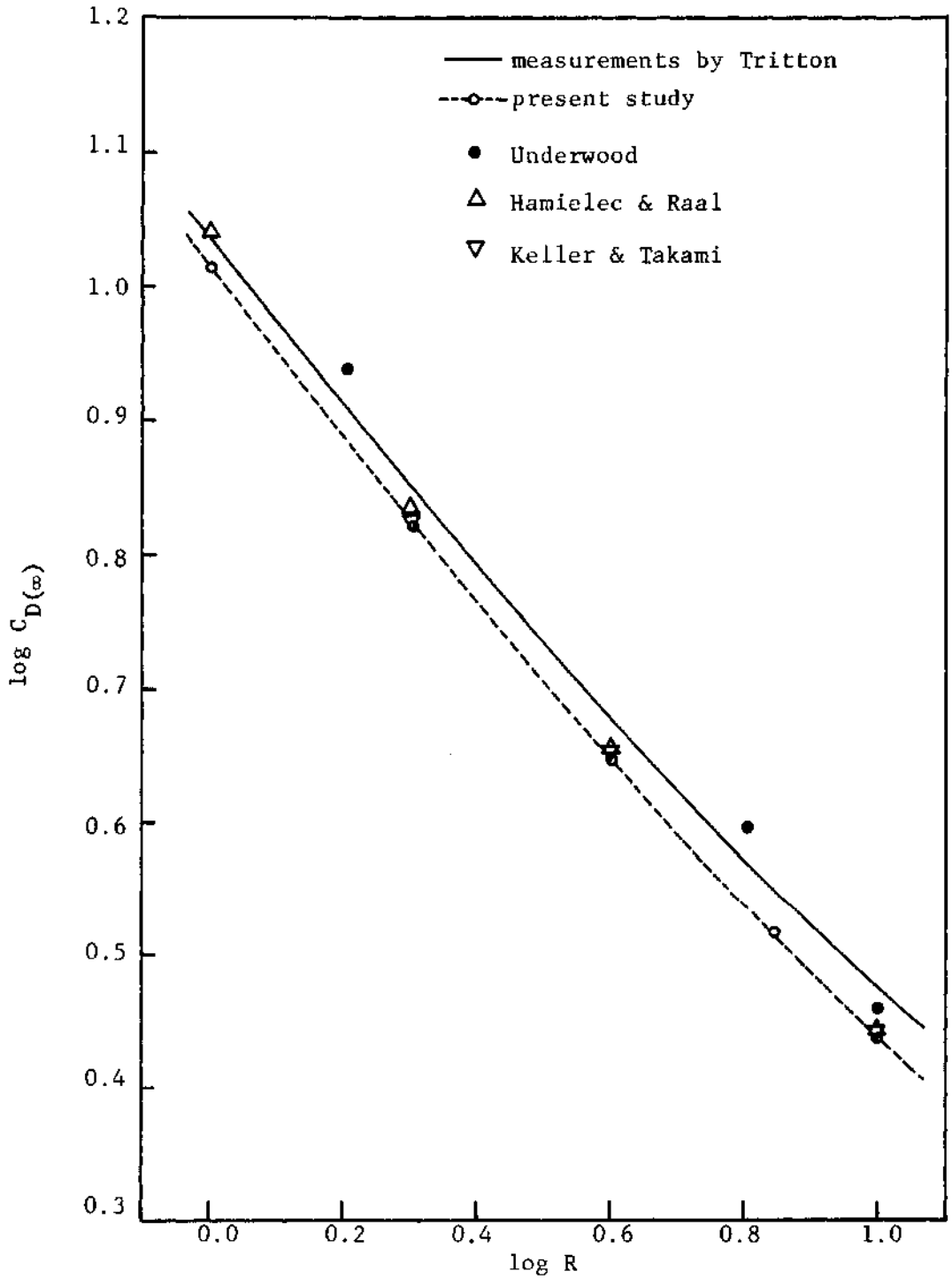

Figure 5. Comparison Between Numerical Calculations and Measurements of the Drag Coefficient

Surface Pressure Distribution

The pressure on the cylindrical surface is given in the form of the pressure coefficient C_p defined by Equation (3-45). Calculated surface pressure distributions are shown in Figure 6 for Reynolds numbers of 1, 2, 4, 7, and 10. Also shown in Figure 6 is the pressure distribution for ideal flow (zero viscosity). It is seen that the minimum pressure occurs at the rear stagnation point at a Reynolds number of 1. Underwood obtained this result at a Reynolds number of 0.4. The position of the minimum pressure moves towards the upstream side of the cylinder with increasing Reynolds numbers. It is also noticed that as the Reynolds number increases, the rear stagnation pressure rises while the front stagnation pressure falls to one, which is the result of the ideal flow solution.

In Figures 7 to 9 the calculated surface pressure distributions are compared with numerical solutions by Keller and Takami and by Underwood for Reynolds numbers of 2, 4, and 10, respectively. The agreement is excellent in the front portion of the cylinder. However, there is a slight difference in the rear of the cylinder.

Surface Vorticity Distribution

The vorticity distributions around the surface of the cylinder are shown in Figure 10 for Reynolds numbers of 1, 2, 4, 7, and 10. It is seen that the surface vorticity increases in the front portion of the cylinder and decreases in the rear portion of the cylinder with increasing Reynolds numbers. As the Reynolds number increases to some extent, the vorticity at a certain position becomes negative. The position at which the

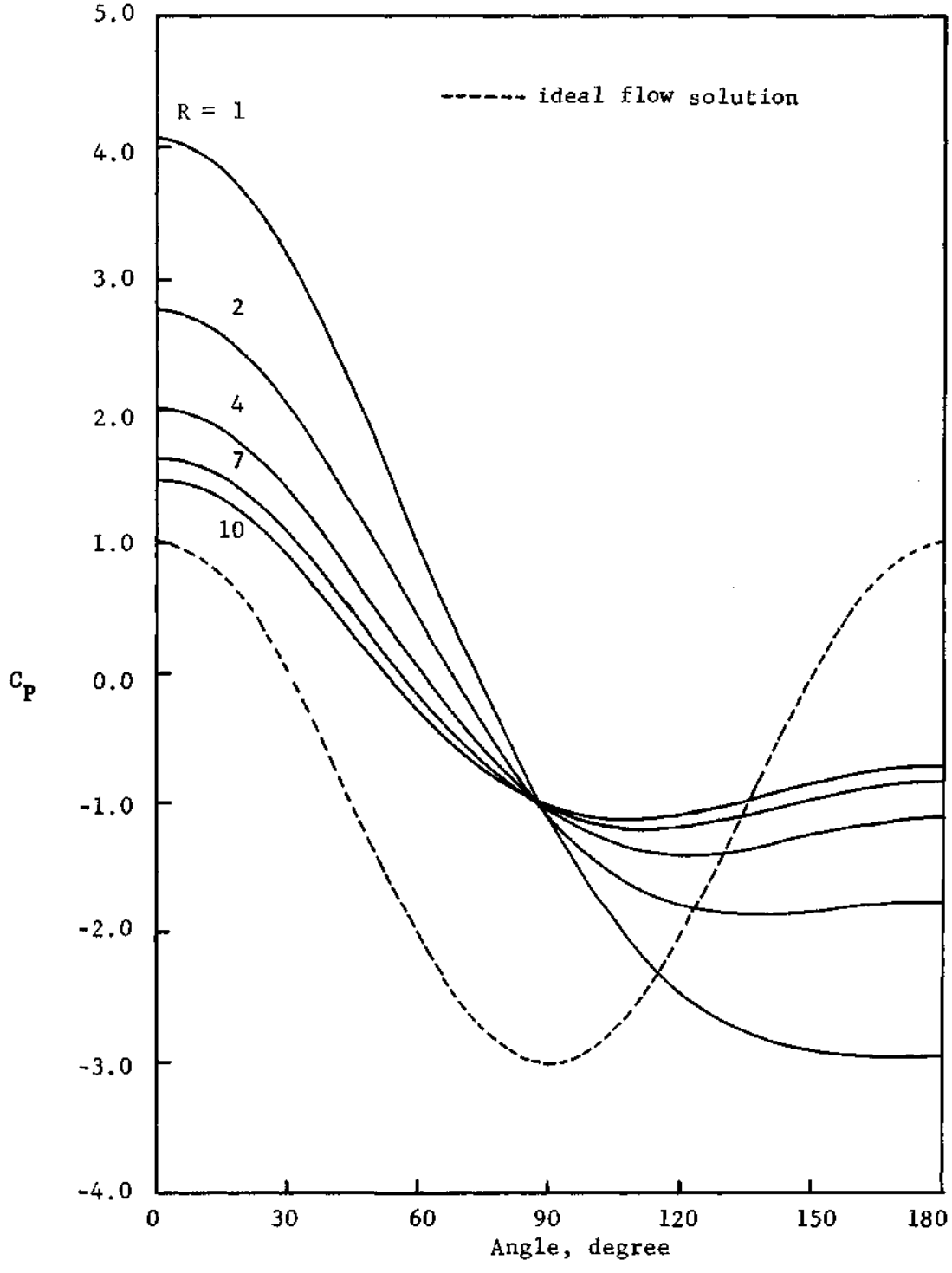

Figure 6. Surface Pressure Distribution Calculated for Various Reynolds Numbers

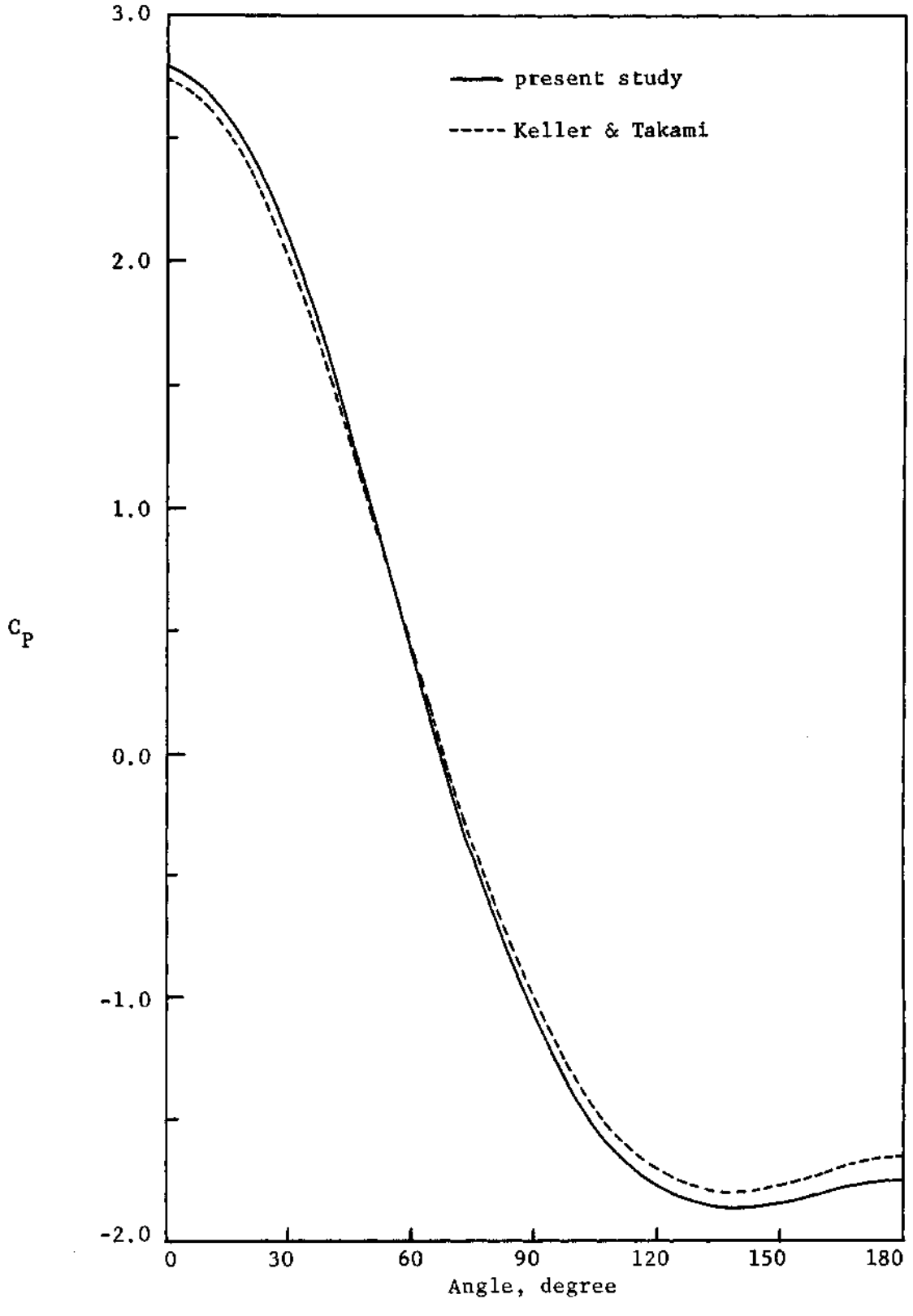

Figure 7. Surface Pressure Distribution for R = 2.0

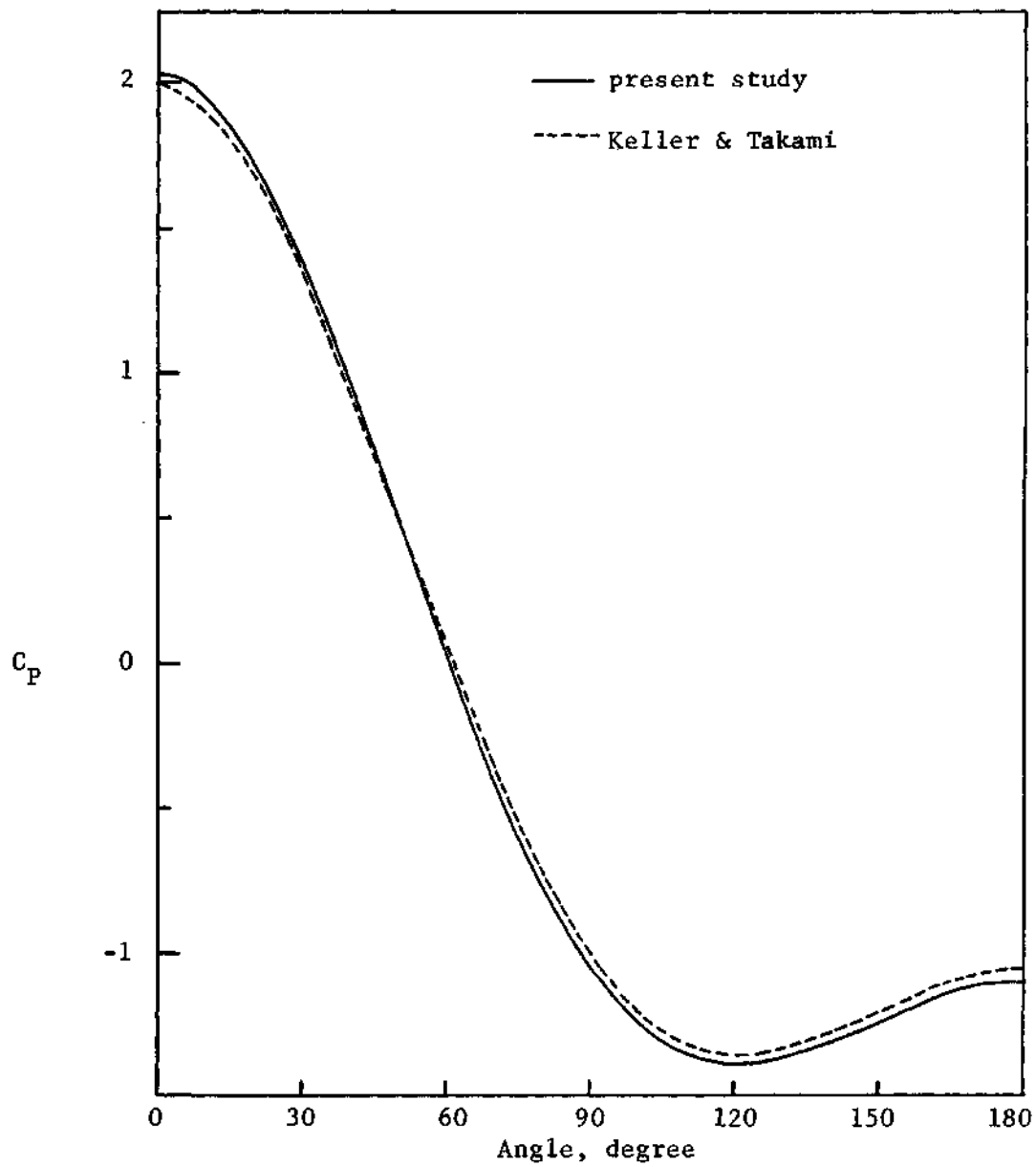

Figure 8. Surface Pressure Distribution for R = 4.0

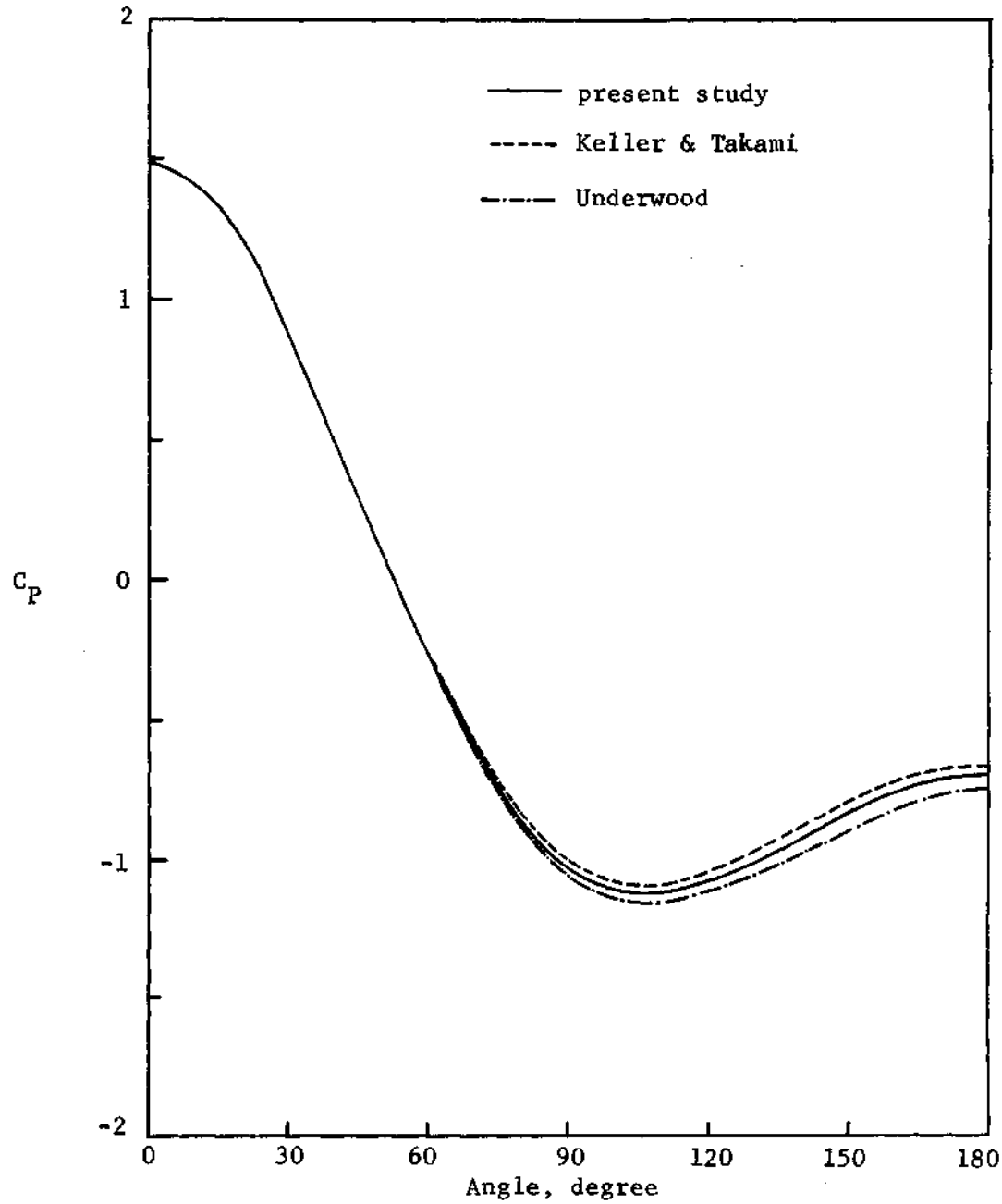

Figure 9. Surface Pressure Distribution for R = 10.0

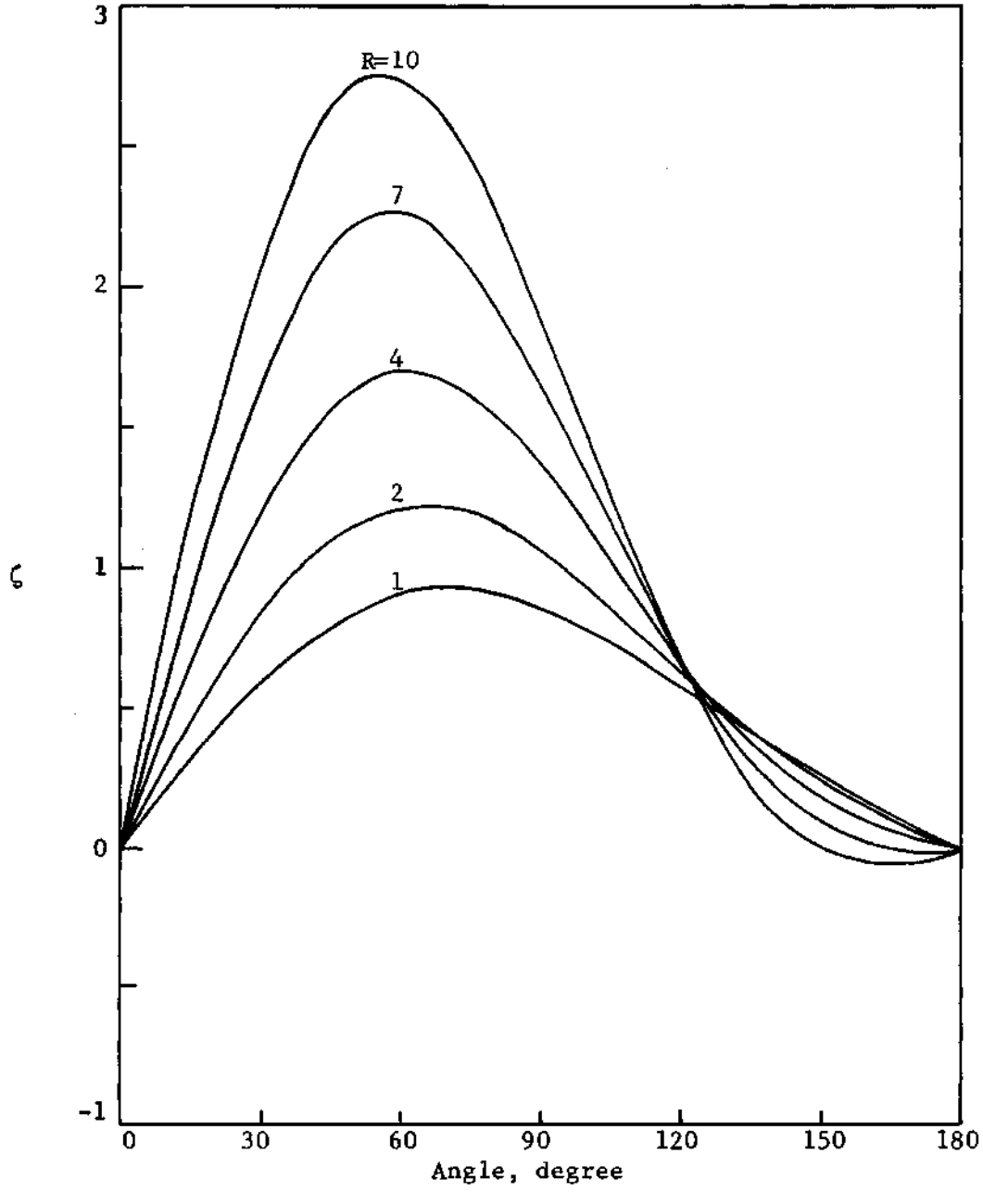

Figure 10. Surface Vorticity Distributions Calculated for Various Reynolds Numbers

vorticity changes sign indicates the flow separation point. It is seen in the present study that a pair of standing eddies form behind the cylinder at Reynolds numbers greater than 7.0.

The calculated surface vorticity distributions are compared with numerical solutions by Keller and Takami for Reynolds numbers of 2, 4, and 10 in Figures 11 to 13, respectively. The agreement is excellent.

Flow Patterns

Streamlines of this study were obtained with the aid of a Contouring Program by California Computer Products (49). Some interesting flow patterns are shown in Figures 14 to 18 for Reynolds numbers of 1, 2, 4, 7, and 10, respectively. These streamlines are important because they represent the fluid flow patterns around the cylinder. At a Reynolds number of 1 (Figure 14), the flow patterns are almost symmetrical fore and aft. As the Reynolds number is increased, asymmetry becomes more pronounced. Figures 17 and 18 show flow separation and the appearance of a pair of standing eddies behind the cylinder.

It is seen that the streamline of $\psi = 2.0$ tends to be less curved with increasing Reynolds number, indicating that the flow becomes undisturbed at a smaller distance from the cylinder as the Reynolds number is increased. This means that the wall effect is less important at higher Reynolds numbers. The same conclusion was reached in the study of the drag coefficient.

At the infinite boundary position the fluid does not feel the existence of the cylinder body. Therefore the streamlines are parallel to the axis of symmetry.

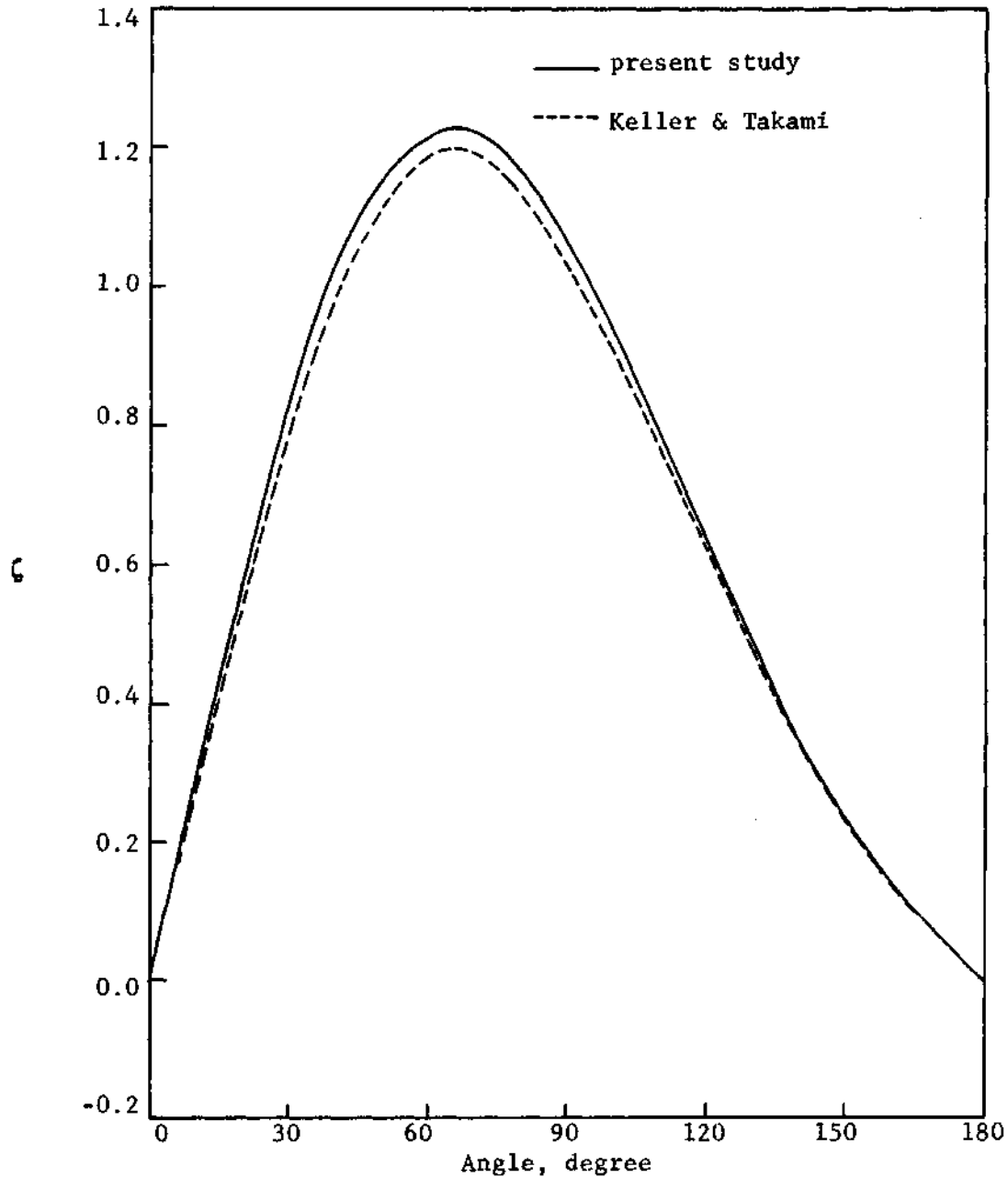

Figure 11. Surface Vorticity Distribution for R = 2.0

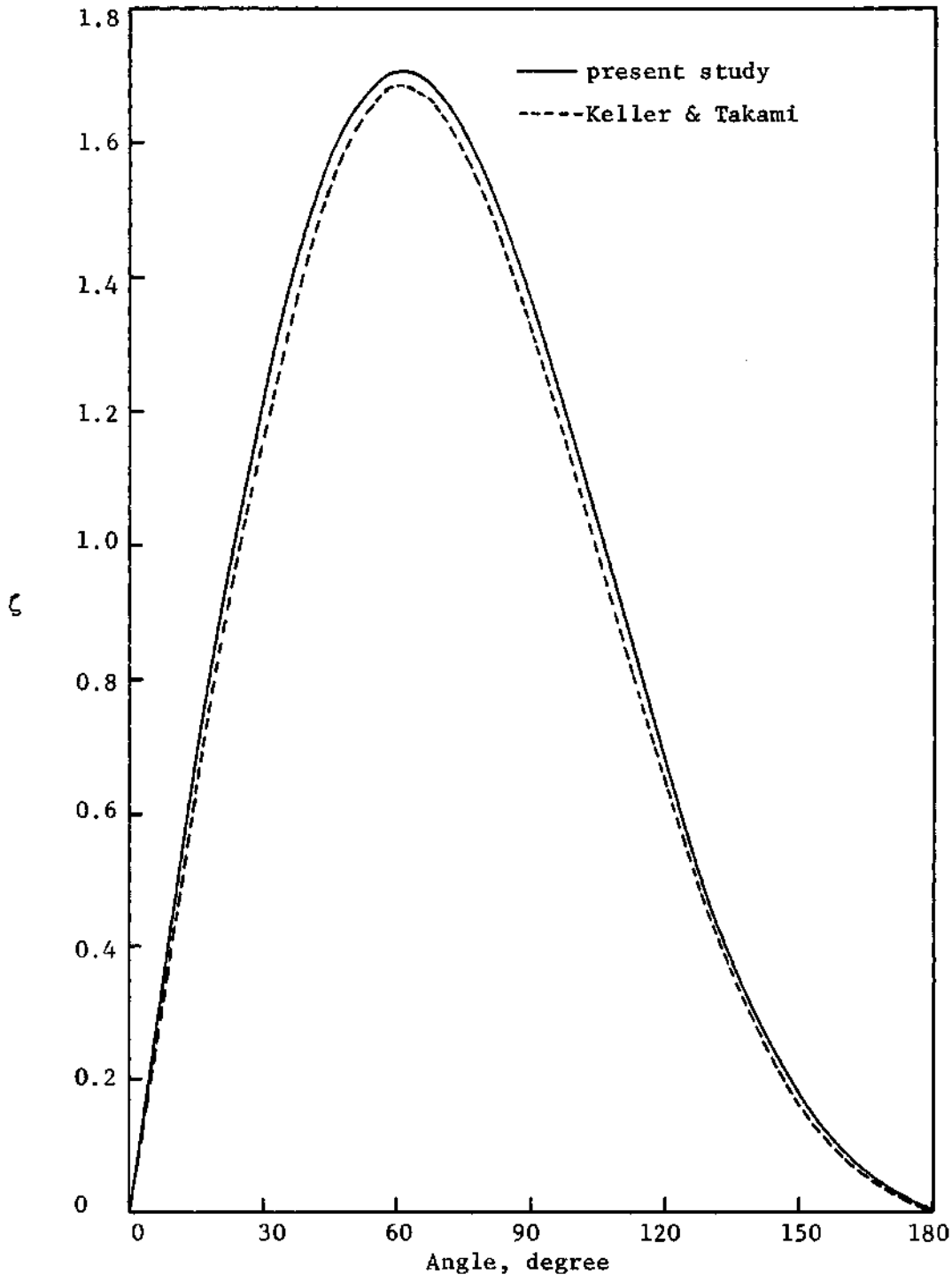

Figure 12. Surface Vorticity Distribution for R = 4

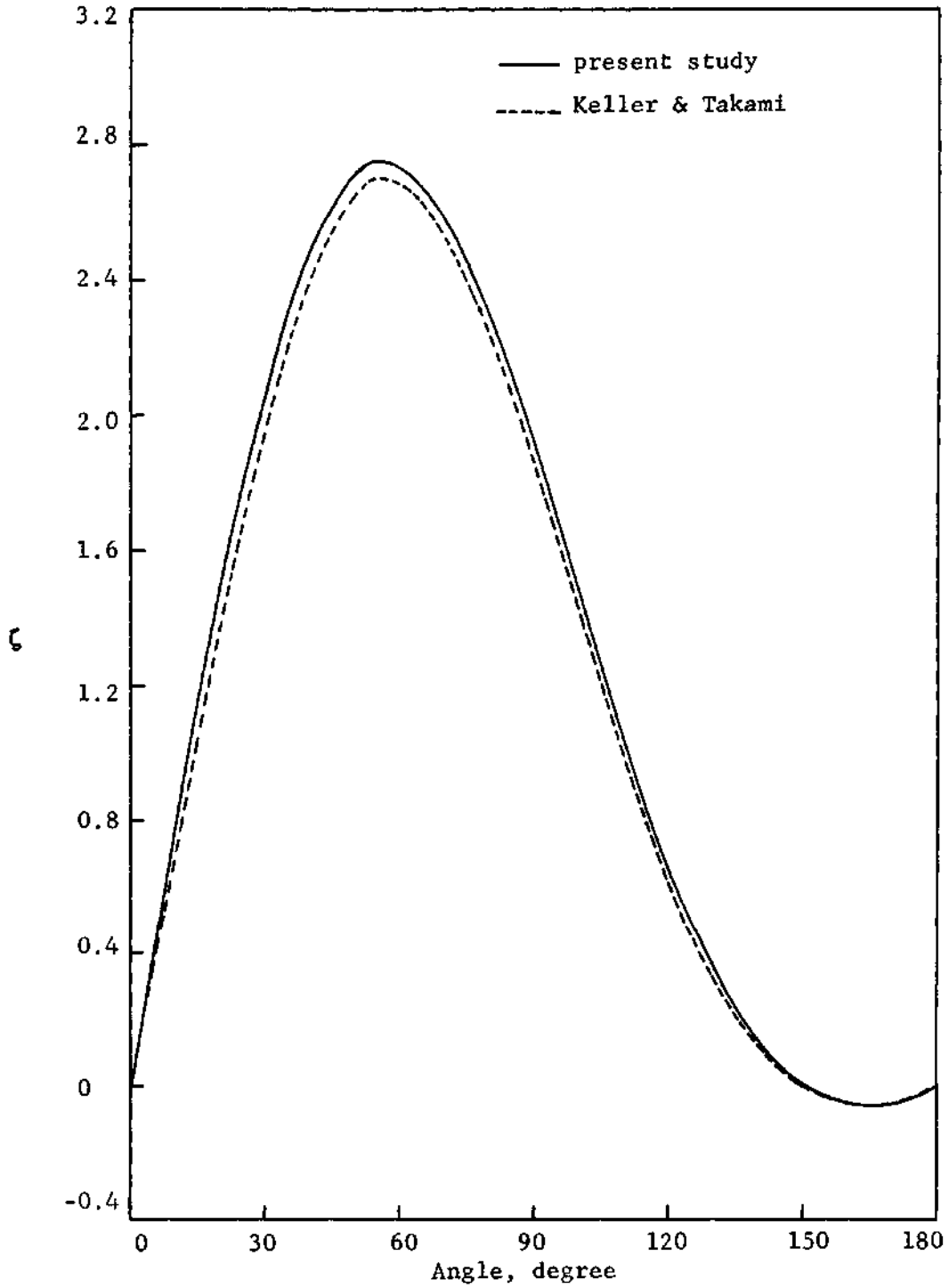

Figure 13. Surface Vorticity Distribution for R = 10

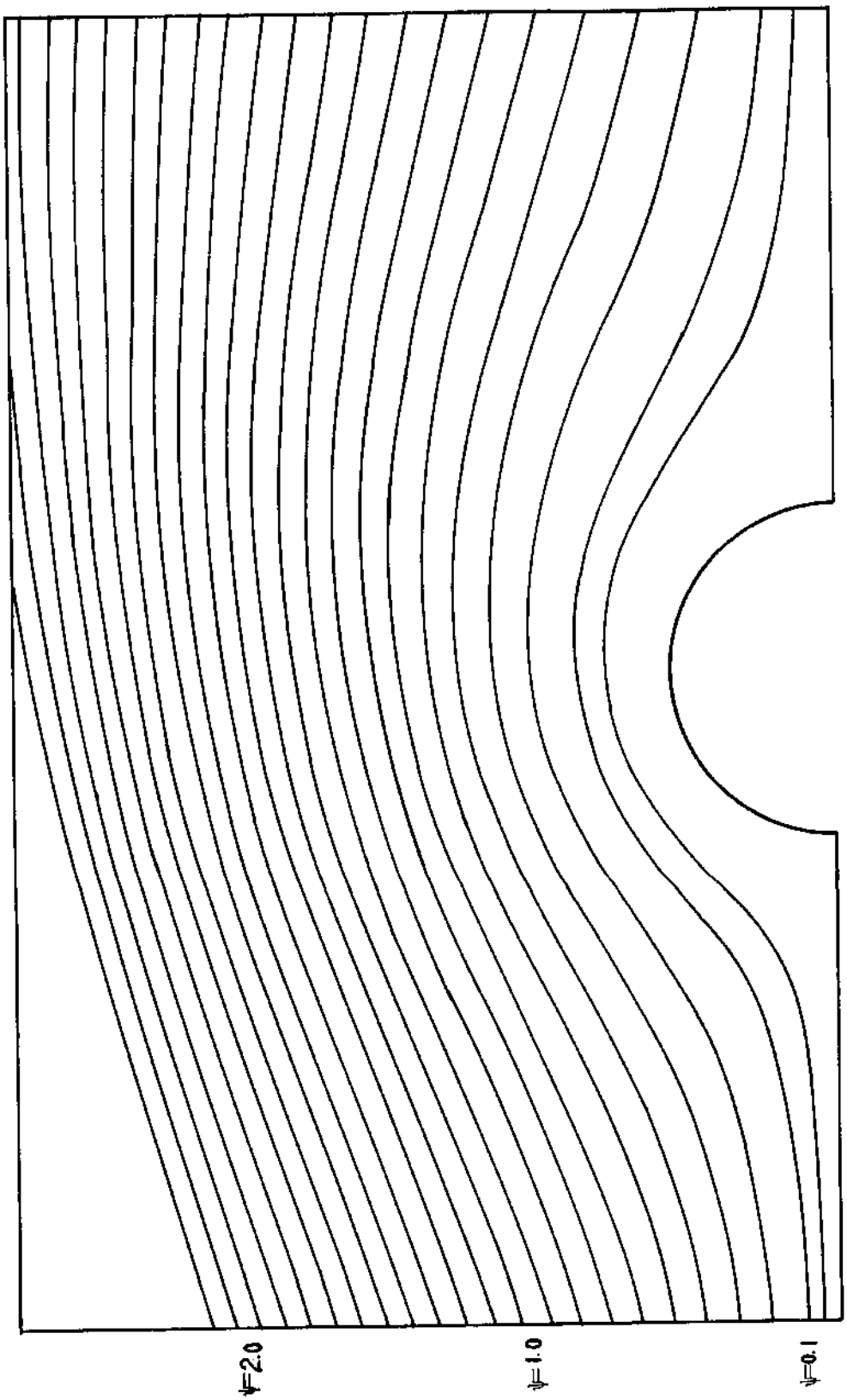

Figure 14. Flow Patterns for R = 1.0

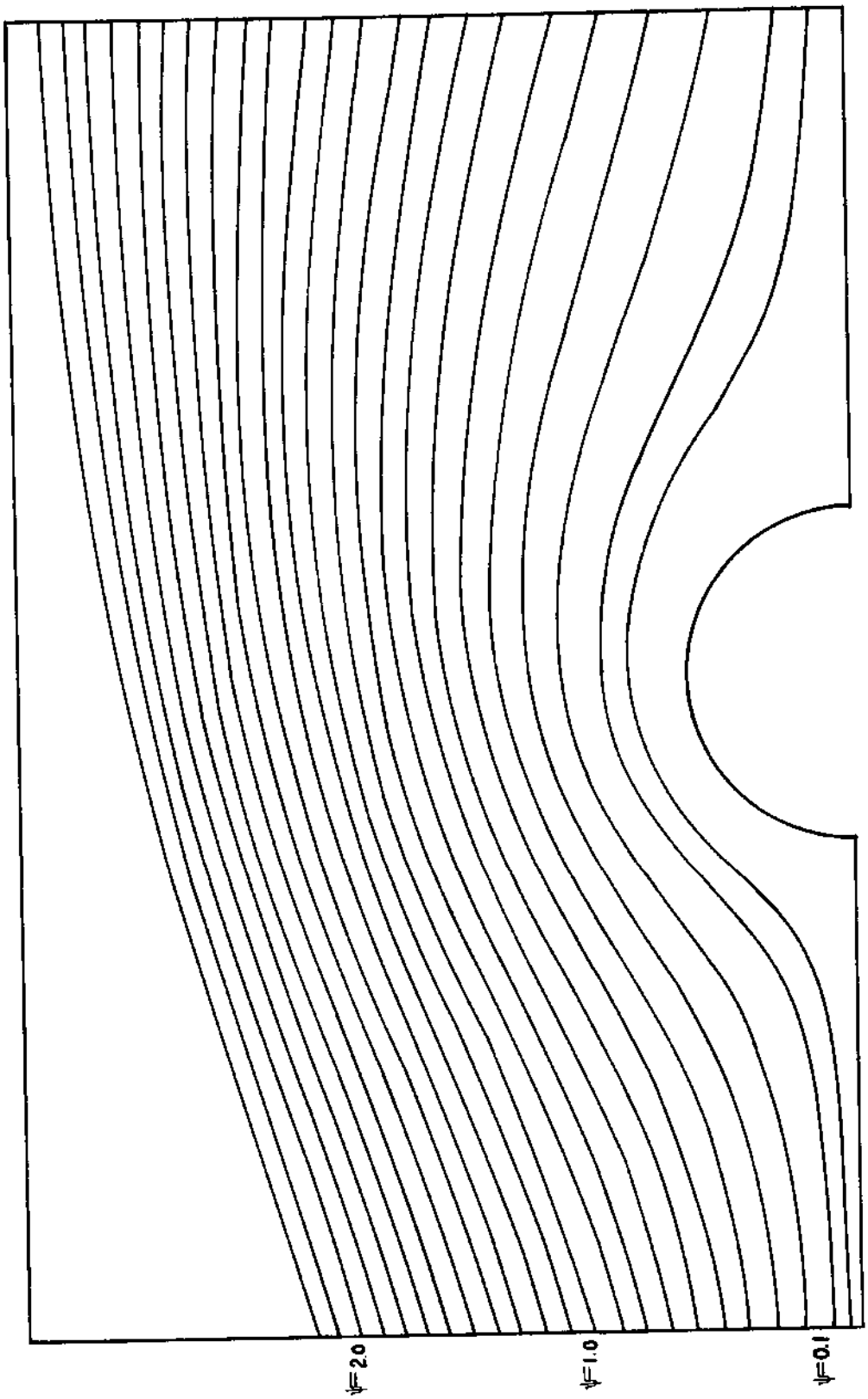

Figure 15. Flow Patterns for R = 2.0

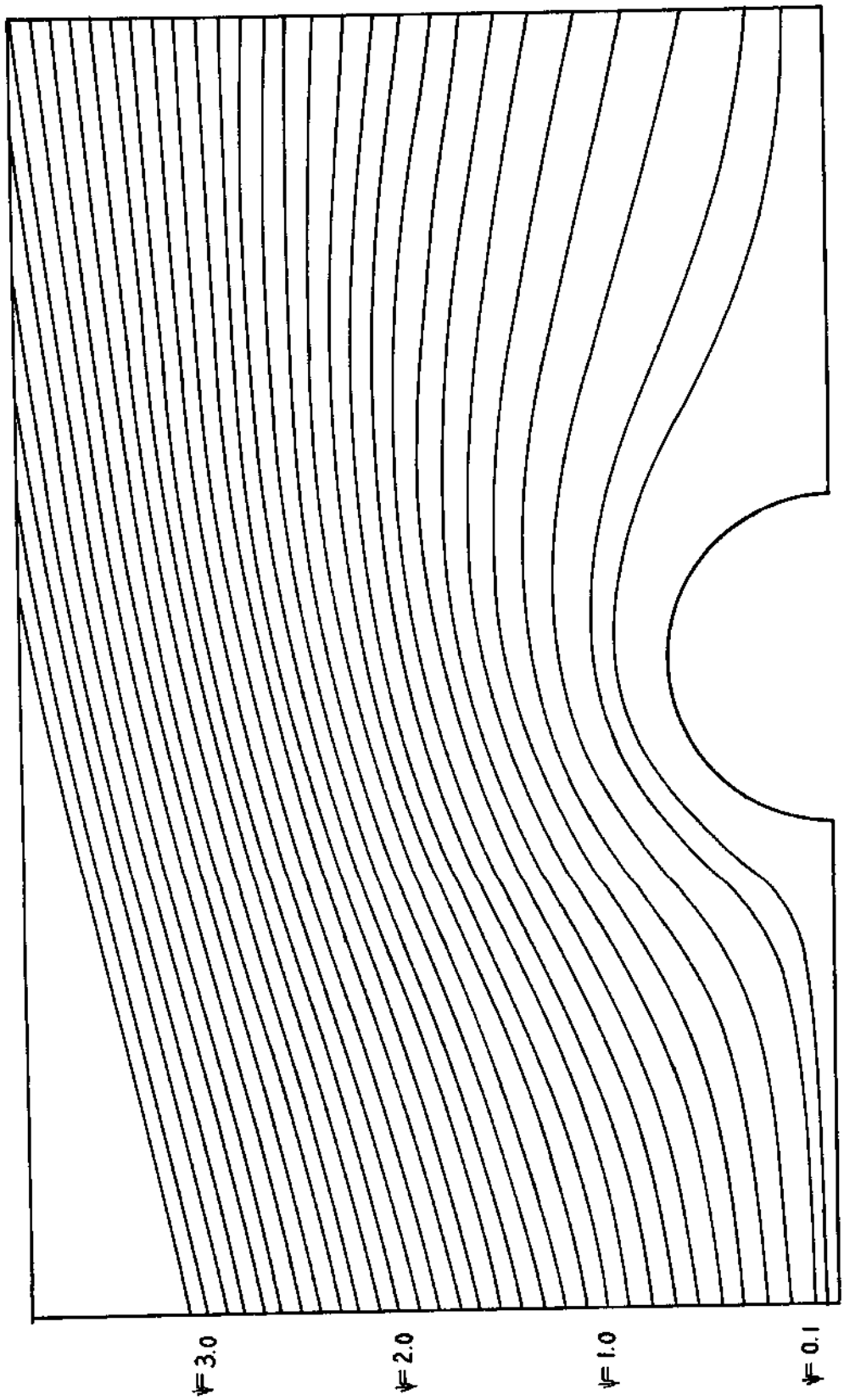

Figure 16. Flow Patterns for R = 4.0

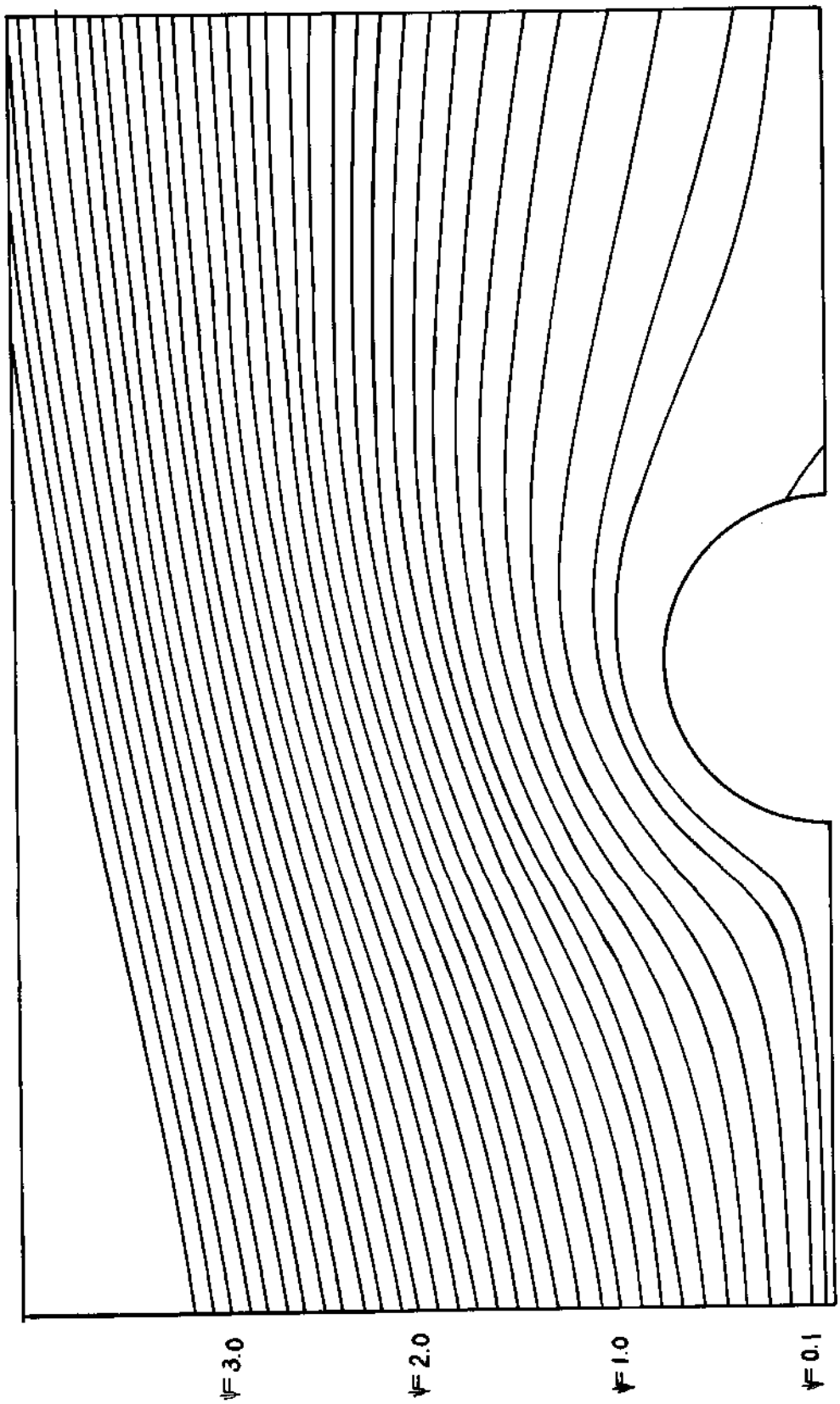

Figure 17. Flow Patterns for R = 7.0

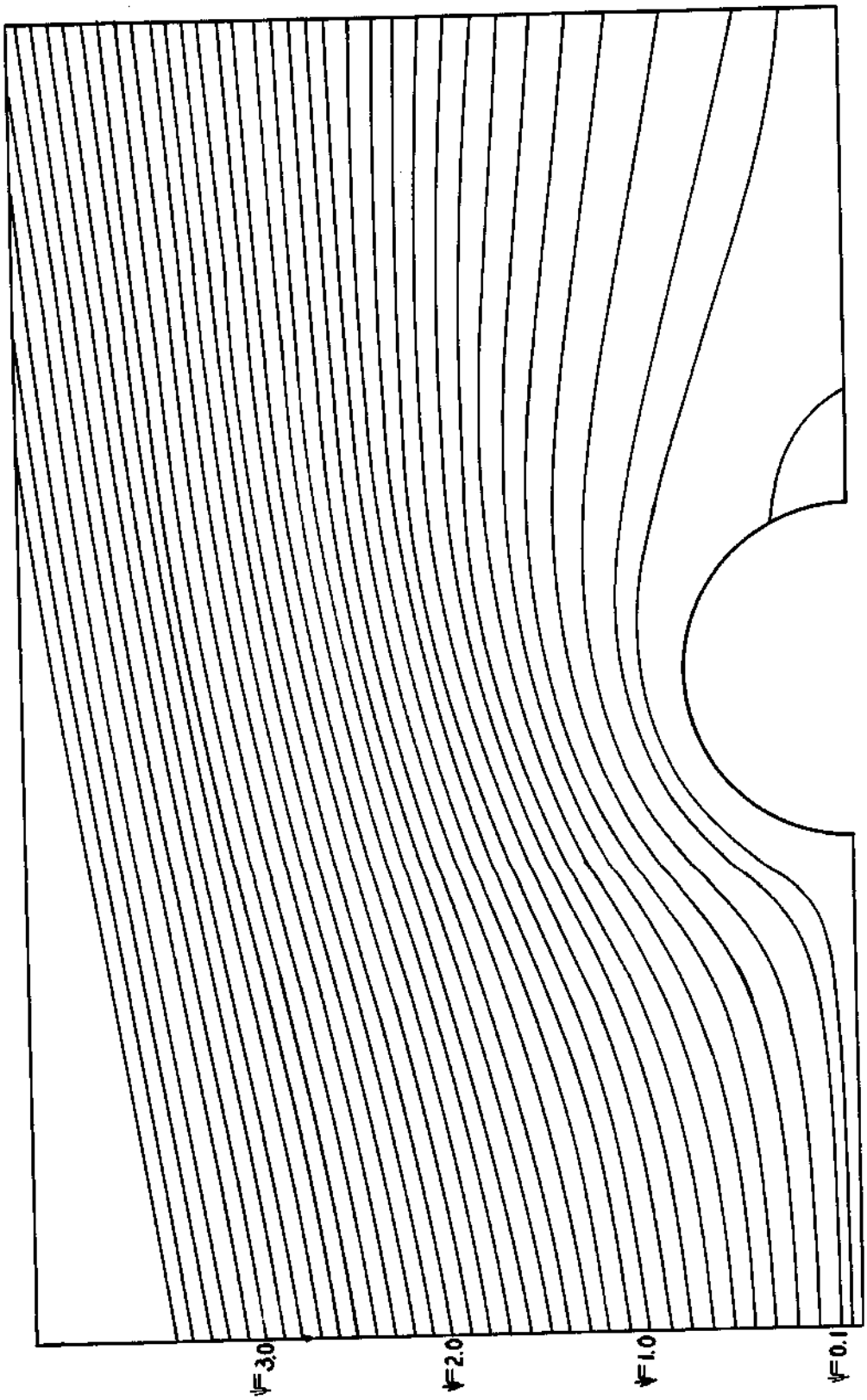

Figure 18. Flow Patterns for R = 10.0

Constant Radial Suction Mass Flux

Low Reynolds number flow perpendicular to a circular cylinder with constant radial suction mass flux was investigated for a pure fluid and for a binary solution. The radial suction flux is expressed in gallons per day per square foot as shown in Appendix C.

Pure Fluid

The constant radial suction fluxes studied ranged from 17 to 115 gallons per day per square foot for a diameter of 100 microns and for Reynolds numbers from 0.5 to 10, and the radial suction fluxes ranged from 3.81×10^3 to 15.27×10^3 gallons per day per square foot for a diameter of 100 microns and for a Reynolds number of 1. The computational parameters used and the drag coefficients calculated at radial suction fluxes less than 120 gallons per day per square foot are summarized in Table 3. The results indicate that under constant radial suction mass fluxes less than 120 gallons per day per square foot the drag coefficients are not significantly affected by the radial suction flux. The effect of very high radial suction mass flux on the drag coefficient is shown in Table 4 for a Reynolds number of 1. The drag coefficient increases as the radial suction flux is increased. The friction drag coefficient increases more rapidly than does the pressure drag coefficient. This result correlates with the fact (to be seen later) that the surface vorticity increases significantly with increasing radial suction flux but the surface pressure distribution is relatively insensitive to this process.

The effect of constant radial suction mass flux on the surface pressure distribution is shown in Figure 19 for a Reynolds number of 1.

Table 3. Computational Parameters Used at Radial Suction Fluxes Less Than 120 gal./day/ft^2

R	Δx	Δz	r_∞	grid	α	β	$-V_o$	G*	C_{DF}	C_{DP}	C_D
0.5	6°	0.075	90.0	31 x 61	1.878	1.15	0.0018	17	9.040	9.115	18.155
0.5	6°	0.075	90.0	31 x 61	1.878	1.15	0.0060	58	9.046	9.109	18.155
0.5	6°	0.075	90.0	31 x 61	1.878	1.15	0.0120	115	9.058	9.117	18.175
1.0	6°	0.075	90.0	31 x 61	1.878	1.05	0.0009	17	5.430	5.545	10.975
1.0	6°	0.075	90.0	31 x 61	1.878	1.10	0.0030	58	5.433	5.548	10.981
1.0	6°	0.075	90.0	31 x 61	1.878	1.10	0.0060	115	5.438	5.544	10.982
1.0	3°	0.075	90.0	61 x 61	1.90	1.25	0.0060	115	5.443	5.553	10.996
2.0	6°	0.070	67.0	31 x 61	1.878	0.90	0.00045	17	3.431	3.610	7.041
2.0	6°	0.070	67.0	31 x 61	1.878	0.90	0.0015	58	3.433	3.612	7.045
2.0	6°	0.070	67.0	31 x 61	1.878	0.90	0.0030	115	3.436	3.612	7.048
4.0	6°	0.055	47.0	31 x 71	1.87	0.70	0.000225	17	2.226	2.485	4.711
4.0	6°	0.055	47.0	31 x 71	1.87	0.70	0.00075	58	2.227	2.485	4.712
4.0	6°	0.055	47.0	31 x 71	1.87	0.70	0.0015	115	2.229	2.486	4.715
6.0	6°	0.045	36.7	31 x 81	1.90	0.70	0.00015	17	1.750	2.059	3.809
6.0	6°	0.045	36.7	31 x 81	1.90	0.70	0.0005	58	1.751	2.063	3.814
6.0	6°	0.045	36.7	31 x 81	1.90	0.70	0.0010	115	1.752	2.061	3.813
10.0	6°	0.035	16.5	31 x 81	1.90	1.00	0.00009	17	1.381	1.802	3.183
10.0	6°	0.035	16.5	31 x 81	1.90	1.00	0.0003	58	1.382	1.806	3.188
10.0	6°	0.035	16.5	31 x 81	1.90	1.00	0.0006	115	1.382	1.804	3.186

*In this column, the results are based on D = 100 microns.

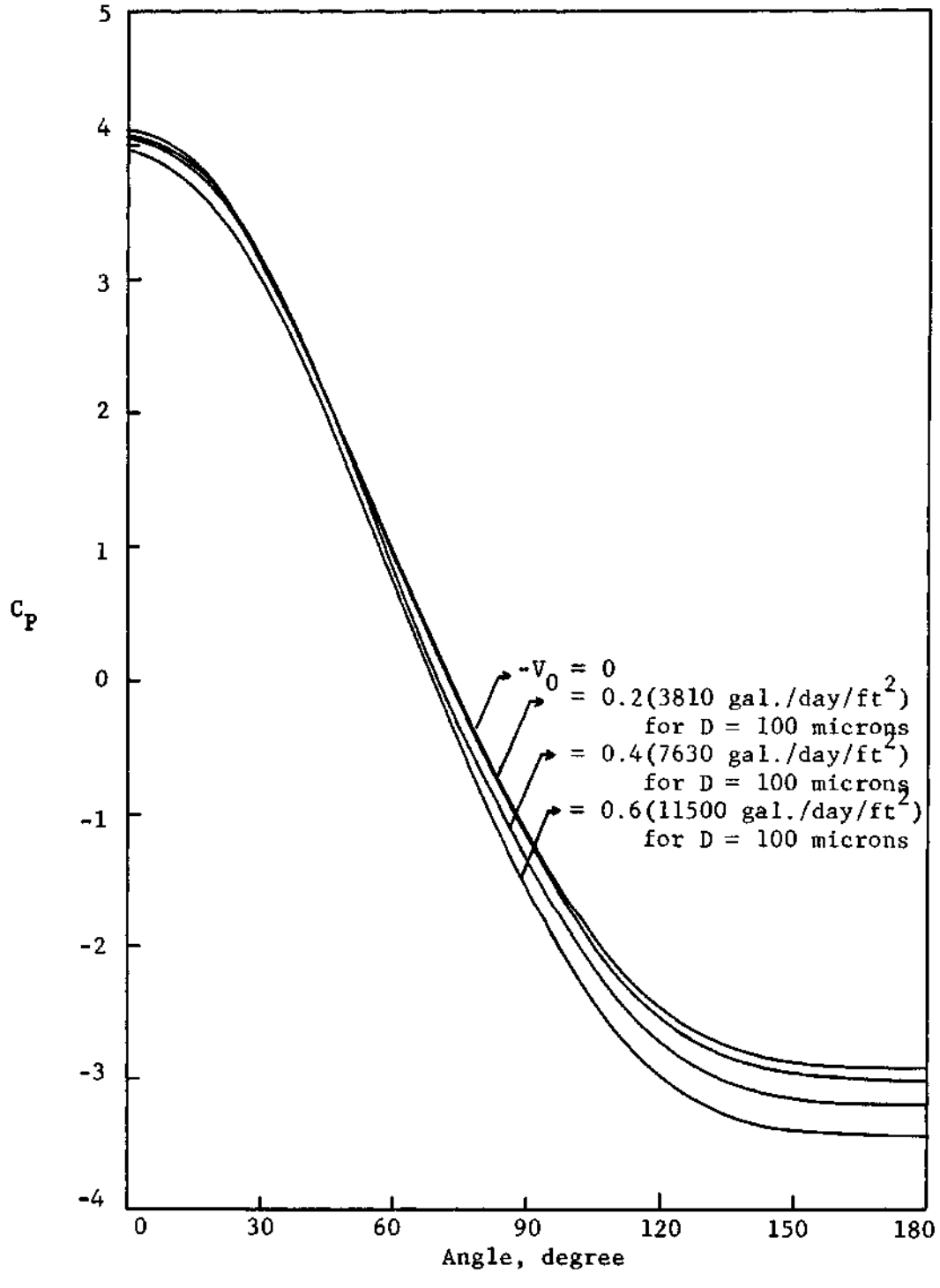

Figure 19. Surface Pressure Distribution Showing the Effect of Radial Mass Flux at a Reynolds Number of 1--Pure Fluid

Table 4. Effect of Radial Suction Flux on Drag Coefficient--Pure Fluid (R = 1.0, grid = 31 by 46, r_∞ = 111.32)

$-V_0$	G* gal./day/ft^2 $\times 10^{-3}$	C_{DF}	C_{DP}	C_D
0.0	0	5.373	5.485	10.858
0.2	3.81	5.750	5.593	11.343
0.4	7.63	6.154	5.704	11.858
0.6	11.50	6.586	5.813	12.399
0.8	15.27	7.050	5.931	12.981

*In this column, the results are based on D = 100 microns.

It is noticed that the surface pressure changes only slightly with increasing radial suction flux. This accounts for the slight change in the pressure drag coefficient.

The effect of constant radial suction mass flux on the surface vorticity distribution is shown in Figure 20 for a Reynolds number of 1. It is noticed that the surface vorticity increases significantly as radial suction flux increases. This accounts for the large increase in the friction drag coefficient C_{DF}, as mentioned in the previous section.

The effect of radial suction flux on the flow patterns is shown in Figure 21 for a Reynolds number of 1. As compared with Figure 14, Figure 21 displays a better fore-and-aft symmetry near the cylinder body. The streamlines have moved closer to the cylinder and their locations are strongly dependent on the magnitude of the radial mass flux. This can be explained as the fluid is being pulled partly towards the cylinder, instead of being carried away completely by the bulk flow. Thus, when there

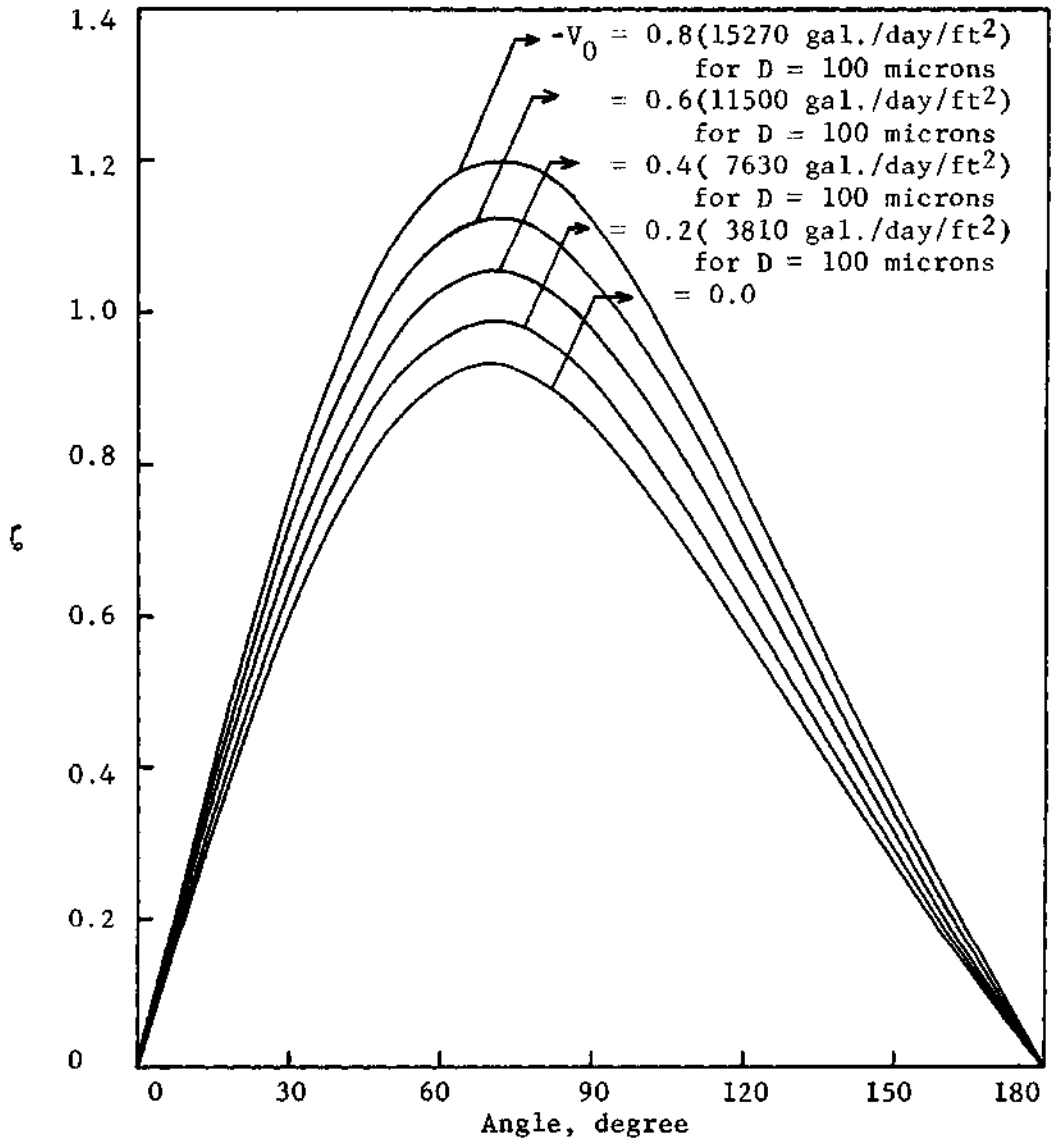

Figure 20. Surface Vorticity Distribution Showing the Effect of Radial Mass Flux at a Reynolds Number of 1--Pure Fluid

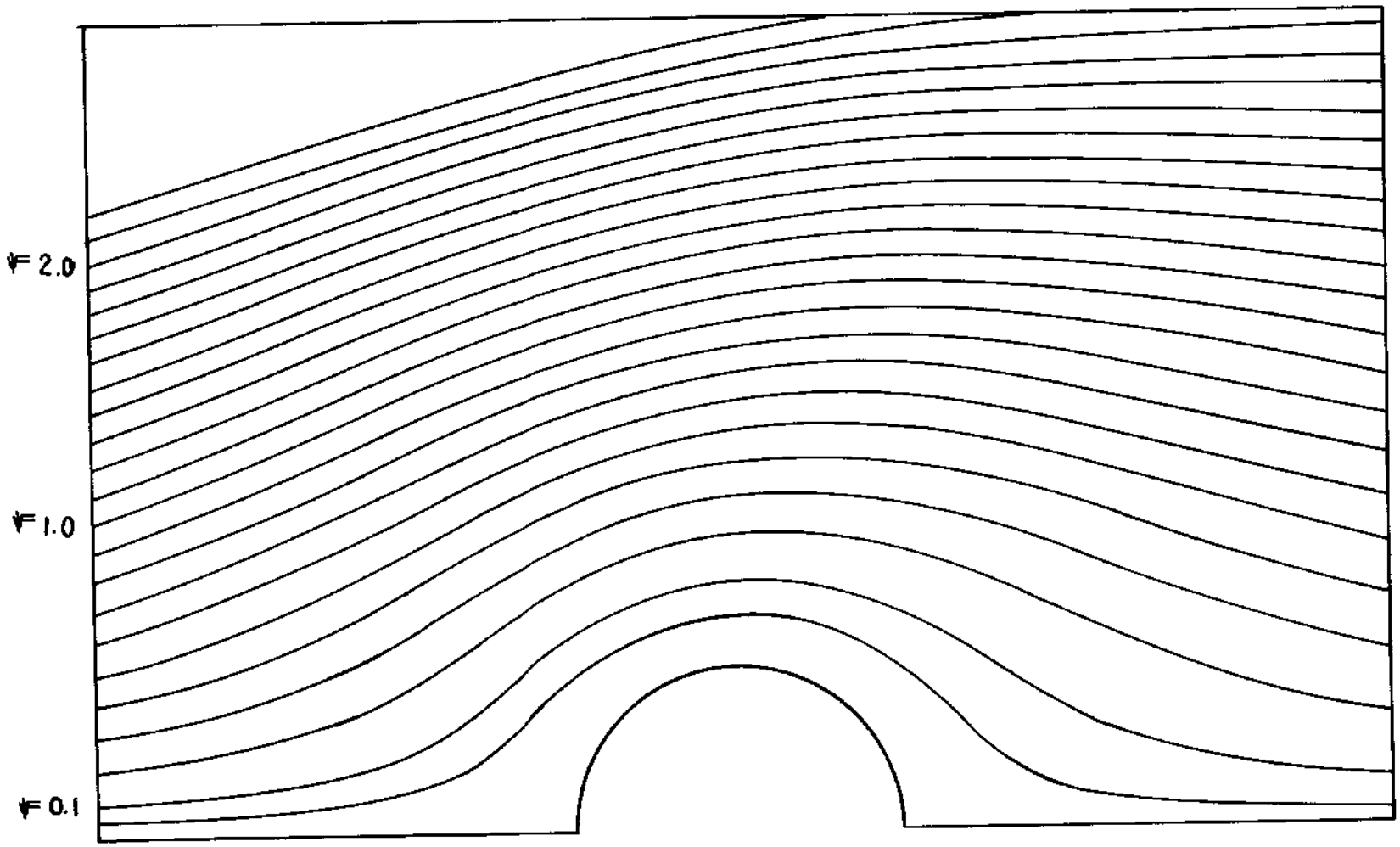

Figure 21. Flow Patterns for R = 1.0 and V_0 = - 0.01 (191 gal./day/ft^2 for D = 100 microns)

is a radial suction flux at the wall, flow separation will be eliminated or delayed, depending on the magnitude of the radial suction flux and the Reynolds number.

Binary Solution

The Reynolds numbers studied ranged from 0.5 to 10, and the constant radial suction mass fluxes ranged from 17 to 115 gallons per day per square foot for a diameter of 100 microns. In addition, brief calculations at radial suction mass fluxes of 2 and 4 gallons per day per square foot for a diameter of 100 microns were made for a Reynolds number of 1 to establish the low mass-transfer data for extrapolation purposes. The concentration distribution was calculated over the whole flow field from which the Nusselt number was obtained by Equations (3-49) and (3-50). The computational parameters used are tabulated in Table 3.

Local Nusselt numbers as a function of angular position are shown in Figures 22 to 27 for Reynolds numbers of 0.5, 1, 2, 4, 6, and 10, respectively. These figures demonstrate the variation of the local Nusselt number over the cylindrical surface. It is seen that the maximum local Nusselt number occurs at the front stagnation point. The local Nusselt number decreases with increasing distance from the front stagnation point and would continue to decrease if there were no flow separation. Thus, the contribution of the rear region to the overall mass transfer is very small. Flow separation occurs near 165° from the front stagnation point for a Reynolds number of 10. The overall Nusselt number at this Reynolds number was estimated by the relation

$$Nu_{overall} = -\frac{2}{\pi}(1 + F)\int_0^{165^\circ}\left(\frac{1}{C - 1}\frac{\partial C}{\partial r}\right)_{r=1} d\theta$$

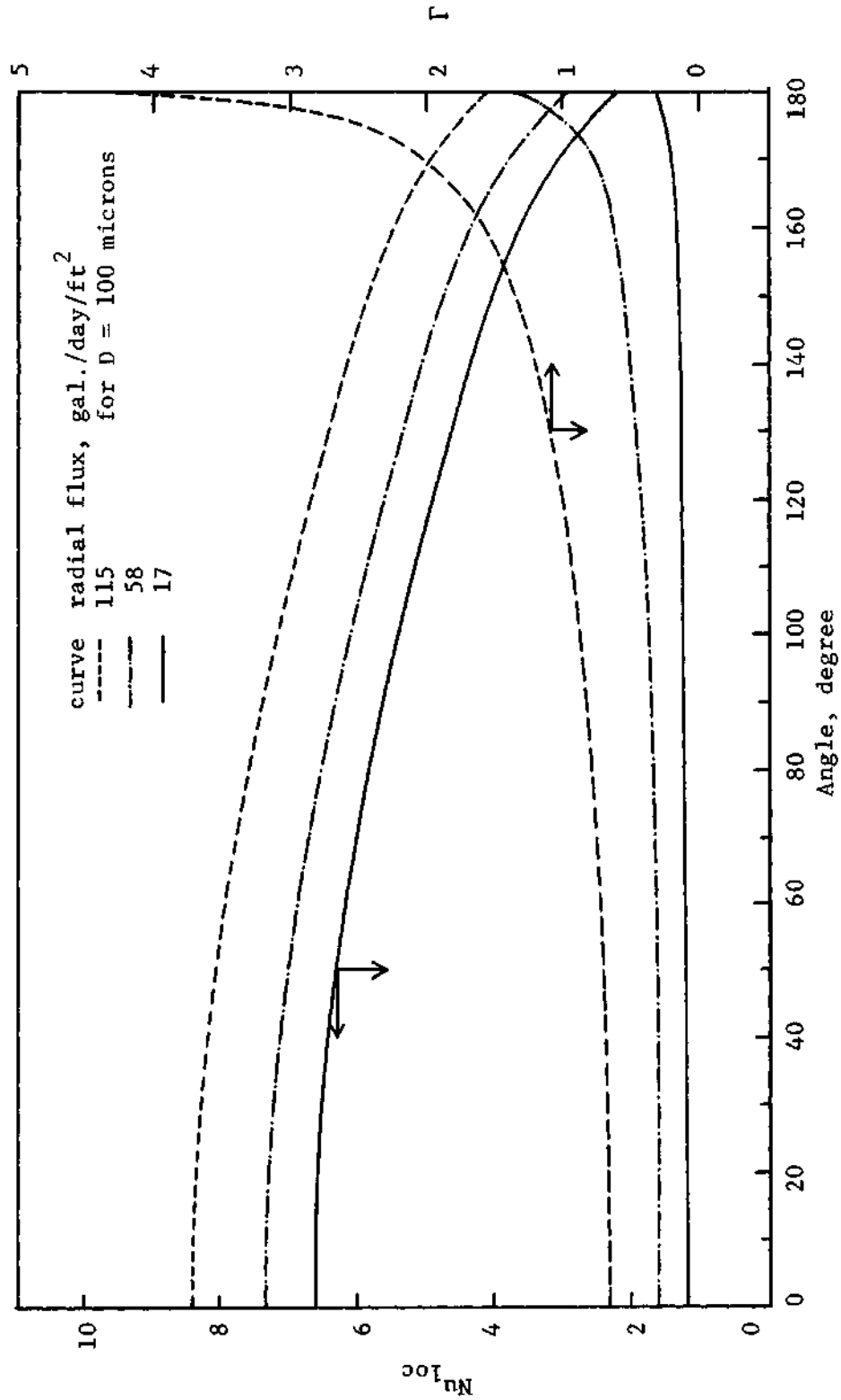

Figure 22. Distribution of Local Nusselt Number and Concentration Polarization Around the Cylindrical Surface for R = 0.5

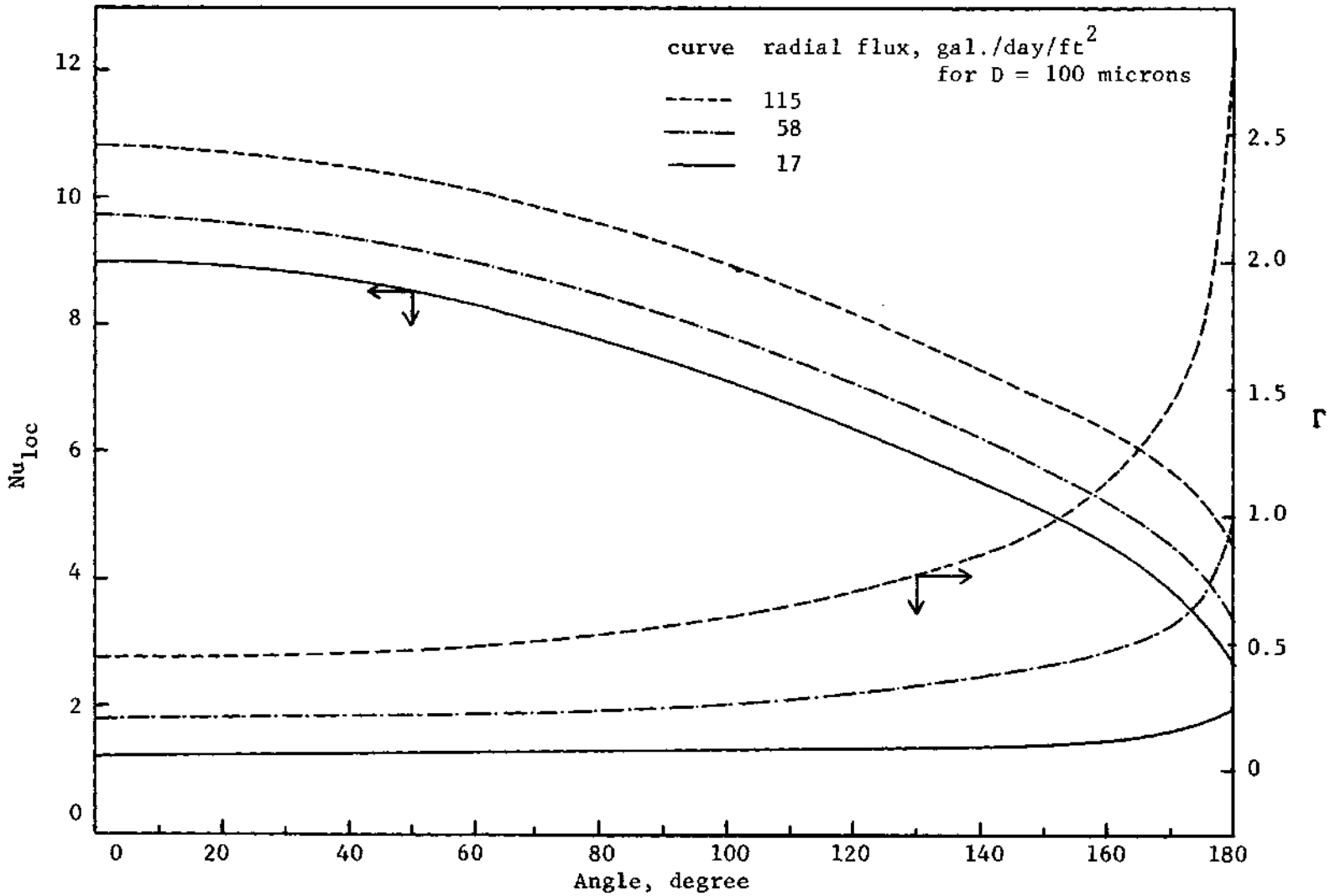

Figure 23. Distribution of Local Nusselt Number and Concentration Polarization Around the Cylindrical Surface for R = 1.0

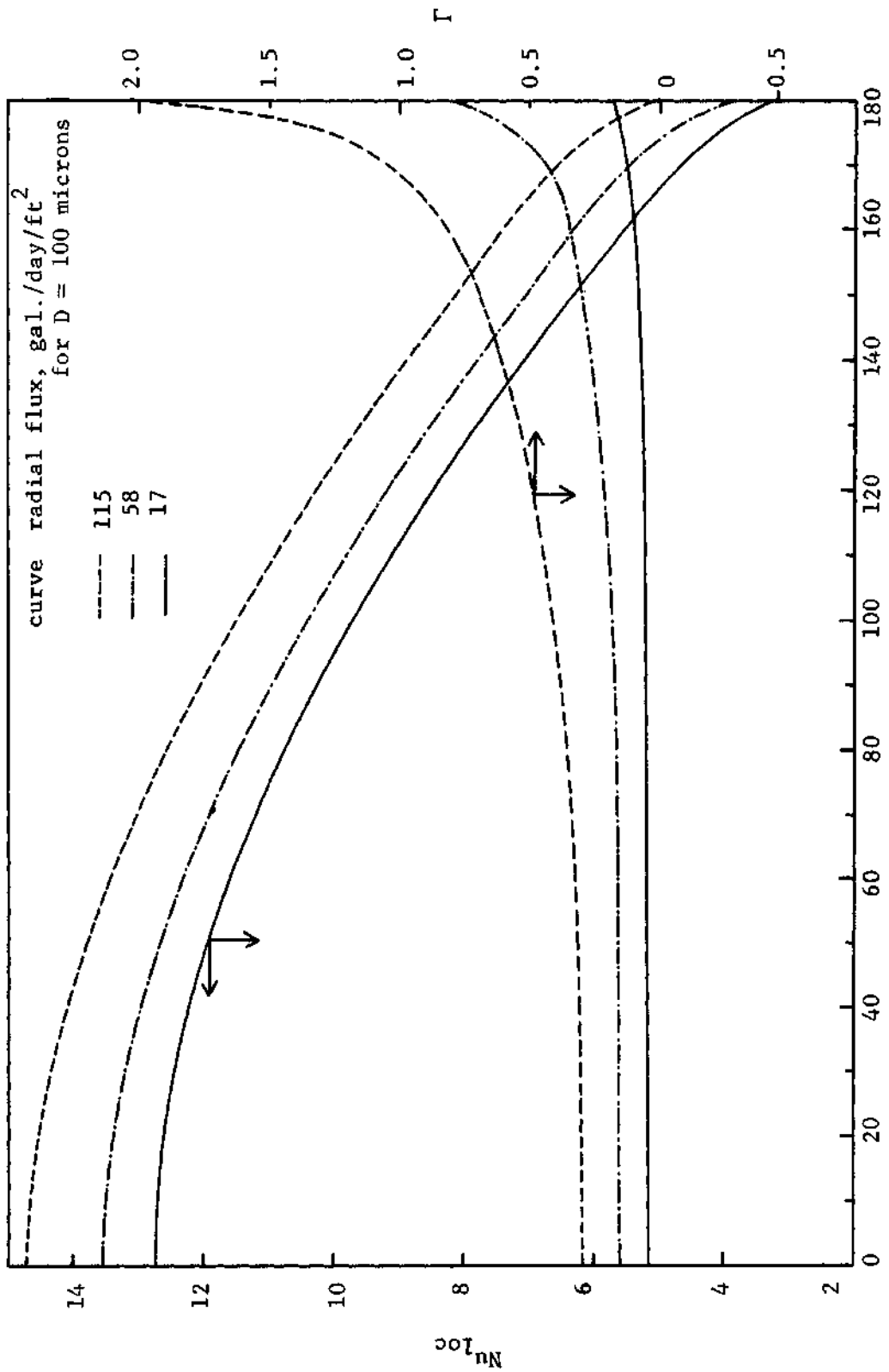

Figure 24. Distribution of Local Nusselt Number and Concentration Polarization Around the Cylindrical Surface for R = 2.0

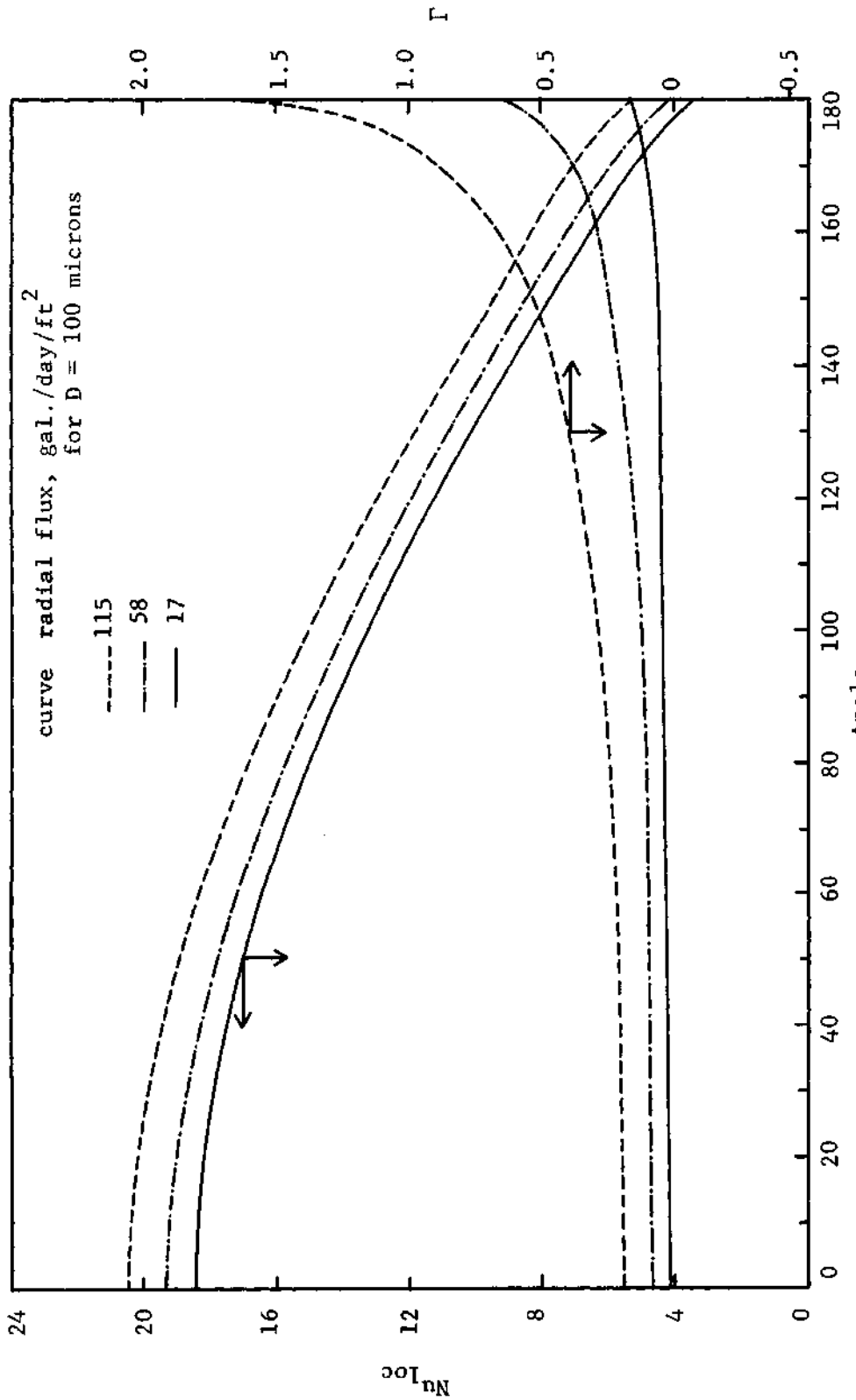

Figure 25. Distribution of Local Nusselt Number and Concentration Polarization Around the Cylindrical Surface for R = 4.0

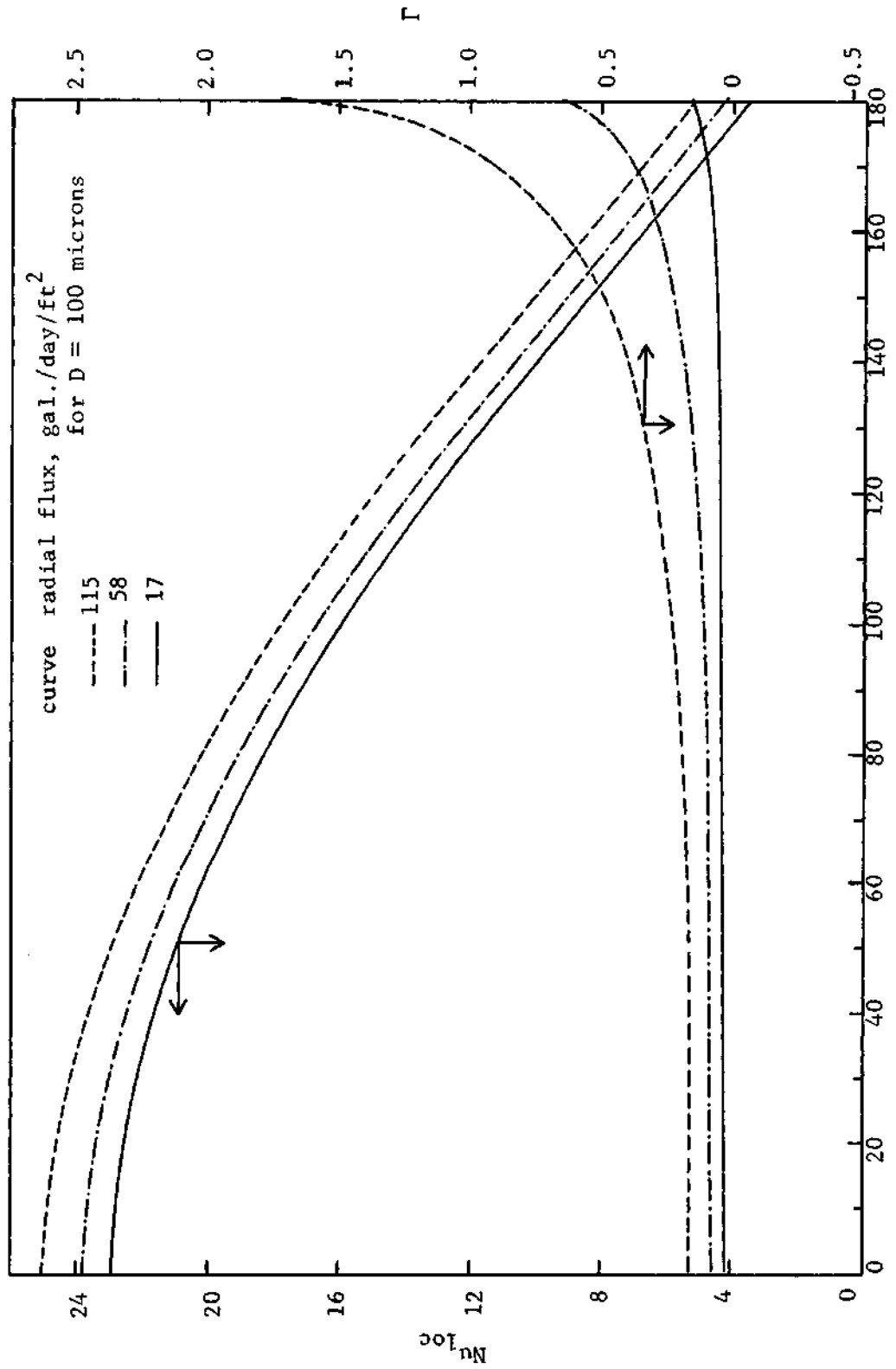

Figure 26. Distribution of Local Nusselt Number and Concentration Polarization Around the Cylindrical Surface for R = 6.0

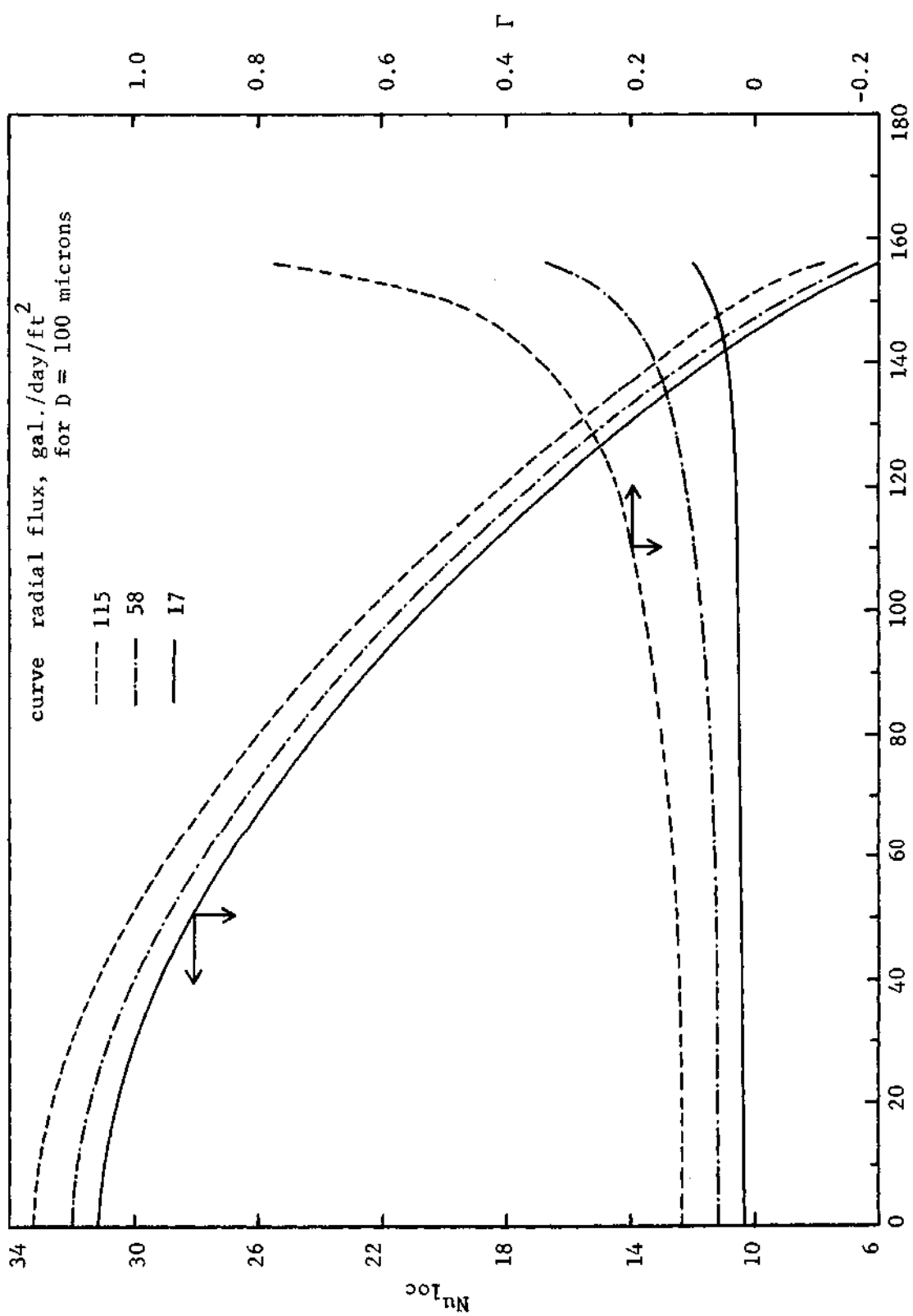

Figure 27. Distribution of Local Nusselt Number and Concentration Polarization Around the Cylindrical Surface for R = 10

where F is defined as the ratio of the mass-transfer rate after flow separation to that before flow separation. Based on the study at Reynolds number of 6, F was found to be 0.045.

Overall Nusselt numbers are shown in Figure 28, which is a plot of $Nu_{overall}/Sch^{1/3}$ versus $R^{1/2}$. A straight line with a slope of 0.75 is obtained for each radial flux condition. These curves may be approximated by the relation

$$Nu_{overall}/Sch^{1/3} = b + 0.75\ R^{1/2}$$

The values of b are 0.12, 0.19, and 0.34 for radial suction fluxes of 17, 58, and 115 gallons per day per square foot for a diameter of 100 microns, respectively. For comparison, the mass-transfer data of Dobry and Finn and Vogtlander and Bakker (50) and the heat-transfer data of Piret, James, and Stacy are also shown in Figure 28. At low radial suction fluxes the present results have a better agreement with those of Vogtlander and Bakker. As the radial suction flux is increased, the deviation from the results of other studies becomes greater. This can be explained by the fact that in the present study the distortion of the velocity and concentration profiles by finite velocity through the cylinder wall is taken into account, whereas in the other studies this effect is neglected.

The results of the mass-transfer study show that the overall Nusselt number depends not only on the Schmidt and Reynolds numbers but also on the mass-transfer rate, indicating that the mass-transfer rates are relatively high within the diffusion layer. Most of the available forced-convection mass-transfer correlations are limited to low mass-

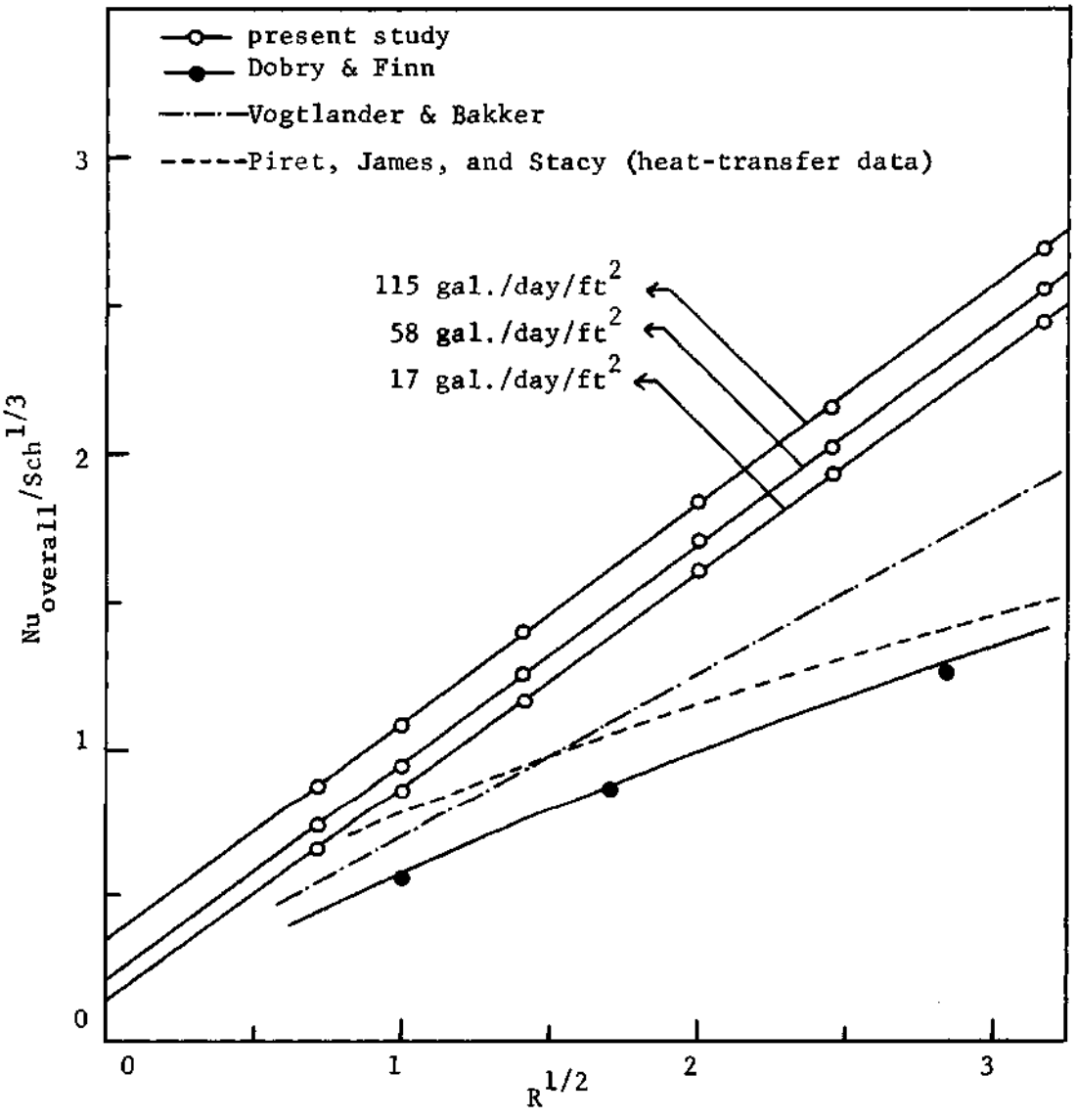

Figure 28. Dimensionless Correlation Showing a Linear Relationship Between $Nu_{overall}$ for Mass Transfer and $R^{1/2}$

transfer rates. The result at high mass-transfer rate may be obtained by multiplying the coefficient at low mass-transfer rates by a correction factor, defined as the ratio of the mass-transfer coefficient at high mass-transfer rates to that at low mass-transfer rates. Based on this study the correction factor as a function of the radial suction mass flux is given in Figure 29. The overall Nusselt number at low mass-transfer rates was obtained by extrapolating to zero mass-transfer rate, as shown in Figure 30.

The concentration buildup along the cylindrical surface was expressed by a dimensionless term Γ defined by

$$\Gamma = \frac{\rho_{A0}}{\rho_{A\infty}} - 1$$

where Γ is called the concentration polarization. The concentration polarization as a function of angular position is shown in Figures 22 to 27 for Reynolds numbers of 0.5, 1, 2, 4, 6, and 10, respectively. For each Reynolds number studied, the concentration polarization increases with an increase in the radial suction flux. At a radial suction flux of 115 gallons per day per square foot for a diameter of 100 microns, the concentration polarization builds up sharply at the very rear portion of the cylinder.

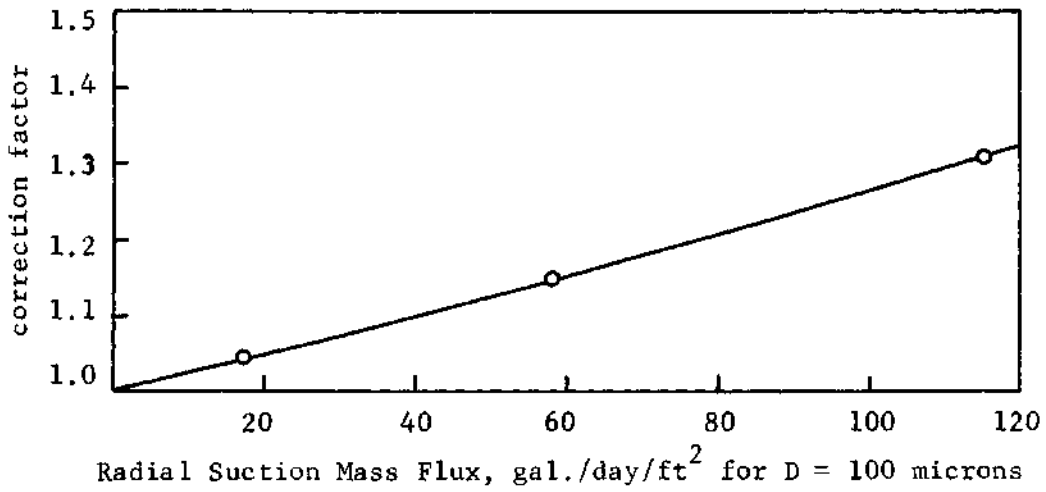

Figure 29. Variation of Correction Factor with Radial Suction Mass Flux

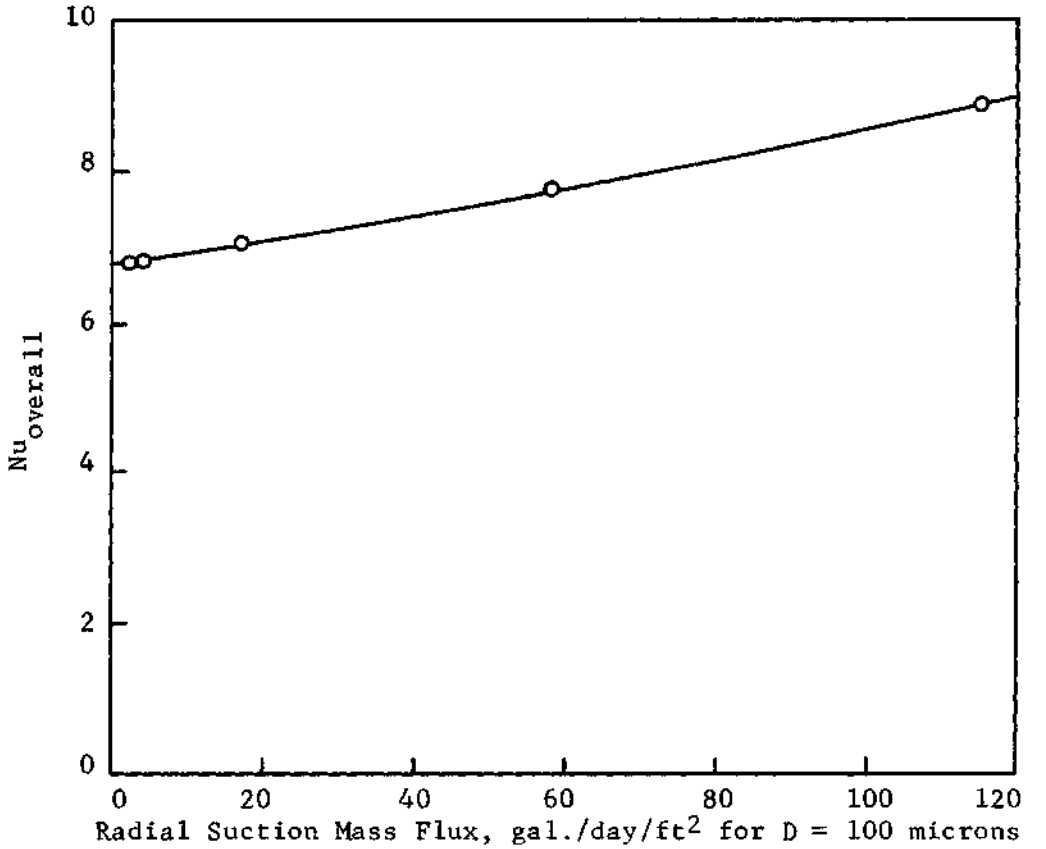

Figure 30. Variation of Overall Nusselt Number with Radial Suction Mass Flux (R = 1)

CHAPTER V

CONCLUSIONS AND SUGGESTIONS FOR FURTHER RESEARCH

Based on the results of this study, the following conclusions are reached:

1. The numerical technique used in this work gives an accurate description of flow characteristics at high Schmidt numbers and low Reynolds numbers, where boundary-layer theory fails to apply.

2. For numerical calculation of viscous flow past a circular cylinder in a fluid of infinite extent, the field of computation must be restricted within an outer circular boundary. This outer boundary position used has an effect on the results of various flow properties calculated, in particular in the low Reynolds number region.

3. The drag coefficient increases as the radial suction flux is increased. The friction drag coefficient increases more rapidly than does the pressure drag coefficient. This result correlates with the fact that the surface vorticity increases significantly with increasing radial suction flux but the surface pressure distribution is relatively insensitive to this process.

4. Without radial suction flux at the cylinder wall, the flow patterns are almost symmetrical fore and aft at a Reynolds number of 1. As the Reynolds number is increased, asymmetry becomes more pronounced. At Reynolds numbers of 7 and 10, the flow patterns show flow separation and the appearance of a pair of standing eddies behind the cylinder.

5. With radial suction flux at the wall, flow separation will be eliminated or delayed, depending on the magnitude of the radial suction flux and the Reynolds number.

6. The maximum local Nusselt number occurs at the front stagnation point. The local Nusselt number decreases with increasing distance from the front stagnation point and would continue to decrease if there were no flow separation.

7. The overall mass-transfer coefficient can be approximated by the relation

$$Nu_{overall}/Sch^{1/3} = b + 0.75\ R^{1/2}$$

where b depends on the magnitude of the radial suction flux.

Suggestions for further study in this area are:

1. This study can be extended to include the case of higher Reynolds numbers without any modification but at the expense of computation time.

2. The numerical technique described here can be applied to study the viscous, incompressible flow past submerged bodies of other shapes.

3. Viscous, incompressible flow past a circular cylinder with variable suction mass flux at the cylinder wall can be studied by the technique developed here.

4. This study can be extended to include the case of flow past tube banks arranged in various configurations such as in-line, triangular, and crossed.

5. The present numerical technique can be applied to study the flow past a circular cylinder with radial injection at the wall.

APPENDICES

APPENDIX A

COMPUTATIONAL ALGORITHM FOR THE METHOD OF THOMAS

L. H. Thomas of the Watson Scientific Computing laboratory suggested a method for solving a special simultaneous equations for which the matrix of coefficients is tridiagonal in form. For a system of equations:

$$B_1 V_1 + C_1 V_2 = D_1$$

$$A_I V_{I-1} + B_I V_I + C_I V_{I+1} = D_I \quad (2 \leqq I \leqq N-2)$$

$$A_{N-1} V_{N-2} + B_{N-1} V_{N-1} = D_{N-1}$$

Let

$$\beta_1 = B_1$$

$$\gamma_1 = D_1/\beta_1$$

$$\beta_I = B_I - A_I C_{I-1}/\beta_{I-1}$$

$$\gamma_I = (D_I - A_I \gamma_{I-1})/\beta_I$$

for I = 2, 3, 4, . . ., N-1.

The solution is

$$V_{N-1} = \gamma_{N-1}$$

$$V_I = \gamma_I - C_I V_{I+1}/\beta_I$$

for I = N-2, N-3, . . ., 1.

Thus β and γ are computed in order of increasing I, and V is then computed in order of decreasing I.

APPENDIX B

COMPUTER PROGRAMS

All the computer programs presented here are written in the Fortran V language for the Univac-1108 electronic digital computer. The main program is given first. Subroutines are given at the end of this appendix. The more important variables appearing in the program are defined:

Program Symbol	Definition
DELX, DELZ	grid spacings Δx, Δz
ALPHA, RHO	relaxation factors, α and β
I, J	subscripts denoting grid point (I,J)
SCHMDT	Schmidt number
PE	Peclet number
PSI	dimensionless radial velocity at the wall
PHI, PHIOLD	new and old values of stream function, ψ
VORT, DUM	new and old values of vorticity, ζ
M, N	total number of grid spacings in the x- and z-directions
VX, VZ	velocities in the x- and z-directions
DCDZ	concentration gradient in the z-direction at the wall
C	concentration
CSTAR	concentration at the wall

```
      COMMON M, R, PSI, XARRAY, YARRAY, PSTAR, VORT
      DIMENSION PHI(31,61), PHIOLD(31,61), VORT(31,61),
     1OUM(31,61), VX(31,61), VZ(31,61), EZ(61),ETWOZ(61),
     2OXSQEZ(61),Y(61), OWOX(61), PX(31),PY(31),OWOZ(31),
     3NZERO(31), OCOZ(31), F(31), PSTAR(31)
      DIMENSION IBUF(1000), XARRAY(33), YARRAY(33)
      DIMENSION A(61), B(61), C(61), D(61), CSTAR(31,61),
     1          CGUESS(31,1)
      PAI = 3.1415926536
    1 READ (5,100) DELT, R, M, N
  100 FORMAT (F6.3,F4.1,2I3)
C     ..... CHECK FOR INVALID DATA .....
      IF (DELT .LT. 0.0) STOP
      DELX = 0.1047197551
      DELZ = 0.075
      ALPHA = 1.878
      RHO = 1.10
      WRITE (6,202) DELT, DELZ, DELX, R, M, N, ALPHA, RHO
  202 FORMAT (1H1, 14X, 'DELT = ', F6.4, 8X, 'DELZ = ',
     1F8.6, 8X, 'DELX = ', F8.6, 8X, 'R = ', F4.1, 8X,
     2'M = ', I2, 8X, 'N = ', I2, /, 15X, 'ALPHA = ',
     3F5.3, 8X, 'RHO = ', F5.3, /)
      SCHMDT = 560.0
      PE = R*SCHMDT
      PSI = - 0.006
      PSISQ = PSI*PSI
      DXSQ = DELX*DELX
      DZSQ = DELZ*DELZ
      DXOVDZ = DELX/DELZ
      RATISQ = DXSQ/DZSQ
      CONST = 0.5*PSI*PE
      B1 = 2.0*(1.0 + RATISQ)
      B2 = R*DXOVDZ/8.0
      F5 = 6.0*DELX
      F6 = 6.0*DELZ
      F7 = 12.0*DELX
      F8 = 12.0*DELZ
      F9 = 2.0*DELX
      F10 = 2.0*DELZ
      F11 = 4.0*DELZ
      F12 = 8.0*DELZ
      G1 = 1.0/(PE*DZSQ)
      G2 = 1.0/(PE*F10)
      MP1 = M + 1
      MP2 = M + 2
      MHALF = M/2 + 1
      NP1 = N + 1
      DO 10  I = 1, MP1
      VX(I,1) = 0.0
      VZ(I,1) = PSI
```

```
      IF (I .GT. MHALF) GO TO 12
      VX(I,NP1) = SIN((I-1)*DELX)
      VZ(I,NP1) = - COS((I-1)*DELX)
      GO TO 10
   12 VX(I,NP1) = VX(MP2-I,NP1)
      VZ(I,NP1) = - VZ(MP2-I,NP1)
   10 CONTINUE
      EPSMAX = 1.0E-5
      DO 15  J = 1, NP1
      EZ(J) = EXP((J-1)*DELZ)
      ETWOZ(J) = EXP(2.0*(J-1)*DELZ)
   15 DXSQEZ(J) = DXSQ*ETWOZ(J)
      DZSQ2 = 2*DZSQ
C     ..... ASSIGN THE INITIAL VALUES OF PHI, VORT .....
      DO 25  I = 1, MP1
      DO 25  J = 1, NP1
      IF (J .EQ. 1) GO TO 20
      VORT(I,J) = 0.0
      IF (I .EQ. 1) GO TO 21
      IF (I .EQ. MP1) GO TO 22
      PHI(I,J) = EZ(J)*VX(I,NP1) - PSI*(I-1)*DELX
      GO TO 25
   20 PHI(I,J) = - PSI*(I-1)*DELX
      GO TO 25
   21 PHI(I,J) = 0.0
      GO TO 25
   22 PHI(I,J) = - PSI*PAI
   25 CONTINUE
      ITERA = 0
      ALPHA = ALPHA/B1
      RHO = RHO/B1
   30 ITERA = ITERA + 1
      DO 32  I = 2, M
      DO 32  J = 2, N
      PHIOLD(I,J) = PHI(I,J)
   32 PHI(I,J) = PHI(I,J) + ALPHA*( - VORT(I,J)*DXSQEZ(J)
     1          + PHI(I+1,J) + PHI(I-1,J) + (PHI(I,J+1)
     2          + PHI(I,J-1))*RATISQ - B1*PHI(I,J))
      IF ((ITERA/20)*20 .NE. ITERA) GO TO 35
      WRITE (6,203) ITERA
  203 FORMAT (23H0                ITERA = , I3)
      WRITE (6,204) (I,(PHI(I,J), J=1,NP1,5),I=1,MP1,5)
  204 FORMAT (6H  I = , I2, /, 13F10.5)
   35 CONTINUE
      IF (ITERA .GT. 200) STOP
      DO 36  I = 2, M
      DO 36  J = 2, N
   36 IF(ABS(PHI(I,J)-PHIOLD(I,J)) .GE. EPSMAX) GO TO 30
      WRITE (6,205)
  205 FORMAT (1H0,25X, 'CONVERGENCE CONDITION HAS BEEN',
     11X, 'REACHED AFTER A NUMBER OF ITERATIONS')
```

```
      WRITE (6,203) ITERA
      WRITE (6,206)
  206 FORMAT (1H0,23X,'STREAM FUNCTION DISTRIBUTION AT',
     11X, 'ALL GRID POINTS')
      WRITE (6,204) (I,(PHI(I,J), J=1,NP1,5),I=1,MP1,5)
      DO 38  I = 1, MP1
   38 VORT(I,1)=(8.0*PHI(I,2)-PHI(I,3)-7.0*PHI(I,1))/DZSQ2
      WRITE (6,213)
  213 FORMAT (1H0,23X,'VORTICITY DISTRIBUTION ON THE',
     11X, 'SURFACE OF THE CYLINDER')
      WRITE (6,208) (VORT(I,1), I = 2, MP1)
  208 FORMAT (1H ,10F12.6)
      EPSMAX = 1.0E-6
      ICOUNT = 0
   99 ICOUNT = ICOUNT + 1
      DO 40  I = 2, M
      DO 40  J = 2, N
      DUM(I,J) = VORT(I,J)
   40 VORT(I,J)=VORT(I,J) + RHO*(VORT(I+1,J)+VORT(I-1,J)
     1           + (VORT(I,J+1) + VORT(I,J-1))*RATISQ
     2           -B1*VORT(I,J)+B2*((PHI(I+1,J)-PHI(I-1,J))
     3           *(VORT(I,J+1)-VORT(I,J-1))-(PHI(I,J+1)
     4           -PHI(I,J-1))*(VORT(I+1,J)-VORT(I-1,J))))
      DO 13  I = 2, M
      DO 13  J = 2, N
   13 IF (VORT(I,J) .GT. 200.0) STOP
      IF ((ICOUNT/100)*100 .NE. ICOUNT) GO TO 42
      WRITE (6,214) ICOUNT
  214 FORMAT (24H0                ICOUNT = , I4)
      WRITE (6,207)
  207 FORMAT (1H0,23X, 'VORTICITY DISTRIBUTION AT ALL',
     11X, 'GRID POINTS')
      WRITE (6,204) (I,(VORT(I,J), J=1,NP1,5),I=1,MP1,5)
   42 CONTINUE
      DO 45  I = 2, M
      DO 45  J = 2, N
      PHIOLD(I,J) = PHI(I,J)
   45 PHI(I,J) = PHI(I,J) + ALPHA*( - VORT(I,J)*DX5QEZ(J)
     1          + PHI(I+1,J) + PHI(I-1,J) + (PHI(I,J+1)
     2          + PHI(I,J-1))*RATISQ - B1*PHI(I,J))
      IF ((ICOUNT/100)*100 .NE. ICOUNT) GO TO 47
      WRITE (6,206)
      WRITE (6,204) (I,(PHI(I,J), J=1,NP1,5),I=1,MP1,5)
   47 CONTINUE
      DO 46  I = 1, MP1
   46 VORT(I,1)=(8.0*PHI(I,2)-PHI(I,3)-7.0*PHI(I,1))/DZSQ2
      IF ((ICOUNT/100)*100 .NE. ICOUNT) GO TO 95
      WRITE (6,213)
      WRITE (6,208) (VORT(I,1), I = 2, MP1)
      GO TO 95
```

```
 46   DO 50  I = 2, M
      VX(I,2) = (-2.0*PHI(I,1) - 3.0*PHI(I,2)
     1          + 6.0*PHI(I,3) - PHI(I,4))/(F6*EZ(2))
      VX(I,N) = (PHI(I,N-2)-6.0*PHI(I,N-1)+3.0*PHI(I,N)
     1          + 2.0*PHI(I,NP1))/(F6*EZ(N))
      NM1 = N - 1
      DO 50  J = 3, NM1
 50   VX(I,J) = (8.0*(PHI(I,J+1)-PHI(I,J-1))+PHI(I,J-2)
     1          - PHI(I,J+2))/(F8*EZ(J))
      DO 55  J = 2, N
      VX(1,J) = 0.0
      VX(MP1,J) = 0.0
      VZ(1,J) =(11.0*PHI(1,J)-18.0*PHI(2,J)+9.0*PHI(3,J)
     1          - 2.0*PHI(4,J))/(F5*EZ(J))
      VZ(MP1,J) = (2.0*PHI(M-2,J) - 9.0*PHI(M-1,J)
     1         +18.0*PHI(M,J)-11.0*PHI(MP1,J))/(F5*EZ(J))
      VZ(2,J) = (2.0*PHI(1,J) +3.0*PHI(2,J)-6.0*PHI(3,J)
     1          + PHI(4,J))/(F5*EZ(J))
      VZ(M,J) = (-PHI(M-2,J)+6.0*PHI(M-1,J)-3.0*PHI(M,J)
     1          - 2.0*PHI(MP1,J))/(F5*EZ(J))
      MM1 = M - 1
      DO 55  I = 3, MM1
 55   VZ(I,J) = (8.0*(PHI(I-1,J) -PHI(I+1,J))+PHI(I+2,J)
     1          - PHI(I-2,J))/(F7*EZ(J))
      WRITE (6,209)
209   FORMAT (1H0, 22X, 'X-COMPONENT VELOCITY', 1X,
     1'DISTRIBUTION AT ALL GRID POINTS')
      WRITE (6,204) (I,(VX(I,J), J=1,NP1,5),I=1,MP1,5)
      WRITE (6,210)
210   FORMAT (1H0, 22X, 'Y-COMPONENT VELOCITY', 1X,
     1'DISTRIBUTION AT ALL GRID POINTS')
      WRITE (6,204) (I,(VZ(I,J), J=1,NP1,5),I=1,MP1,5)
      DO 65  J = 1, MP1
 65   DWDX(J) = (-11.0*VORT(1,J) + 18.0*VORT(2,J)
     1          - 9.0*VORT(3,J)+2.0*VORT(4,J))/F5
      PSTAR0=1.0-PSISQ+(4.0/R)*SIMPS (DWDX,DELZ, 1, NP1)
      WRITE (6,300) PSTAR0
300   FORMAT (1H0, 30X, 'PSTAR0 = ', F9.5)
      DO 60  I = 1, MP1
      DWDZ(I) = ( - 11.0*VORT(I,1) + 18.0*VORT(I,2)
     1          - 9.0*VORT(I,3) + 2.0*VORT(I,4))/F6
      WZERO(I) = VORT(I,1)
      PX(I) = (2.0/R)*SIMPS (DWDZ, DELX, 1, I)
     1        - PSI*SIMPS (WZERO, DELX, 1, I)
      PSTAR(I) = PSTAR0 + 2.0*PX(I)
 60   PY(I) = PX(I)*COS((I-1)*DELX)
      WRITE (6,301)
301   FORMAT (1H0, 23X, 'PRESSURE DISTRIBUTION ON THE', 1X,
     1'SURFACE OF THE CYLINDER')
      WRITE (6,208) (PSTAR(I), I = 2, MP1)
```

```
      DO 58  I = 1, MP1
   58 Y(I) = VORT(I,1)*VX(I,NP1)
      CDF = (4.0/R)*SIMPS (Y, DELX, 1, MP1)
      WRITE (6,211) CDF
  211 FORMAT (1H0, 22X, 'DRAG COEFFICIENT CDF = ',F10.5)
      CDP = 2.0*SIMPS (PY, DELX, 1, MP1)
      WRITE (6,212) CDP
  212 FORMAT (1H0, 22X, 'DRAG COEFFICIENT CDP = ',F10.5)
      CD = CDF + CDP
      WRITE (6,215) CD
  215 FORMAT (1H0, 22X, 'TOTAL DRAG COEFF. CD = CDF +',1X,
     1'CDP = ', F10.5)
      IF (ICOUNT .EQ. IMAX) GO TO 199
   95 DO 98  I = 2, M
      DO 98  J = 2, N
   98 IF (ABS(PHI(I,J)-PHIOLD(I,J)) .GE. EPSMAX .AND.
     1ABS(DUM(I,J)-VORT(I,J)) .GE. EPSMAX) GO TO 99
      WRITE (6,205)
      IMAX = ICOUNT
      WRITE (6,214) ICOUNT
      WRITE (6,206)
      WRITE (6,204) (I,(PHI(I,J), J=1,NP1,5),I=1,MP1,5)
      WRITE (6,207)
      WRITE (6,204) (I,(VORT(I,J), J=1,NP1,5),I=1,MP1,5)
      WRITE (6,213)
      WRITE (6,208) (VORT(I,1), I = 2, MP1)
      GO TO 48
  199 CONTINUE
      XARRAY(32) = 0.0
      XARRAY(33) = 30.0
      YARRAY(32) = - 4.0
      YARRAY(33) = 1.0
      CALL PLOTS (IBUF(1), 1000, 2)
      CALL PLOT1
      YARRAY(32) = -0.4
      YARRAY(33) = 0.2
      CALL PLOT2
      CALL PLOT (0.0, 0.0, 999)
      WRITE (6,209)
      DO 302  I = 1, MP1
  302 WRITE (6,310) (VX(I,J), J = 1, NP1)
      WRITE (6,210)
      DO 304  I = 1, MP1
  304 WRITE (6,310) (VZ(I,J), J = 1, NP1)
      K = N
      KP1 = K + 1
      KM1 = K - 1
      I = 1
      CGUESS(1,1) = 1.36
      CSTAR(1,1) = CGUESS(1,1)
      CSTAR(1,KP1) = 1.0
```

```
      DO 500  J = 2, K
      G3 = VZ(1,J)*EZ(J)/F11
      A(J) = G1 + G3
      B(J) = - 2.0*G1
      C(J) = G1 - G3
500   D(J) = 0.0
      ITERA = 0
      GO TO 502
490   CSTAR(1,1) = CGUESS(1,1)
502   D(2) = - A(2)*CSTAR(1,1)
      D(K) = - C(K)*CSTAR(1,KP1)
      CALL TRIDAG (2, K, A, B, C, D, Y)
      ITERA = ITERA + 1
      DO 501  J = 2, K
      CSTAR(1,J) = Y(J)
      IF (CSTAR(1,J) .LT. 1.0) GO TO 495
501   CONTINUE
495   DO 496  L = J, K
496   CSTAR(1,L) = 1.0
      CGUESS(1,1) = (18.0*CSTAR(1,2) - 9.0*CSTAR(1,3)
     1              + 2.0*CSTAR(1,4))/(11.0 + CONST*F6)
      IF (ABS(CGUESS(1,1)-CSTAR(1,1)) .GE. EPSMAX)
     1 GO TO 490
      CSTAR(1,1) = CGUESS(1,1)
      WRITE (6,205)
      WRITE (6,218) I, ITERA
218   FORMAT (1H0, 25X, 'I = ', I2, 4X, 'ITERA = ', I3)
      WRITE (6,310) (CSTAR(1,J), J = 1, K)
310   FORMAT (1H , 10F13.7)
      DCDZ(1) = ( - 11.0*CSTAR(1,1) + 18.0*CSTAR(1,2)
     1            - 9.0*CSTAR(1,3) + 2.0*CSTAR(1,4))/F6
      WRITE (6,313) DCDZ(1)
313   FORMAT (1H0, 22X, 'LOCAL CONC. GRADIENT DCDZ = ',
     1F10.6)
      F(1) = DCDZ(1)/(CSTAR(1,1) - 1.0)
      ALOCNU = - 2.0*F(1)
      WRITE (6,314) ALOCNU
314   FORMAT (1H0,22X, 'LOCAL NUSSELT NUMBER ALOCNU = ',
     1F10.6)
      DO 700  I = 2, M
      CGUESS(I,1) = 1.01*CSTAR(I-1,1)
      CSTAR(I,1) = CGUESS(I,1)
      CSTAR(I,KP1) = 1.0
      DO 600  J = 2, K
      G3 = (VZ(I,J) + VZ(I-1,J))*EZ(J)/F12
      G4 = (VX(I,J) + VX(I-1,J))*EZ(J)/F9
      A(J) = G1 + G3
      B(J) = - (2.0*G1 + G4)
      C(J) = G1 - G3
600   D(J) = - A(J)*CSTAR(I-1,J-1) + (2.0*G1-G4)
     1       *CSTAR(I-1,J) - C(J)*CSTAR(I-1,J+1)
```

```
      ITERA = 0
      GO TO 594
590   CSTAR(I,1) = CGUESS(I,1)
      DO 592  J = 2, K
      G4 = (VX(I,J) + VX(I-1,J))*EZ(J)/F9
592   D(J) = - A(J)*CSTAR(I-1,J-1) + (2.0*G1-G4)
     1       *CSTAR(I-1,J) - C(J)*CSTAR(I-1,J+1)
594   D(2) = D(2) - A(2)*CSTAR(I,1)
      D(K) = D(K) - C(K)*CSTAR(I,KP1)
      CALL TRIDAG (2, K, A, B, C, D, Y)
      ITERA = ITERA + 1
      DO 601  J = 2, K
      CSTAR(I,J) = Y(J)
      IF (CSTAR(I,J) .LT. 1.0) GO TO 595
601   CONTINUE
595   DO 596  L = J, K
596   CSTAR(I,L) = 1.0
      CGUESS(I,1) = (18.0*CSTAR(I,2) - 9.0*CSTAR(I,3)
     1              + 2.0*CSTAR(I,4))/(11.0 + CONST*F6)
      IF (ABS(CGUESS(I,1)-CSTAR(I,1)) .GE. EPSMAX)
     1GO TO 590
      CSTAR(I,1) = CGUESS(I,1)
      WRITE (6,205)
      WRITE (6,218) I, ITERA
      WRITE (6,310) (CSTAR(I,J), J = 1, K)
      DCDZ(I) = ( - 11.0*CSTAR(I,1) + 18.0*CSTAR(I,2)
     1            - 9.0*CSTAR(I,3) + 2.0*CSTAR(I,4))/F6
      WRITE (6,313) DCDZ(I)
      F(I) = DCDZ(I)/(CSTAR(I,1) - 1.0)
      ALOCNU = - 2.0*F(I)
      WRITE (6,314) ALOCNU
700   CONTINUE
      I = MP1
      CGUESS(MP1,1) = 1.30*CSTAR(M,1)
      CSTAR(MP1,1) = CGUESS(MP1,1)
      CSTAR(MP1,KP1) = 1.0
      DO 800  J = 2, K
      G3 = (VZ(MP1,J) + VZ(M,J))*EZ(J)/F12
      G4 = (VX(MP1,J) + VX(M,J))*EZ(J)/F9
      A(J) = G1 + G3
      B(J) = - (2.0*G1 + G4)
      C(J) = G1 - G3
800   D(J) = - A(J)*CSTAR(M,J-1) +(2.0*G1-G4)*CSTAR(M,J)
     1       - C(J)*CSTAR(M,J+1)
      ITERA = 0
      GO TO 794
790   CSTAR(MP1,1) = CGUESS(MP1,1)
      DO 792  J = 2, K
      G4 = (VX(MP1,J) + VX(M,J))*EZ(J)/F9
792   D(J) = - A(J)*CSTAR(M,J-1) +(2.0*G1-G4)*CSTAR(M,J)
     1       - C(J)*CSTAR(M,J+1)
```

```
794   D(2) = D(2) - A(2)*CSTAR(MP1,1)
      D(K) = D(K) - C(K)*CSTAR(MP1,KP1)
      CALL TRIDAG (2, K, A, B, C, D, Y)
      ITERA = ITERA + 1
      DO 801  J = 2, K
      CSTAR(MP1,J) = Y(J)
      IF (CSTAR(MP1,J) .LT. 1.0) GO TO 695
801   CONTINUE
695   DO 696  L = J, K
696   CSTAR(MP1,L) = 1.0
      IF (ITERA .GT. 150) STOP
      CGUESS(MP1,1) =(18.0*CSTAR(MP1,2)-9.0*CSTAR(MP1,3)
     1                + 2.0*CSTAR(MP1,4))/(11.0+CONST*F6)
      IF (ABS(CGUESS(MP1,1)-CSTAR(MP1,1)) .GE. EPSMAX)
     1GO TO 790
      CSTAR(MP1,1) = CGUESS(MP1,1)
      WRITE (6,205)
      WRITE (6,218) I, ITERA
      WRITE (6,310) (CSTAR(MP1,J), J = 1, K)
      DCDZ(MP1)= ( - 11.0*CSTAR(MP1,1)+18.0*CSTAR(MP1,2)
     1           - 9.0*CSTAR(MP1,3)+2.0*CSTAR(MP1,4))/F6
      WRITE (6,313) DCDZ(MP1)
      F(MP1) = DCDZ(MP1)/(CSTAR(MP1,1) - 1.0)
      ALOCNU = - 2.0*F(MP1)
      WRITE (6,314) ALOCNU
      AVEGRA = GRAD (M, DCDZ, DELZ)
      WRITE (6,315) AVEGRA
315   FORMAT (1H0,22X,'AVERAGE CONC. GRADIENT AVEGRA = '
     1, F10.6)
      OVERNU = - (2.0/PAI)*SIMPS (F, DELX, 1, MP1)
      WRITE (6,316) OVERNU
316   FORMAT (1H0,22X,'OVERALL NUSSELT NUMBER OVERNU = '
     1, F10.6)
      GO TO 1
      END
      SUBROUTINE TRIDAG (IF, L, A, B, C, D, V)
      DIMENSION A(1), B(1), C(1), D(1), V(1),
     1          BETA(101), GAMMA(101)
      BETA(IF) = B(IF)
      GAMMA(IF) = D(IF)/BETA(IF)
      IFP1 = IF + 1
      DO 1  I = IFP1, L
      BETA(I) = B(I) - A(I)*C(I-1)/BETA(I-1)
    1 GAMMA(I) = (D(I) - A(I)*GAMMA(I-1))/BETA(I)
      V(L) = GAMMA(L)
      LAST = L - IF
      DO 2  K = 1, LAST
      I = L - K
    2 V(I) = GAMMA(I) - C(I)*V(I+1)/BETA(I)
      RETURN
      END
```

```
      FUNCTION GRAD (M, F, DZ)
      DIMENSION F(1)
      DCDZ = 0.0
      MP1 = M + 1
      DO 1  I = 1, MP1
      IF (I .EQ. 1 .OR. I .EQ. MP1) GO TO 2
      DCDZ = DCDZ + F(I)
      GO TO 1
    2 DCDZ = DCDZ + 0.5*F(I)
    1 CONTINUE
      DCDZ = DCDZ/M
      GRAD = DCDZ
      RETURN
      END
      FUNCTION SIMPS (F, H, IR, IS)
      DIMENSION F(1)
      N = (IS - IR)/2
C     ..... N WILL BE TRUNCATED, IF (IS - IR) IS NOT EVEN .....
      IF (IS-IR-1) 10, 20, 30
   10 SIMPS = 0.0
      RETURN
   20 SIMPS = (F(IR) + F(IS))*H/2.0
      RETURN
   30 SUM = F(IR)
      NM1 = N - 1
      IF (NM1 .LT. 1) GO TO 3
      DO 1  I = IR, NM1
    1 SUM = SUM + 4.0*F(IR+2*I-1) + 2.0*F(IR+2*I)
    3 IF ((IS - IR) .NE. (2*N)) GO TO 2
      SUM = SUM + 4.0*F(IR+2*N-1) + F(IR+2*N)
      SIMPS = H*SUM/3
      RETURN
    2 SUM = SUM + 4.0*F(IR+2*N-1) + 2.5*F(IR+2*N)
      SIMPS = H*(SUM/3 + F(IS)/2)
      RETURN
      END
      SUBROUTINE PLOT1
      COMMON M, R, PSI, XARRAY, YARRAY, PSTAR
      DIMENSION Z(1), XARRAY(33), YARRAY(33), PSTAR(31)
      CALL PLOT (0.0, -0.5, 3)
      Z(1) = 'X-ABSC'
      Z(2) = 'ISSA..'
      CALL AXIS (0.0, 0.0, Z, -10, 6.0, 0.0, XARRAY(32),
     1XARRAY(33))
      Z(1) = 'Y-ORDI'
      Z(2) = 'NATE..'
      CALL AXIS (0.0, 0.0, Z, 10, 10.0, 90.0,
     1YARRAY(32), YARRAY(33))
      CALL PLOT (6.0, 0.0, 3)
      CALL PLOT (6.0, 10.0, 2)
      CALL PLOT (0.0, 10.0, 2)
```

```
      Z(1) = 'SURFAC'
      Z(2) = 'E PRES'
      Z(3) = 'SURE D'
      Z(4) = 'ISTRIB'
      Z(5) = 'UTION '
      CALL SYMBOL (1.0, 9.7, 0.14, Z, 0.0, 29)
      Z(1) = 'PLOTTE'
      Z(2) = 'D ON A'
      Z(3) = ' CALCO'
      Z(4) = 'MP PLO'
      Z(5) = 'TTER..'
      CALL SYMBOL (1.0, 9.4, 0.14, Z, 0.0, 28)
      CALL SYMBOL (1.0, 9.1, 0.14,18HREYNOLDS NUMBER = ,
     10.0, 18)
      CALL NUMBER (999.0, 999.0, 0.14, R, 0.0, 1)
      CALL SYMBOL (1.0, 8.8, 0.14, 6HPSI = , 0.0, 6)
      CALL NUMBER (999.0, 999.0, 0.14, PSI, 0.0, 2)
      MP1 = M + 1
      DO 500  I = 1, MP1
      XARRAY(I) = (I-1)*6.0
  500 YARRAY(I) = PSTAR(I)
      CALL LINE (XARRAY(1), YARRAY(1), 31, 1, 1, 4)
      RETURN
      END
      SUBROUTINE PLOT2
      COMMON M, R, PSI, XARRAY, YARRAY, PSTAR, VORT
      DIMENSION Z(1), XARRAY(33), YARRAY(33), PSTAR(31),
     1          VORT(31,1)
      CALL PLOT (7.0, 0.0, -3)
      Z(1) = 'X-ABSC'
      Z(2) = 'ISSA..'
      CALL AXIS (0.0, 0.0, Z, -10, 6.0, 0.0, XARRAY(32),
     1XARRAY(33))
      Z(1) = 'Y-ORDI'
      Z(2) = 'NATE..'
      CALL AXIS (0.0, 0.0, Z, 10, 10.0, 90.0,YARRAY(32),
     1YARRAY(33))
      CALL PLOT (6.0, 0.0, 3)
      CALL PLOT (6.0, 10.0, 2)
      CALL PLOT (0.0, 10.0, 2)
      Z(1) = 'SURFAC'
      Z(2) = 'E VORT'
      Z(3) = 'ICITY '
      Z(4) = 'DISTRI'
      Z(5) = 'BUTION'
      CALL SYMBOL (1.0, 9.7, 0.14, Z, 0.0, 30)
```

```
      Z(1) = 'PLOTTE'
      Z(2) = 'D ON A'
      Z(3) = ' CALCO'
      Z(4) = 'MP PLO'
      Z(5) = 'TTER..'
      CALL SYMBOL (1.0, 9.4, 0.14, Z, 0.0, 28)
      CALL SYMBOL (1.0, 9.1, 0.14,18HREYNOLDS NUMBER = ,
     10.0, 18)
      CALL NUMBER (999.0, 999.0, 0.14, R, 0.0, 1)
      CALL SYMBOL (1.0, 8.8, 0.14, 6HPSI = , 0.0, 6)
      CALL NUMBER (999.0, 999.0, 0.14, PSI, 0.0, 2)
      MP1 = M + 1
      DO 600  I = 1, MP1
      XARRAY(I) = (I-1)*6.0
600   YARRAY(I) = VORT(I,1)
      CALL LINE (XARRAY(1), YARRAY(1), 31, 1, 1, 1)
      RETURN
      END
```

APPENDIX C

CALCULATION OF RADIAL MASS FLUX

The following is a sample calculation of radial mass flux at a dimensionless radial velocity V_0 of 0.006 and a diameter of 100 microns.

$R = 1$

$2a = 100$ microns

$\nu = 0.009$ cm/sec.

$v_0 = V_0 \times U_\infty$

$R = \frac{2a}{\nu} U_\infty$

$U_\infty = \frac{\nu}{2a} R$

$= \frac{0.009}{0.01} \times 1$

$= 0.9$ cm/sec.

$v_0 = V_0 \times U_\infty$

$= 0.006 \times 0.9$ cm/sec.

$= 0.006 \times 0.9 \times 2.12 \times 10^4$ gal./day/ft^2

radial suction mass flux $G = 115$ gal./day/ft^2

BIBLIOGRAPHY

1. G. G. Stokes, "On the Effect of the Internal Friction of Fluids on the Motion of Pendulums," Trans. Camb. Phil. Soc., 9, 8 (1851).

2. C. W. Oseen, "Ueber die Stokes'sche Formel, und über eine verwandte Aufgabe in der Hydrodynamik," Ark. Math. Astronom. Fys., 6, 29 (1911).

3. H. Lamb, "On the Uniform Motion of a Sphere through a Viscous Fluid," Philos. Mag., 21, 112 (1911).

4. S. Tomotika and T. Aoi, "The Steady Flow of Viscous Fluid Past a Sphere and Circular Cylinder at Small Reynolds Numbers," Quart. J. Mech. Appl. Math., 3, 140 (1950).

5. S. Taneda, "Experimental Investigation of the Wakes behind Cylinders and Plates at Low Reynolds Numbers," J. Phys. Soc. Japan, 11, 302 (1956).

6. H. Yamada, "On the Slow Motion of Viscous Liquid Past a Circular Cylinder," Rep. Res. Inst. Appl. Mech., Kyushu Univ., 3, 11 (1954).

7. S. Kaplun, "Low Reynolds Number Flow Past a Circular Cylinder," J. Math. Mech., 6, 595 (1957).

8. I. Proudman and J. R. A. Pearson, "Expansions at Small Reynolds Numbers for the Flow Past a Sphere and a Circular Cylinder," J. Fluid Mech., 2, 237 (1957).

9. D. J. Tritton, "Experiments on the Flow Past a Circular Cylinder at Low Reynolds Numbers," J. Fluid Mech., 6, 547 (1959).

10. A. Thom, "An Investigation of Fluid Flow in Two Dimensions," British Aero. Res. Council, R. & M., no. 1194 (1928).

11. A. Thom, "The Flow Past Circular Cylinders at Low Speeds," Proc. Royal Soc. London, A141, 651 (1933).

12. M. Kawaguti, "Numerical Solution of the Navier-Stokes Equations for the Flow Around a Circular Cylinder at Reynolds Number 40," J. Phys. Soc. Japan, 8, 747 (1953).

BIBLIOGRAPHY (Continued)

13. D. N. de G. Allen and R. V. Southwell, "Relaxation Methods Applied to Determine the Motion, in Two Dimensions, of a Viscous Fluid Past a Fixed Cylinder," Quart. J. Mech. Appl. Math., 8, 129 (1955).

14. M. Kawaguti, "Note on Allen and Southwell's Paper 'Relaxation Methods Applied to Determine the Motion, in Two Dimensions, of a Viscous Fluid Past a Fixed Cylinder,'" Quart. J. Mech. Appl. Math., 12, 261 (1959).

15. S. C. R. Dennis and M. Shimshoni, "The Steady Flow of a Viscous Fluid Past a Circular Cylinder," Aero. Res. Council, London, no. 797 (1965).

16. R. L. Underwood, "Calculation of Incompressible Flow Past a Circular Cylinder at Moderate Reynolds Numbers," J. Fluid Mech., 37, 95 (1969).

17. M. D. Van Dyke, "A Method of Series Truncation Applied to Some Problems in Fluid Mechanics," Stanford University SUDAER no. 247 (1965).

18. R. B. Payne, "Calculations of Unsteady Viscous Flow Past a Circular Cylinder," J. Fluid Mech., 4, 81 (1958).

19. M. Kawaguti and P. Jain, "Numerical Study of a Viscous Flow Past a Circular Cylinder," J. Phys. Soc. Japan, 21, 2055 (1966).

20. J. S. Son and T. J. Hanratty, "Numerical Solution for the Flow Around a Cylinder at Reynolds Numbers of 40, 200 and 500," J. Fluid Mech., 35, 369 (1969).

21. D. W. Peaceman and H. H. Rachford, Jr., "The Numerical Solution of Parabolic and Elliptic Partial Differential Equations," J. Soc. Indust. Appl. Math., 3, 28 (1955).

22. H. B. Keller and H. Takami, "Numerical Studies of Steady Viscous Flow about Cylinders," Numerical Solutions of Nonlinear Differential Equations, ed. by D. Greenspan, John Wiley & Sons, Inc., New York, pp. 115-140 (1966).

23. A. E. Hamielec and J. D. Raal, "Numerical Studies of Viscous Flow Around Circular Cylinders," Phys. Fluids, 12, 11 (1969).

24. W. Lohrisch, "Bestimmung von Waermeuebergangszahlen durch Diffusionsversuche," Mitt. Forsch., 322, 46 (1929).

BIBLIOGRAPHY (Continued)

25. W. H. Linton, Jr. and T. K. Sherwood, "Mass Transfer from Solid Shapes to Water in Streamline and Turbulent Flow," Chem. Eng. Progr., 46, 258 (1950).

26. R. Dobry and R. K. Finn, "Mass Transfer to a Cylinder at Low Reynolds Numbers," Ind. Eng. Chem., 48, 1540 (1956).

27. A. H. Davis, "Convective Cooling of Wires in Streams of Viscous Liquids," Phil. Mag. & J. of Sci., 47, 1057 (1924).

28. S. K. Friedlander, "Mass and Heat Transfer to Single Spheres and Cylinders at Low Reynolds Numbers," A. I. Ch. E. J., 3, 43 (1957).

29. M. J. Lighthill, "Contributions to the Theory of Heat Transfer through a Laminary Boundary Layer," Proc. Royal Soc. London, A202, 359 (1950).

30. P. H. Sih and J. Newman, "Mass Transfer to the Rear of a Sphere in Stokes Flow," Intern. J. Heat Mass Transfer, 10, 1749 (1967).

31. J. Newman, "Mass Transfer to the Rear of a Cylinder at High Schmidt Numbers," Ind. Eng. Chem. Fundamentals, 8, 553 (1969).

32. R. W. Grafton, "Prediction of Mass Transfer from Spheres and Cylinders in Forced Convection," Chem. Eng. Sci., 18, 457 (1963).

33. W. H. McAdams, Heat Transmission, 3rd ed., McGraw-Hill Book Company, Inc., New York (1954).

34. R. L. Piret, W. James, and M. Stacy, "Heat Transmission from Fine Wires to Water," Ind. Eng. Chem., 39, 1098 (1947).

35. E. R. G. Eckert and E. E. Soehngen, "Distributions of Heat Transfer Coefficients Around Circular Cylinders in Cross-Flow at Reynolds Numbers from 20 to 500," Trans. ASME, 74, 343 (1952).

36. E. E. Soehngen, "Experimental Studies on Heat Transfer at Very High Prandtl Numbers," Progress in Heat and Mass Transfer, Volume 2, Pergamon Press, Inc., London, pp. 125-150 (1969).

37. J. Cole and A. Roshko, "Heat Transfer from Wires at Reynolds Numbers in the Oseen Range," Proceedings of Heat Transfer and Fluid Mechanics Institute, University of California, Berkeley, pp. 13-23 (1954).

BIBLIOGRAPHY (Concluded)

38. C. R. Ellingworth, "Flow at Small Reynolds Number, in Laminary Boundary Layer," ed. by L. Rosenhead, Oxford, Clarendon Press (1963).

39. W. W. Wood, "Calculations for Anemometry with Fine Hot Wires," J. Fluid Mech., 32, 9 (1968).

40. C. A. Hieber and B. Gebhart, "Low Reynolds Number Heat Transfer from a Circular Cylinder," J. Fluid Mech., 32, 21 (1968).

41. R. B. Bird, W. E. Stewart, and E. N. Lightfoot, Transport Phenomena, John Wiley & Sons, Inc., New York (1960).

42. H. Schlichting, Boundary-Layer Theory, 6th ed., McGraw-Hill Book Company, Inc., New York (1968).

43. V. G. Levich, Physicochemical Hydrodynamics, Prentice-Hall, Englewood Cliffs, N. J. (1962).

44. L. Lapidus, Digital Computation for Chemical Engineers, McGraw-Hill Book Company, Inc., New York (1962).

45. B. Carnahan, H. A. Luther, and J. O. Wilkes, Applied Numerical Methods, John Wiley & Sons, Inc., New York (1969).

46. V. G. Jenson, "Viscous Flow Round a Sphere at Low Reynolds Numbers (< 40)," Proc. Royal Soc. London, A249, 346 (1959).

47. J. Crank and P. Nicholson, "A Practical Method for Numerical Evaluation of Solutions of Partial Differential Equations of the Heat-Conduction Type," Proc. Camb. Phil. Soc., 43, 50 (1947).

48. G. H. Bruce, D. W. Peaceman, H. H. Rachford, and J. D. Rice, "Calculation of Unsteady-State Gas Flow through Porous Media," Trans. Amer. Inst. Mining and Met. Engrs., 198, 79 (1953).

49. "General Purpose Contouring Program," by California Computer Products, Inc., 1968.

50. P. H. Vogtlander and C. A. P. Bakker, "An Experimental Study of Mass Transfer from a Liquid Flow to Wires and Gauzes," Chem. Eng. Sci., 18, 583 (1963).

VITA

The author was born on June 22, 1939 in Taiwan, China. He received his elementary education in his native town. He then attended Ping-Tung Senior High School, where he graduated in the summer of 1959. In the fall of that year he entered the Engineering College of Taiwan Provincial Chen Kung University. Under the practical training program of his alma mater, he worked for the Taiwan Aluminum Corporation during the summer of his sophomore year. In 1963 he graduated with a degree of Bachelor of Science in Chemical Engineering. Shortly after his graduation from the college, he entered service in the Chinese Army as a Second Lieutenant, where he was assigned as a Unit Administration Officer. After his military service was completed, he enrolled at the Georgia Institute of Technology with the award of a graduate teaching assistantship. He received his Master of Science in Chemistry in 1967 and continued his studies towards a doctorate degree in the School of Chemical Engineering.

He served as a graduate teaching assistant from September, 1968 to August, 1969 in the School of Chemical Engineering. From September, 1968 to December, 1970 he worked half-time as a graduate research assistant at the Georgia Institute of Technology Engineering Experiment Station, Atlanta, Georgia.

He is a member of the Chinese Engineers' Association.